Effects of impurities on an industrial crystallization process of ammonium sulfate

Dissertation

zur Erlangung des akademischen Grades

Doktoringenieur (Dr.-Ing.)

vorgelegt dem

Zentrum für Ingenieurwissenschaften

der Martin-Luther-Universität Halle-Wittenberg

als organisatorische Grundeinheit für Forschung und Lehre im Range einer Fakultät
(§ 75 Abs. 1 HSG LSA, § 1 Abs. 1 Grundordnung)

von

Herrn Dipl.-Ing. Robert Buchfink

geboren am 18.04.1983

Gutachter: 1. Prof. Dr.-Ing. Dr. h.c. Joachim Ulrich

          2. Prof. Dr. rer. nat. habil. Axel König

Datum der Verteidigung: 02.05.2011

Halle (Saale), den 01.06.2011

Acknowledgment

First of all I want to thank my family including my parents Gunter und Sigrid, my sister Lydia and my grandfather Walter. I wished my grandmother Hanni could have seen me getting a PhD degree. All of them gave me a great support, both financial and moral, over the long period of study and up to now we have a fantastic relationship. Furthermore, I want to acknowledge the support of my girlfriend Elli who was always there for me in good and in bad times.

No PhD thesis without a supervisor, an institute and a topic. In this context I want to thank Prof. Dr.-Ing. Dr. h.c. Joachim Ulrich who gave me the great opportunity to work at his institute and who supervised my research in the interesting field of crystallization. Moreover, I also want to thank Prof. Ulrich for creating the institute as a melting pot of international students which opened my mind in many ways and gave me the opportunity to get close friendships and learn much about the culture of different nations.

Moreover I want to thank Prof. Dr. Axel König for his willingness to be the second examiner for this work and my special thanks also go to all the members of the examination committee.

Concerning the life at "TVT" I, especially, want to thank the four musketeers Mr. Weißbarth, Canerinho, Angus and Püpp for the nice days full of laughing, the afternoons full of sports and the evenings full of "scientific stuff".

Mr. Weißbarth was and he still is irreplaceable concerning his work as technician, for interesting discussions on science and as a fellow for after work activities. Over the years I had so much fun with my colleagues at TVT, so thank you Essa, Javetti, Claudi, Christiane, Patrugi, Isabell, Yi, Anika, Danovitsch, Kesarinho, Chilli, Vivi, Jingfei, Mehrdad, James, Lydi, Micha, Torsten, Frau Höser and Claudia K. for making the work at TVT unforgettable.

I think this thesis would not be possible without the hard work of the students I supervised during my time at TVT. With this in mind I want to thank Bernd, Rene, Sebastian, Agnes, Christiane, Omar, Steffen² and Iwona for their help and the friendly collaboration.

In addition, I would like to thank SKW Piesteritz for giving me the topic of this work. Therefore I acknowledge Prof. Dr. Dr. h.c. Niclas for the helpful discussions and the promotion of the status seminars, Dr. Niendorf and his lab stuff for performing the

Table of Contents

1. Introduction

In general, crystallization is a process including a liquid-solid phase transition. This process was used for a very long time by mankind and one famous example is the production of the so-called "white gold", the sodium chloride. The Martin Luther University is situated in Halle at the river Saale which is famous for its history in the production of food grade salt. Archaeological findings of tools for the salt production at the "Hallmarkt" close to river Saale from the year 2000 before Christ are evidence for a considerable salt production of Celtic, German and Slavic tribes. In 13th century saltwater was taken from springs and was brought to so-called boiling houses, where the water was evaporated and therefore salt was produced. Afterwards the wet salt was dried in big baskets and the final product table salt could be sold. From this example for early and simple evaporation crystallizations there was a steep development and today crystallization processes are highly efficient and generate very pure products with high yields.

These industrial crystallization processes for the production of inorganic salts like ammonium sulfate are large scale processes. By taking a look at the crystallization unit of such a process and fading out all upstream or downstream process operations like centrifugation, filtration, drying or storage, the dimension become clear.

The most important criterion for the success of the process is the product stream which contains the desired crystalline product. This product should have specified properties after leaving the crystallizer. On the one hand the quantity (yield) of the crystallization should be as high as possible to make the process profitable. On the other hand there is the product quality which includes parameters like crystal size and crystal size distribution, the shape of the product crystals and their purity. All of these parameters depend on the design of the crystallizer (and process conditions) and on the properties of the feed stream.

Common types of crystallizers are the FC (Forced Circulation) crystallizer, the DTB (Draft Tube Baffle) crystallizer or the Oslo-type crystallizer [Hof04]. All of these types are continuous crystallizers which are often used for mass products like inorganic salts. Already by choosing the one or the other type of crystallizer the size of the product crystals is fixed into a defined range.

So with the FC crystallizer crystal sizes from 0.2-0.8 mm can be produced, whereas the Oslo-type crystallizer is used to achieve crystals in the size range of >1.5-5 mm [Hof04].

Up to this point there is no problem, but also the feed stream can affect the properties of the product. Industrial mass productions of inorganic compounds like ammonium sulfate need a production which leads to the desired properties of the product at low costs. Therefore, often waste streams of other chemical reaction pathways are used as feed stream which can contain different impurities in various concentrations. These impurities can be e.g. metal ions like Fe^{3+}, Al^{3+} or Cr^{3+} originating from the previous process, the transport or from storage. Since the process is continuous these impurities can get enriched within the mother liquor. If their concentrations reach a critical level, the undesired ions have to be removed from time to time by renewing the mother liquor (time and money consuming process).

If the critical concentrations are exceeded this would have a strong effect on the following parameters. The most important effects are the influences on the nucleation and metastable zone width (MZW), the crystal growth rates and the crystal morphology. If the nucleation is affected, this would have a direct influence on the crystal size distribution which is an important parameter for the crystal quality. If the growth rate of the crystals is reduced by impurities the yield or the retention time of the crystallization will decrease or increase, respectively, and therefore the profitability of the process. Another important parameter for the product quality is the morphology of the crystals because these will directly affect the downstream processes namely centrifugation and filtration on the one hand and also transport and storage problems could be created on the other hand.

It is therefore essential to know the critical concentrations for the impurities which might be present in the feed streams of a process. Furthermore, the concentrations should be controlled within the process and suitable action should be taken if these critical values are exceeded.

So one major task of this work is to define process windows for the common impurities Fe^{3+}, Cr^{3+}, Al^{3+}, Zn^{2+}, K^+ and Na^+ concerning their effect on growth rates, MZW/nucleation and crystal morphology of ammonium sulfate. Furthermore, a proof of concept should be carried out for the treatment of contaminated solutions by the help of oxalic acid as suggested already long time ago [Mes70].

2. Basics of Crystallization

2.1 Crystal State

By definition a crystal is a solid which contains periodically arranged units (e.g. atoms, ions or molecules) into all three dimensions. A simple model for crystals is a point lattice in which every point is characterized by the three dimensions a, b and c and by three angles α, β and γ. From these parameters an unit cell can be created. Figure 2.1 shows a schematic unit cell.
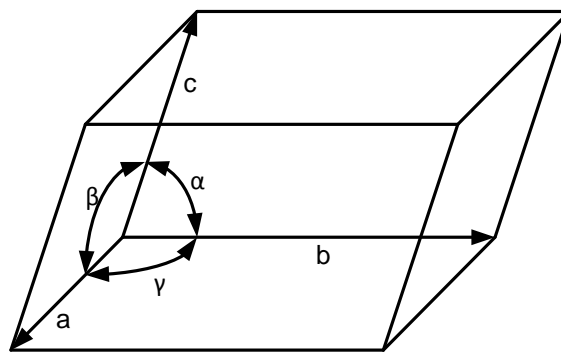
Fig. 2.1: Schematic unit cell (see e.g. [Mul93])

Using the parameters of the unit cell one can define seven crystal systems called cubic, tetragonal, orthorhombic, rhombohedral, hexagonal, monoclinic and triclinic. These systems can be refined into 13 Bravais lattices. Detailed information can be achieved from the literature (e.g. [Mul93, Mye02]). Ammonium sulfate crystallizes in an orthorhombic crystal system.

All these facts give information on the internal structure of crystals including the arrangement of growth units, but a crystal also shows an external appearance which is called the crystal habit. The habit of a crystal is defined by the internal structure on the one hand, but also on factors like growth rate, used solvent and presence or absence of impurities on the other hand. The shape of the crystal is restricted by specific faces. Miller indices are used to index all faces appearing at one crystal. Every plane could be described by three parameters (hkl) which are defined to be the reciprocals of the intercepts between plane and the three crystal axis (see e.g. [Mye02]). Figure 2.2 shows a theoretical habit of ammonium sulfate with its characteristic faces.
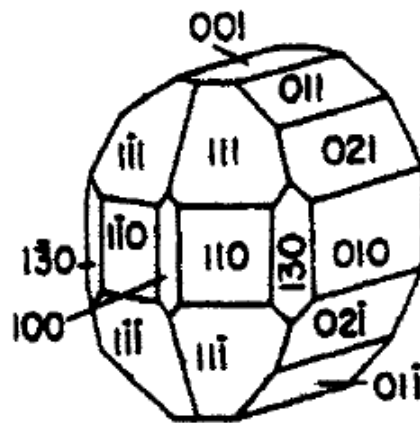
Fig. 2.2: Characteristic crystal habit of ammonium sulfate [Mul93]

2.2 Phase Diagram

2.2.1 Solubility

Per definition the solubility gives information on the amount of a compound which can be dissolved within a specific solvent under defined conditions (see e.g. [Sch04]). The correct term for the definition is the equality of chemical potentials of the solute within the solution and the species in the solid phase – a solid-liquid-equilibrium [Mye01].

In literature there are long lists of different expressions and units for the solubility and also on how to translate one into another (e.g. [Mul93]). Within this work solubility will be expressed as [g/L] which means the mass of a salt in [g] is dissolved in 1 L of solvent, in this case distilled water or as [Ma%] which means the percentage of the mass of salt based on total mass of the solution.

The thermodynamically fixed solubility only depends on pressure, temperature and concentration. For the most commercially used crystallization processes the pressure only plays a minor role. Hence the phase equilibrium can be reduced to a temperature-concentration-diagram as shown exemplary in Figure 2.3 [Xu98]. For industrial crystallization processes frequently only a specific section of the complete phase diagram is of interest (solubility curve) shown in Fig 2.3 (right).
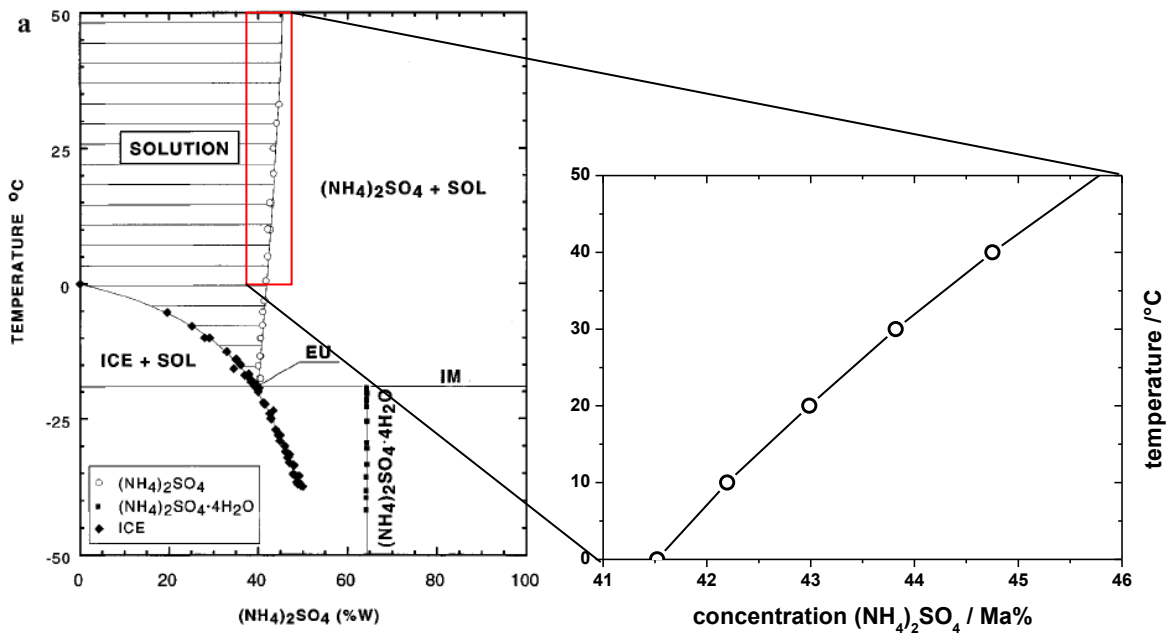
Fig. 2.3: Phase diagram of ammonium sulfate (left) [Xu 98] and solubility curve as a part of it (right) (data taken from [Mul93])

2.2.2 Supersolubility and Metastable Zone Width (MZW)

Additionally to the solubility curve the phase diagram of Fig. 2.3 (right) can be extended by adding a supersolubility curve (a non-thermodynamic factor) (see Fig. 2.4).
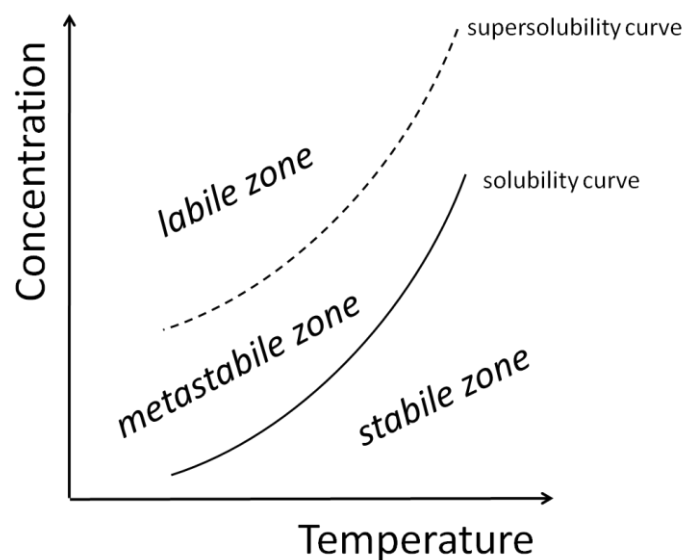
Fig. 2.4: Schematic phase diagram

In contrary to the solubility curve which is exactly defined by the thermodynamic parameters pressure, temperature and concentration, the supersolubility curve

always depends on process parameters like presence or absence of crystals, stirrer speed, rate of achieving the supersaturation and presence of impurity.

Both, solubility and supersolubility curve, separate the phase diagram into three zones (see Fig. 2.4). At the stable zone the solution is unsaturated which means crystallization is not possible and existing crystals will be dissolved. Within the metastable zone the solution is supersaturated. Existing crystals grow, but no primary nucleation will occur in the metastable zone. If the solution gets further supersaturated, e.g. by cooling or evaporation of the solvent, the supersolubility curve will be crossed and nucleation will appear instantly [Mul93].

2.3 Nucleation

2.3.1 Basic and Energetic Considerations

For crystal growth two main conditions have to be given within a system, a supersaturated solution or supercooled melt on the one hand and first very small crystals, the so-called nuclei, on the other hand. These nuclei can be formed during different processes and therefore different classes of nucleation can be defined.

Primary Nucleation can be divided into two sub items, homogeneous and heterogeneous nucleation. While in case of homogeneous nucleation the nuclei are formed from absolute pure solution, in case of heterogeneous nucleation foreign particles give base for inducing nucleation. For industrial crystallization processes as well as scientific studies absolutely pure conditions cannot be achieved which means homogeneous nucleation is more a theoretical term.

Secondary Nucleation always implies the presence of crystals. In practice new nuclei can appear by attrition or breakage of the existing crystals when there are collisions between crystals and stirrer, crystals and reactor walls or internals and also crystal and crystal. Secondary nucleation can be also induced by seed crystals or the dust on their surfaces.

For the different nucleation mechanisms the supersolubility curve will change and hence there is also a difference in the metastable zone width. Therefore the supersolubility curve for secondary nucleation will be closer to the solubility curve than for primary heterogeneous nucleation. An even higher supersaturation would be needed to induce primary homogeneous nucleation.

The nucleation process itself can be explained as a stochastic gathering of molecules or ions within the solution or melt. This process can be reduced to an energetic level and can be expressed by Equation 2.1.

$$\Delta G = \Delta G_S + \Delta G_V \qquad (2.1)$$

The total excess free energy ΔG is the sum of surface excess free energy ΔG_S and volume excess free energy ΔG_V. Both, ΔG_S and ΔG_V depend on the particle radius r as can be seen in Equation 2.2.

$$\Delta G = 4\pi \cdot r^2 \cdot \gamma + \frac{4}{3}\pi \cdot r^3 \cdot \Delta G_\vartheta \qquad (2.2)$$

Plotting Equation 2.2 into a $\Delta G - r -$ diagram (see Fig. 3.5) opens the possibility to understand the energetically point of view on nucleation processes. For very small nuclei it is energetically more favorable that nuclei dissolve again, while once a critical size r_c is reached the free energy will decrease with increasing size which makes the growth process energetically favorable. The critical size and critical free energy level could be calculated from Equations 2.3 and 2.4, respectively.

$$r_{3D}{}^* = \frac{-2 \cdot \gamma}{\Delta G_V} \qquad (2.3)$$

$$\Delta G_{3D}{}^* = \frac{4}{3} \cdot \pi \cdot \gamma \cdot r_{3D}{}^{*2} \qquad (2.4)$$
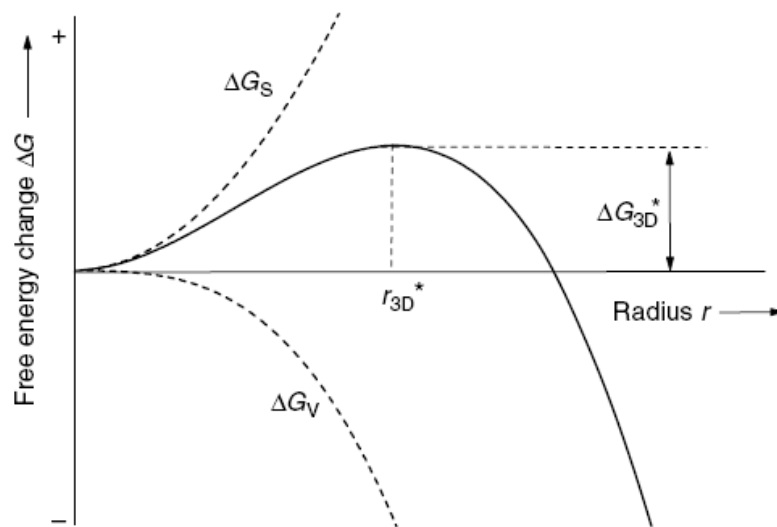
Fig. 2.5: Diagram of free energy vs. radius of nucleus (taken from [San07b])

The rate of nucleation which means the number of nuclei created during a specific time period within a specific volume can be expressed by following Equation 2.5 [Mul93]. From this so-called Arrhenius reaction velocity equation it is possible to form Equation 2.6 wherein all parameters influencing the nucleation rate are included.

$$J = A_1 \cdot e^{\frac{-\Delta G}{k \cdot T}} \tag{2.5}$$

$$J = A_1 \cdot e^{\left[-\frac{16\pi \cdot \gamma^3 \cdot \Omega^2}{3k^3 \cdot T^3 \cdot (\ln \sigma)}\right]} \tag{2.6}$$

As can be seen from Equation 2.6 the nucleation rate depends on temperature T, supersaturation level σ, the molecular volume Ω and interfacial tension γ. So normally the nucleation rate should increase very fast with increasing supersaturation, but in practice another behavior could be detected as can be seen in Figure 2.6.
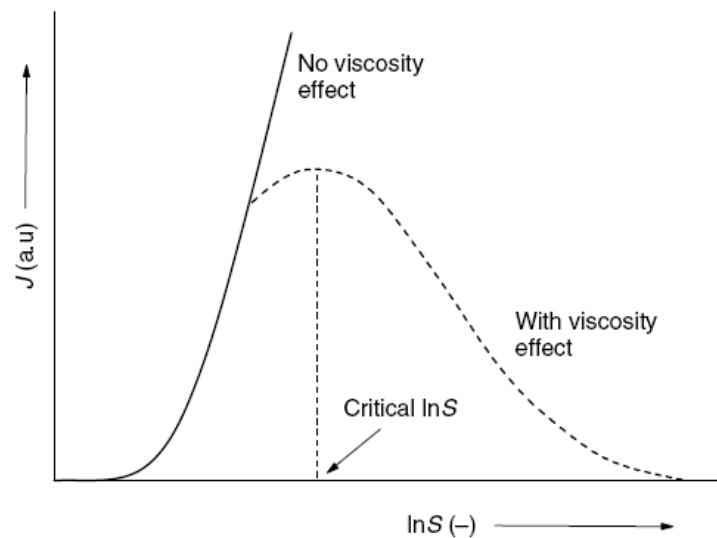
Fig. 2.6: Dependence of nucleation on the supersaturation (taken from [San07b])

With increasing supersaturation the viscosity for some compounds reaches a critical level which reduces the molecular movement within the solution or melt. Therefore the nucleation rate in practice will show a maximum and with further increase of supersaturation the nucleation rate J will decrease again.

In connection to nucleation processes one has to mention the induction time for nucleation. By definition the induction time is the time which elapses between adjusting supersaturation and the first appearance of crystal nuclei [Mul93]. This time

depends on various parameters like supersaturation level, agitation, viscosity or the presence of impurities.

Induction time t_{ind} could be divided into different parts which are based on theoretically considerations, but cannot easily be investigated separately from each other (see Eq. 2.7).

$$t_{ind} = t_r + t_n + t_g \qquad (2.7)$$

Thereby t_r is the so-called relaxation time which is needed by the system to reach a quasi-steady-state distribution of molecular clusters, t_n is the time which is needed to form a stable nucleus and t_g is the time for the growth of the nucleus to a detectable size.

2.3.2 Effect of Impurities

In the past decades many works were published concerning the influence of impurities on the nucleation rates and kinetics of nucleation. But unfortunately up to now and based on the available data no general relationships can be formulated. However, it is known that especially trivalent metal ions show an effect on the nucleation of inorganic compounds like e.g. ammonium sulfate.

The possible effects could be explained by taking a closer look at Eq. 2.6 where all parameters concerning the nucleation rates are included. Sangwal [San07b] specified two possible mechanisms of the impurity effects. The first includes the effect of impurities on the solid-liquid interfacial energy γ which could be reduced by impurity adsorption at the crystal surface. Thereby the nucleation rate J is increased (see Eq. 2.6). The other possible mechanism is also based on impurity adsorption, but in this case at relevant growth sites which leads to a blockage and thus to a change in the rate of the growth of the nuclei. So J is decreased by a decreasing A_1 which is the kinetic parameter of the nucleation process (Eq. 2.6) [San07b]. However, the very short life time of the first nuclei (nano- to microseconds) sometimes does not allow any impurity adsorption onto the surface of the nuclei, because impurity molecules cannot reach the surface by diffusion. In this case no effect of the impurities can be expected [Kas02].

Another imaginable reason could be the indirect effect of impurities on the nucleation by changing the solubility and thus supersaturation level σ which is a

thermodynamic effect. If σ is increased by the impurity, the nucleation rate J will also be increased (Eq. 2.6). Even small amounts of additives can cause strong changes in the solubility of a compound (see Chapter 3.2.1).

2.4 Crystal Growth

2.4.1 Theories on Crystal Growth

During the long term of research on crystallization processes a multitude of different theories and models for crystal growth were defined. Within this chapter an overview on the most important models will be given.

Crystal growth can be explained as a three-step process which includes the transport of solute molecules, so called growth units, from the bulk solution to the crystal surface (diffusion step), the integration of these units into the crystal lattice (reaction step) and the transfer of arising crystallization heat from the surface into the bulk. The slowest of these steps always is the limiting step of a crystallization process [Kru93].

Heat transfer: Often the third step can be neglected, as proven e.g. by Kruse [Kru93], but Matzuoka et al. [Mat91] gave a critical parameter for which negligence is not valid anymore. Especially, for heat transfer effects in aqueous solutions the third step could be neglected if the criteria $-\Delta H/(1-w_b) < 700$ J/g is fulfilled [Hay73]. The heat of solution $-\Delta H$ for ammonium sulfate is 6.57 kJ/mol (at 30 °C) [Ull05] what is 49.74 J/g. The solubility of ammonium sulfate at 20 °C is 754 g/L and therefore the concentration of ammonium sulfate in solution w_b is 43 %(w/w). The criteria $-\Delta H/(1-w_b) = 87.26$ J/g < 700 J/g is fulfilled and the heat transfer could be assumed to show no influence on the crystal growth.

Reaction (integration step): Dealing with the integration of growth units into an existing crystal surface one should have detailed information on the surface structure of the crystal. For an attaching growth unit there are three theoretical attachment sites on crystal surfaces which are schematically shown in Fig. 2.7 A. Taking energetic considerations into account the attachment at kinks is the most favorable followed by the attachment at ledges and the attachment at terraces of crystal surfaces (see e.g. [Mye02]). By applying the Periodic Bond Chain (PBC) which was introduced by Hartmann and Perdok [Har55] in 1955 it is possible to define three different types of crystal surfaces which are shown in Fig. 2.7 B.

A   **B**
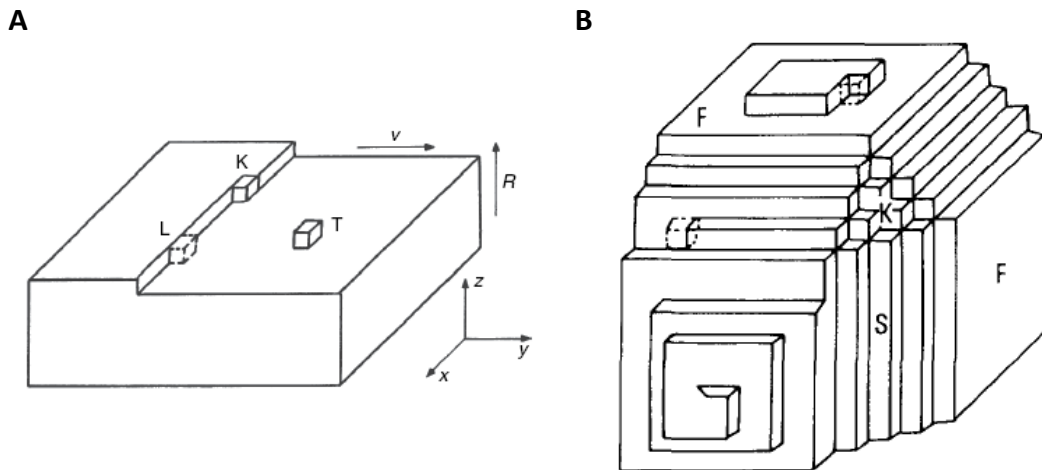
Fig.2.7: A: different attachment sites - kinks (K), ledges (L) and terraces (T) [San07]
B: Crystal including flat (F), stepped (S) and kinked (K) faces [Boi88]

The so called K faces contain only kinks which enable them to grow by direct incorporation of growth units. In contrary to the K faces the F faces contain no or nearly no kink sites (Fig. 2.8). These F faces show other growth mechanisms like two-dimensional surface nucleation. The S faces show e.g. spiral growth as shown in Fig. 2.9.
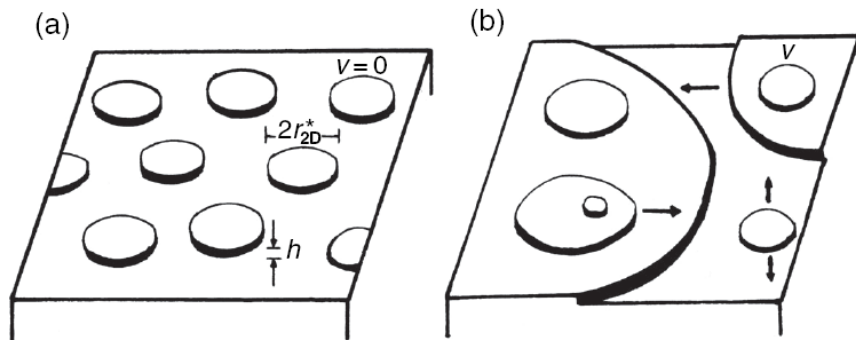
Fig. 2.8: 2D-nucleation models: polynuclear model (a) and multiple nucleation model or Birth and Spread model (B+S) (b) (taken from [San07b])

The 2D-nucleation on the crystal surface proceeds similar to the 3D-nucleation which was already described in Chapter 2.3. Once a nucleus reached a critical size $2r^*_{2D}$ it becomes stable and at its edges it offers kink sites where other growth units could be integrated easily. It has to be distinguished between the polynuclear model where many 2D-nuclei (with a monomolecular height) arises on the surface and on the other hand the B+S model which involves simultaneous birth and spread of nuclei also in a polynuclear height [San07b].

The B+S model could be described by the following face growth rate – supersaturation relationship (see Eq. 2.8).

$$v = A_2 \cdot \sigma^{\frac{5}{6}} \cdot e^{\frac{A_3}{\sigma}} \qquad (2.8)$$

A_2 and A_3 are constants related to the system, v is the face growth rate and σ describes the supersaturation within the system.
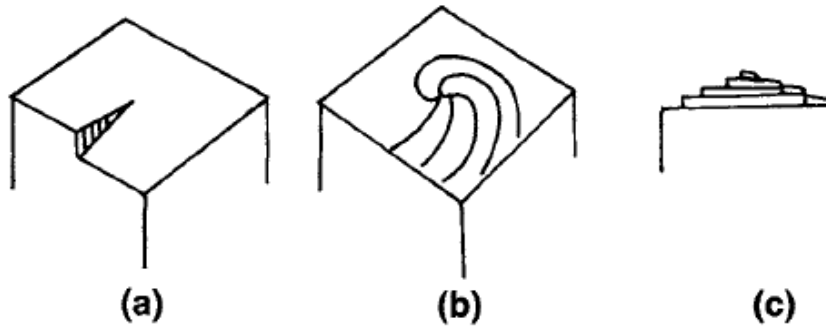
Fig 2.9: Crystal spiral growth originated from a screw dislocation [Mul93]

Based on a screw dislocation (Fig. 2.9 (a)) existing on the crystal surface kinks and ledges are provided for the integration of growth units. So theoretically the screw dislocation propagates along the crystal surface (Fig. 2.9 (b)) until the crystal surface becomes a spiral (Fig. 2.9 (c)) [Mul93].

In this context the Burton-Cabrera-Frank (BCF) – relationship has to be mentioned (see Eq. 2.9) [Mul93].

$$v = A_4 \cdot \sigma^2 \cdot \tanh\left(\frac{A_5}{\sigma}\right) \qquad (2.9)$$

A_4 and A_5 are constants which depend on temperature and step spacing, v is the crystal growth velocity and σ stands for the supersaturation of the system.

Transport (Diffusion step): If the diffusion of growth units from bulk to crystal surface is slower than surface diffusion and integration of growth units into the crystal lattice the process becomes diffusion controlled [San07b]. This happens especially if the viscosity of a system increases.

The diffusion layer model divides the overall growth rate R_G into the two steps diffusion and surface integration. Equations 2.10 to 2.12 describe the growth rates

and from Fig. 2.10 one can get an idea about the crystallization driving forces present during the crystallization process.
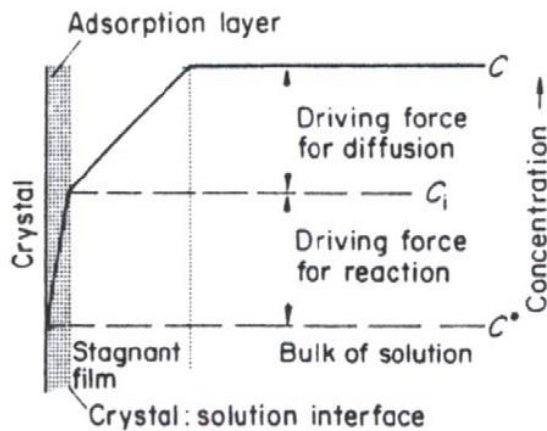
$$R_G = \frac{1}{A} \cdot \frac{dm}{dt} = k_d \cdot (c - c_i) \qquad (2.10)$$

$$R_G = \frac{1}{A} \cdot \frac{dm}{dt} = k_r \cdot (c_i - c^*)^r \qquad (2.11)$$

$$R_G = \frac{1}{A} \cdot \frac{dm}{dt} = K_G \cdot (c - c^*)^g \qquad (2.12)$$

Fig 2.10: Driving forces for crystallization from solution [Mul93]

Equation 2.10 stands for the diffusion term of the overall growth rate, while Eq. 2.11 represents the reaction term. If the value of k_d is large the growth process is surface integration (reaction) controlled and if k_r is large compared to k_d the growth is diffusion controlled.

2.4.2 Effect of Impurities on Crystal Growth

For industrial crystallization processes the influence of impurities on the crystal growth rate is an important parameter, because it can affect the purity, the yield, the crystal morphology and the efficiency of the process and therefore the economic potential of the process. So in the past many investigations concerning the effect of different impurities on crystal growth rates of several compounds were carried out and on the base of these results models were introduced.

One of the first models was given by Blisnakov [Bli57]. This model describes the mobile impurity adsorption at the crystal surface and could be mathematically explained by Equation 2.13:

$$v = v_0 - (v_0 - v_{\theta = 1}) \cdot \theta \qquad (2.13)$$

Another model was defined by Cabrera and Vermilyea [Cab58] with the so-called pinning mechanism. Pinning in this case means the immobile adsorption of impurity

molecules on the crystal surface which reduces the step velocity (see Equation 2.14) within the growing face.

$$v \; = \; v_0 \cdot \sqrt{1 - 2 \cdot \rho_c \cdot d^{0,5}} \qquad \qquad (2.14)$$

Later other models based on the original model of Cabrera and Vermilyea tried to imply the influence of impurity concentration on crystal surface and within the bulk solution. So the model of Davey and Mullin [Dav74] was introduced which uses adsorption isotherms to describe the amount of adsorbed impurity molecules (Equation 2.15) [Dav74].

$$v = v_0\big(1 - \theta_{eq}\big) \; = \; v_0 \left(1 - \frac{K \cdot c_i}{1 + K \cdot c_i}\right) \qquad (2.15)$$

In this case the Langmuir isotherm was used to describe the impurity adsorption Θ_{eq} at the crystal surface, but also other common isotherms like Freundlich isotherms and Tempkin isotherm could be used connected to this model [San07b].
Another parameter for the impurity effect was introduced by Kubota and Mullin [Kub95a] which is called the impurity effectiveness factor α. This model (Equation 2.16) contains two parameters, the fractional surface coverage Θ_{eq} on the one hand which stands for the quantity of adsorbed impurity and the impurity effectiveness factor α on the other hand which stands for the quality of effect caused by an impurity [Kub95a].

$$v \; = \; v_0 \, (1 - \alpha \cdot \theta_{eq}) \qquad \qquad (2.16)$$

At α = 0 there is no impurity effect on crystal growth. At α = 1 the growth rate becomes zero asymptotically with increasing impurity concentration and at α > 1 there is a very strong influence which leads to growth stoppage even at low impurity concentrations. These cases are clearly shown in Figure 2.11.
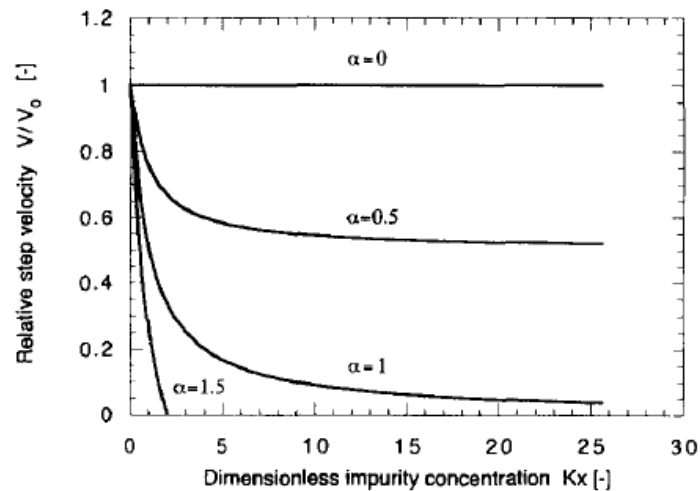
Fig. 2.11: Effect of impurity effectiveness factor on crystal growth rate [Kub95a]

Thereby the relative step velocity v/v_0 is the growth rate of the contaminated system normalized to the pure system and Kx is the dimensionless impurity concentration which means the adsorption constant multiplied with the impurity concentration.

2.5 Crystal Habit and Effect of Impurities

Especially, for industrial crystallization processes the morphology of the product is a very important parameter of quality. Often a product with a special habit is required to optimize the efficiency of the following process steps like centrifugation or filtration.

The crystal habit is the term for the external appearance of the crystal. As mentioned before (Chapter 2.1) the appearance of a crystal is influenced by both, the internal structure defined by the unit cell and the external factors like supersaturation level or concentration of impurities.

So crystals of one and the same crystal lattice can appear in different habits depending on the external conditions during growth (see Fig. 2.12).

(a) Tabular   (b) Prismatic   (c) Acicular
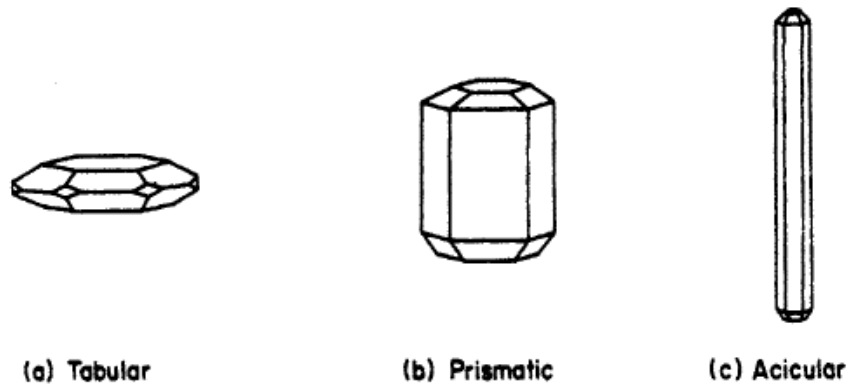
Fig. 2.12: Different crystal habits of hexagonal crystal system [Mul93]

In order to change or manipulate the habit of the product crystals the concentration of impurities should be controlled. In the literature the effect of different amounts of various impurities on the morphology of organic and inorganic compounds is described. One common example from a long list of effects of impurities on the crystal morphology is gypsum ($CaSO_4$). Gypsum crystallizes as long thin needles from pure solution, but with the addition of 50 ppm polymaleate spherical crystals are formed [VDL89].

But how can these changes in morphology be explained?

As explained in Chapter 2.1 a crystal is laterally confined by specific faces. These faces contain different molecules at their surfaces depending on the unit cell and thereby the surfaces gain different properties. As a consequence the impurities adsorb in various amounts on the different surfaces and cause a reduction in the growth velocity of specific faces. On this account the morphology of the crystal changes based on the mechanism explained by Fig. 2.13.
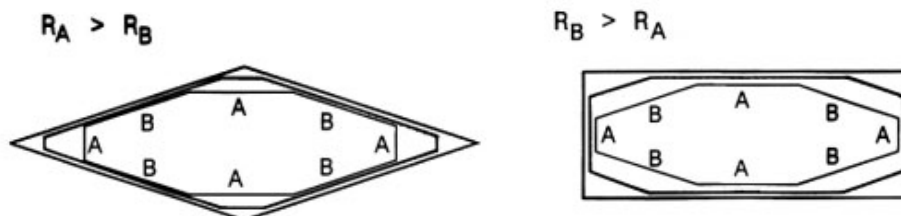
Fig. 2.13: Example for changes in morphology depending on growth velocities [Ulr04]

On the basis of one crystal morphology, during crystal growth the habit can change into other appearances depending on the ratio of the growth velocities of the faces existing on the crystal.

2.6 Metal Ions in Aqueous Solution

In order to understand the effect of metal ions on the crystallization parameters of an inorganic salt like ammonium sulfate one should know the basics of the chemistry of metal ions in aqueous solution.

If a salt like e.g. $NH_4Fe(SO_4)_2$ is dissolved in an aqueous solution, the arising Fe^{3+} ions will not appear as bare metal ions, but they will be coordinated by different kinds and numbers of ligands and form complexes. In aqueous solutions often water molecules are these ligands and therefore metal-aquo-complexes are formed. Normally di- and trivalent metal ions are surrounded by 4 to 6 water molecules and in Fig. 2.14 exemplary a hexa-aqua-iron complex is shown which means the Fe^{3+} ion is coordinated by six water molecules (simulated by GAUSSIAN Software – see Chapter 4.7.2).
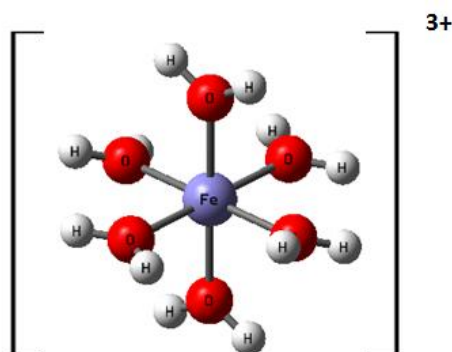
Fig. 2.14: Model of a hexaaqua-iron-complex (simulated by GAUSSIAN Software)

Metal-aquo-complexes are Bronsted acids which mean that they can act as proton donors. The mentioned hexa-aqua-iron-complex is a fairly strong acid with a pKa value of 2.19 [Ste07]. This is the reason for the acidic behavior of especially trivalent metal ions in aqueous solutions.

Depending on solution pH the metal-aquo-complexes undergo hydrolysis reactions as shown by the following equations:

$$[Me(H_2O)_6]^{3+} \rightleftarrows [Me(H_2O)_5OH]^{2+} + H^+ \qquad \text{pKa}_1 \qquad (2.17)$$
$$[Me(H_2O)_6]^{2+} \rightleftarrows [Me(H_2O)_4(OH)_2]^+ + H^+ \qquad \text{pKa}_2 \qquad (2.18)$$
$$[Me(H_2O)_6]^+ \rightleftarrows Me(OH)_3(s) + H^+ \qquad \text{pKa}_3 \qquad (2.19)$$
$$Me(OH)_3(s) \rightleftarrows [Me(H_2O)_3(OH)_4]^- + H^+ \qquad \text{pKa}_4 \qquad (2.20)$$
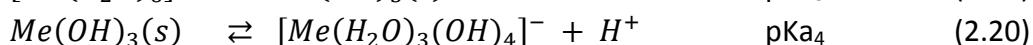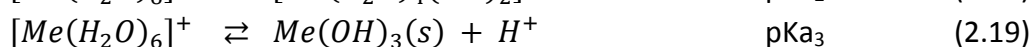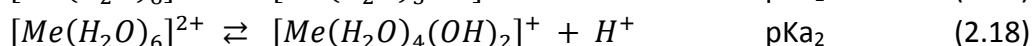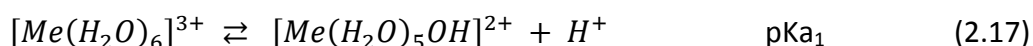
The reactions could be continued, but for the pH value ranges used within this work only the first three hydrolysis products are of interest.

Me stands for the metal ion like iron, aluminum or chromium. Table 2.1 shows the hydrolysis constants pKa_1, pKa_2 and pKa_3 taken from literature for the three trivalent ions observed within this work.

Table 2.1: Hydrolysis constants of trivalent metal ions in aqueous solutions

Metal	Nr.	pK_{a1}	pK_{a2}	pK_{a3}	I /M	T /°C	p /bar	Reference
Fe^{3+}	1	**2.19±0.02**	**5.76±0.06**	**14,30±0.32**	0	25	1	[Ste07]
	2	2.19	5.67±0.1	13.1	0	25	-	[Bae76]
	3	2.18±0.01			-			[Byr00]
Al^{3+}	1	**4.97±0.02**	**8.7±0.3**	**15.0±0.3**	0	25	-	[Bae76]
	2	4.99	10.13	-	-	25		[May79]
	3	5.33	10.91	-	-	25		[Bro85]
Cr^{3+}	1	-0.49	5.78	9.35	0	-	-	[Rai87]
	2	**3.52±0.02**	**9.3±0.87**	**17.18±0.16**	-	-	-	[Lop10]

As can be seen from Table 2.1 the pK_a values vary between the listed references. One possible reason could be a different determination technique like potentiometric or spectrophotometric measurements. Here not only the method of determination, but also other parameters like temperature, pressure or ionic strength could have a strong effect on the hydrolysis constants as shown by Fig. 2.15 right and left exemplary for the pKa_1 values of Fe^{3+} [Byr00].
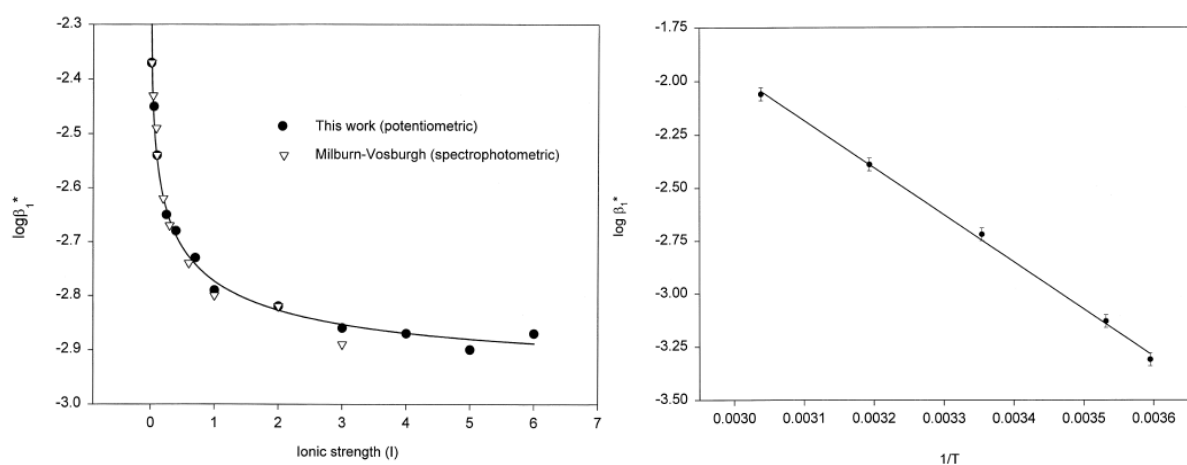
Fig. 2.15: log β_1^* (= -pK_a) as a function of ionic strength (T = 25 °C) (left) and of temperature (I = 0.72 M $NaClO_4$) (right) [Byr00]

Based on these hydrolysis constants the distribution of the different hydrolysis products depending on the pH value of the solution can be calculated by the help of different computer-based software. Fig. 2.16 shows the results for a distribution of hydrolysis products taken from Stefannson et al. [Ste07].
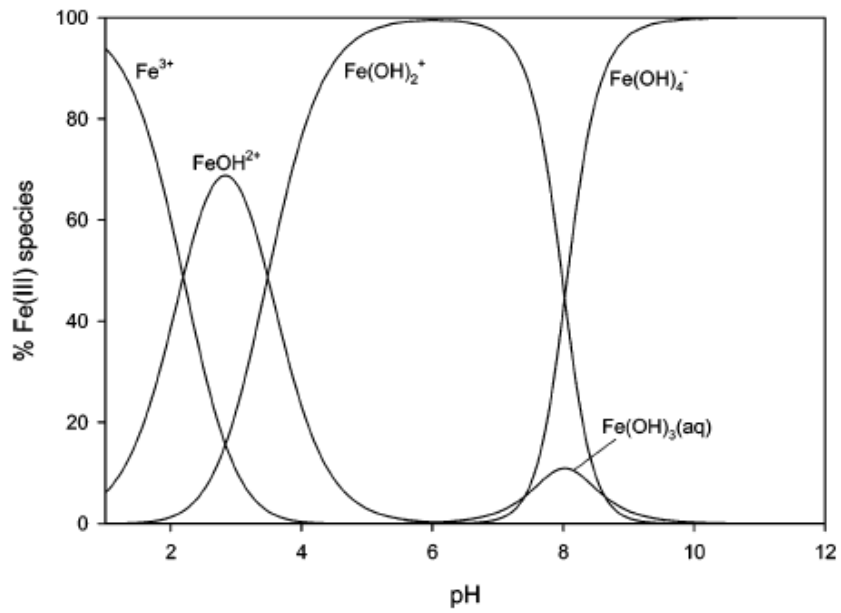
Fig. 2.16: Distribution of hydrolysis products of Fe^{3+} in aqueous solution (I = 0) [Ste07]

For the simulation of distributions of hydrolysis products for all the observed metals, within this work the software HYSS is used which is described more detailed in Chapter 4.7.1.

As shown before, the chemistry of metal ions in aqueous solution can become arbitrary complicated, especially, if all possible complexes would be taken into consideration.

3. Aim of the Work

The previous Chapter 2 showed the actual state of the art concerning the crystallization of inorganic compounds. In recent years a huge number of papers, books and reviews were published concerning the crystallization of inorganic compounds and especially ammonium sulfate as a model substance (e.g. [Mul70], [Lar73], [Tav92], [Kit92], [Rau00]). The well-disposed reader would now think why there is another PhD thesis on the crystallization of ammonium sulfate. The simple answer is that in comparison to other common separation techniques like distillation, extraction or adsorption the crystallization process is a little bit more like a "black box" due to phenomena like nucleation (primary and secondary), attrition, agglomeration, polymorphism, growth rate dispersion and the complex effects caused by impurities. There are no reliable simulation tools for a complete crystallization process and up to now in industry the experience in connection with the own process is the most important foundation of a successful crystallization and a high quality product.

This results in the urgent need for a deeper understanding in thermodynamics and kinetics of nucleation and crystal growth processes, especially, with respect to the effect of impurities. Figure 3.1 shows the complex interrelations between an impurity and its possible effects on an industrial crystallization process and the final product.

Fig. 3.1: Effects of impurities and their network (taken and modified from [AlS96])

From this overview the main aims of this work can be derived. They can be divided into two different sections. On the one hand there is some kind of *fundamental research* concerning the mode of action of impurity adsorption and the effects caused by changing the pH value. On the other hand there is an *industrial*

crystallization process affected by impurities, where there is actually no clear strategy how to deal with this in literature.

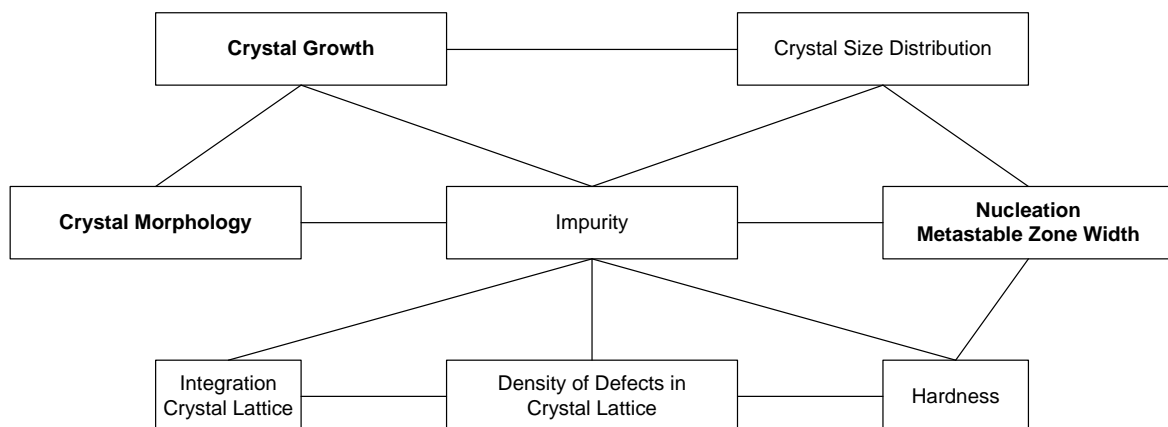In general it can be stated that the effects on crystallization caused by different impurities is not completely understood with respect to the complexity of the topic although there are many different theories and models as explained in the previous Chapter.

Within this work a further step in order to gain a deeper understanding in the mechanisms should be performed which stand behind the impurity effects:

- Where is the influence of the pH value based on?
- Why different impurities cause different effects – main influencing parameter?
- Which impurity species in aqueous solution are responsible for what effects?
- Can the observed effects be referred to impurity adsorption?
- Is molecular modeling an appropriate tool to explain the effects of impurities on the crystallization of an inorganic compound like ammonium sulfate?

Answering these questions on the effects of several impurities in the case study of crystallization of ammonium sulfate is a contribution to a general understanding in terms of the mechanisms of impurity impact. If once the problem is completely understood, the knowledge can be used to optimize existing industrial crystallization processes regarding the undesired effect of impurities. Up to date it is essential, at least, to know about the effects caused by certain amounts of impurities and to define critical impurity concentrations which allow a stable crystallization process and desired product quality.

In the available literature no recommendations can be found in terms of critical impurity concentrations regarding an industrial crystallization process of ammonium sulfate. For the industrial crystallization process an overview on the effects of commonly appearing impurities on the most important crystallization parameters (mentioned in Fig. 3.1) has to be performed since up to now there is no satisfying overview available in the literature. Based on the results of the fundamental studies, operational windows of critical impurity concentrations have to be defined which, once exceeded, lead to lower productivity or an undesired product quality.

Furthermore, the applicability of oxalic acid to reduce the effects of impurities has to be proved and discussed since there is a lack of information obtainable from literature.

4. Materials and Methods

4.1 Chemicals

Ammonium sulfate as the main compound of this work was provided by SKW Piesteritz. It has a purity of 99.9 % and Table 4.1 shows the impurities present in the ammonium sulfate (the analysis was done by SKW Piesteritz).

Tab. 4.1: Overview over the impurities present in ammonium sulfate from SKW Piesteritz

impurity	conc. [ppm]	impurity	conc. [ppm]	impurity	conc. [ppm]
Aluminium	0.12	Cobalt	< 0.05	Silicium	< 0.05
Lead	0.1	Cupper	0.06	Thallium	< 0.05
Cadmium	< 0.05	Magnesium	< 0.05	Titanium	< 0.05
Calcium	0.54	Mangan	0.21	Vanadium	< 0.05
Chromium	0.1	Molybdenum	0.09	Zinc	< 0.05
Iron	18	Sodium	< 0.05		
Potassium	0.36	Nickel	0.17		

As can be seen from Table 4.1 the used ammonium sulfate already contains these impurities which should be observed as additives during this study. Thus for all experiments a blank for the "pure" solution was made and the results of the contaminated solutions were normalized to this value.

Table 4.2 gives an overview on the most important properties of ammonium sulfate.

Table 4.2: Important properties of ammonium sulfate

Chemical formula	$(NH_4)_2SO_4$
CAS-Number	7783-20-2
Molar Mass	132.14 $gmol^{-1}$ [Ull05]
Heat capacity	1.423 $Jg^{-1}K^{-1}$ [Ull05]
Density	1.77 gcm^{-3} (at 20 °C) [GES10]
Solubility	754 gL^{-1} (at 20 °C) [GES10]
Enthalpy of solution (at 30 °C)	6.57 $kJmol^{-1}$ [Ull05]
Critical humidity	80 % [Xu98]

The impurities (metal ions) were added as their sulfate salts. This has the advantage that no new species of impurity like e.g. Cl^- are added to the solution which could cause changes in the crystallization parameters of ammonium sulfate. The disadvantage is the addition of further sulfate ions which causes only a small shift in the solubility product. The adjustment of the pH value was realized by sulfuric acid in

terms of lowering the pH value and by ammonium hydroxide in terms of raising the pH value. This results in a further addition of ammonium ions or sulfate ions.

An overview about all used chemicals can be seen in Table 4.3.

Table 4.3: Overview about the used chemicals

Chemical	Formula	Concentration	Producer	Molar Mass [gmol^{-1}]
Sulfuric acid	H_2SO_4	95-97 %	Merck	
Ammonium hydroxide	NH_4OH	25 %	Fluka	
Ammonium iron sulfate dodecahydrate	$NH_4Fe(SO_4)_2$ *12 H_2O	> 99.7 %	VWR	482.15
Aluminium sulfate hexadecahydrate	$Al_2(SO_4)_3$ *16 H_2O	> 95 %	Roth	630.39
Chromium sulfate hydrate	$Cr_2(SO_4)_3$*H_2O	-	Alfa Aesar	103.99
Iron sulfate heptahydrate	$FeSO_4$*$7H_2O$	> 99.5 %	Merck	278.02
Zinc sulfate heptahydrate	$ZnSO_4$*$7H_2O$	> 99.5 %	Merck	287.54
Potassium sulfate	K_2SO_4	> 99 %	Roth	174.26
Sodium sulfate	$NaSO_4$	> 99 %	Roth	142.04
Oxalic acid dihydrate	$H_2C_2O_4$*$2H_2O$	>99.5 %	Merck	126.03

The mass of salt (e.g. ammonium iron sulfate) which is needed to adjust a specific concentration of metal ions (e.g. Fe^{3+}) in the solution was calculated by Eq. 4.1.

$$m_i[mg] = c_i\ [ppm] \cdot m_{tot}[kg] \cdot \frac{M_{i_{tot}}[\frac{g}{mol}]}{z \cdot M_i[\frac{g}{mol}]}$$ (4.1)

Thereby m_i is the wanted mass of the salt, c_i is the desired concentration of metal ions in solution, m_{tot} is the total mass of the solution, $M_{i,tot}$ is the molar mass of the salt and M_i is the molar mass of the metal ion. The stoichiometric number of metal ions within the formula of the salt is characterized by z.

4.2 Microscope Cell

The microscope cell is an useful and common tool to observe the effect of additives or impurities on the growth rate of specific crystal faces of a single crystal. Furthermore, any changes in crystal morphology could be observed by the help of the microscope cell. Figure 4.1 shows the schematic setup of the microscope cell used within this study.
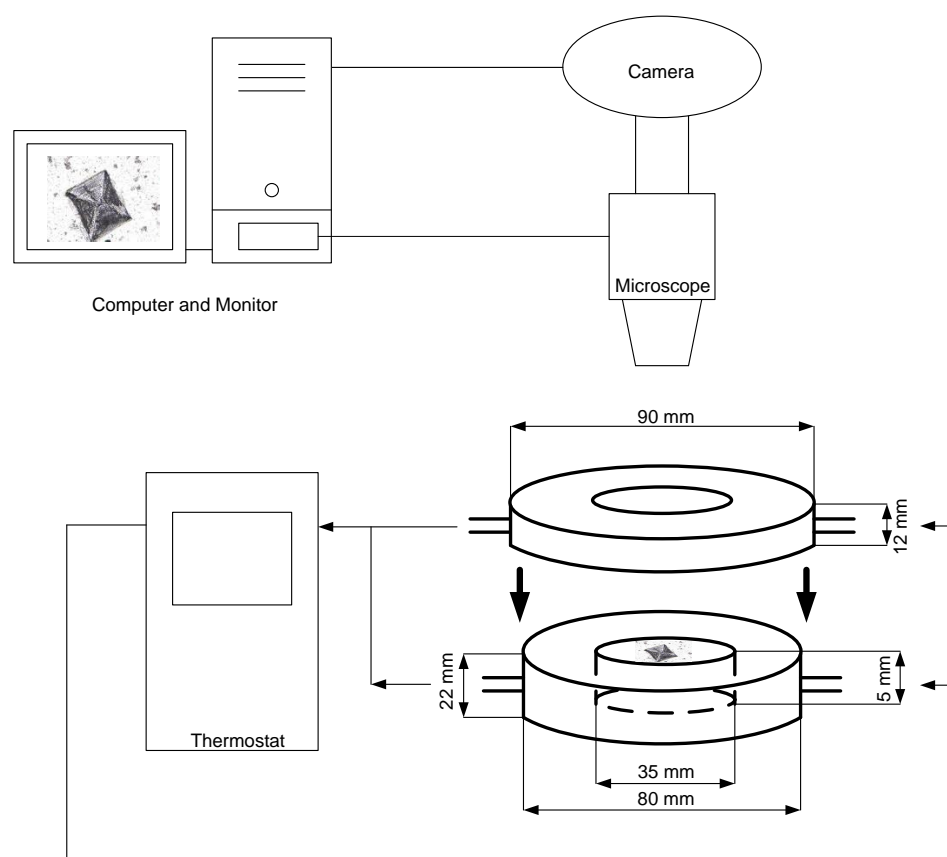
Fig. 4.1: The scheme of the microscope cell setup including detailed design of the cell

The supersaturated mother liquor is located inside the double-wall microscope cell and contains a few seed crystals. Via isolated tubes the cell is connected to a thermostat (Julabo ME) which controls the temperature of the solution in the cell and thus supersaturation of the solution. The growth can be recorded by the help of a microscope (BH2, Olympus) connected to a digital camera (Altra, Soft Imaging). In defined time intervals (5 min) pictures were taken of the crystals which could be analyzed and measured afterwards by the help of the computer program "Analysis".

Further information concerning the use of the microscope cell could be taken from literature (see e.g. ([Nie95] and [Gou09]).

One major disadvantage of a microscope cell is that only stagnant solutions could be observed during growth which sometimes leads to a desupersaturated zone around the crystals, especially, if the diffusion is hindered e.g. by a high viscosity of the mother liquor.

The results concerning those microscope cell experiments could be found in Chapter 5.2.

4.3 Fluidized Bed

Another major disadvantage of the microscope cell which was described in Chapter 4.2 is the small number of crystals that could be analyzed in a reasonable time. For several years the phenomenon called growth rate dispersion is well-known which describes the different growth behavior of crystals under the same growth conditions like supersaturation, temperature and concentration of impurities. Further information concerning growth rate dispersion can be found in literature (see e.g. [Ulr89], [Ulr90]).

Fig. 4.2: Scheme of the fluidized bed and detailed setup of the measurement cell

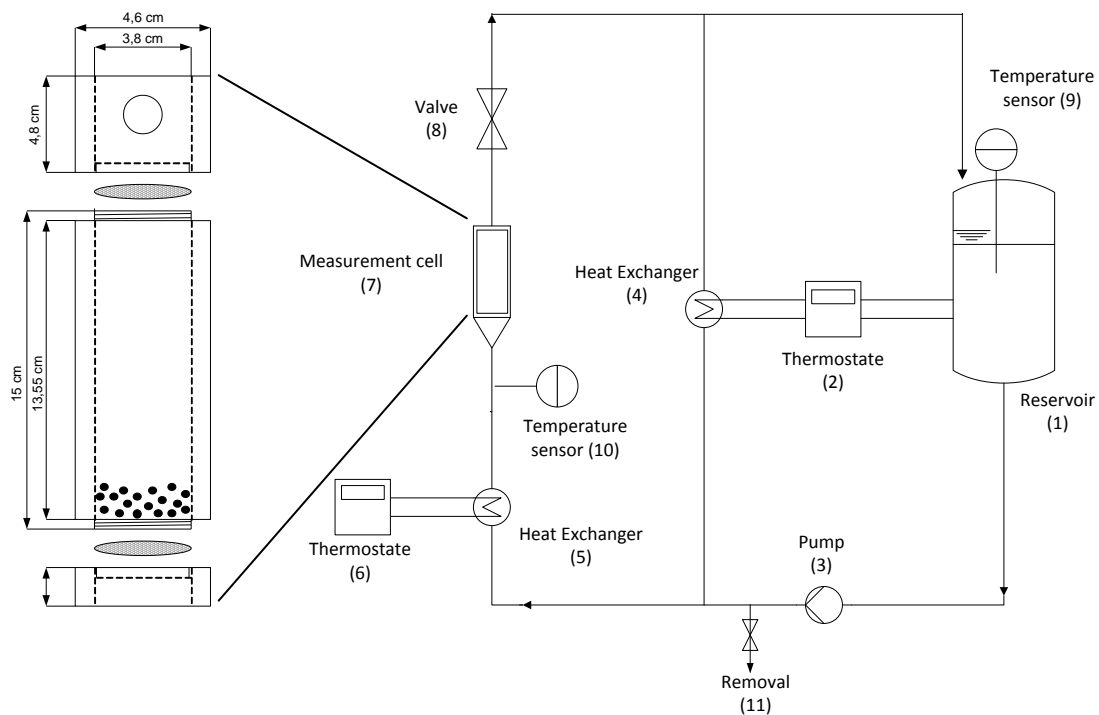On this account another technique was established to measure the growth rate of many crystals within one experiment – the fluidized bed. Its general setup is shown in Figure 4.2 as described and used already before as by e.g. Stepanski [Ste90], Kruse [Kru93], Lühmann [Lüh96],] Al-Jibbouri [AlJ02] and Al-Atia [AlA08].

The stock solution (T_{sol}=30 °C) is stored at the reservoir (1) with a volume of 15 L which is temperature controlled by a thermostat (2) (Julabo HC). A pump (3) provides the circulation of the stock solution into two loops. The first is the *temperature control loop* which contains a heat exchanger (4) connected to a thermostat (2). The temperature control loop sustains a temperature of >30 °C to avoid undesired nucleation and to dissolve small attrition pieces of crystals coming from the measurement cell. The second loop is called *saturation loop* and consists of a heat exchanger (5) connected to another thermostat (6) (Julabo MV) which cools the stock solution until reaching a desired supersaturation level. Afterwards the supersaturated stock solution enters the measurement cell (7) and gets desupersaturated by the growth of the seed crystals. After passing a valve (8) which is used to adjust a specific flow rate, the stock solution returns to the reservoir. The temperature is controlled at two positions of the process by Pt 100 sensors. The first temperature measurement (9) is located in the reservoir and is needed to guarantee a solution temperature above saturation temperature (here 30 °C). Another temperature measurement (10) is needed to control the supersaturation at the measurement cell.

The measurement cell is the core piece of the plant and a detailed scheme is shown in Fig. 4.2 left side. It is a cylindrical cell with a top and a bottom part which can be connected to the main part including two sieves (here mesh width 400 µm).

The stock solution with a concentration of ammonium sulfate which corresponds to a saturation of 30 °C, with or without impurities and with a desired pH value, was prepared externaly. Before filling the stock solution into the reservoir, the stock solution was filtered (particle filter 413, VWR) to remove remaining crystals. To reach the exact saturation at 30 °C, crystals were given to the measurement cell and the system could reach the equilibrium (saturation at 30 °C).

For every measurement 3 g of seed crystals (here sieve fraction 560-710 µm) were given into the measurement cell. After placing the cell in the fluidized bed equipment, the pump was turned on and the measurement time started. Each experiment takes 20 min or 10 min in case of high undersaturations to avoid the

crystals dissolving to a size below 400 µm. Afterwards the crystals were removed from the cell by washing with saturated ammonium sulfate solution into a filter funnel (particle filter 413, VWR). The filter paper then was dried overnight at 50 °C in an oven and the dried crystals were weight. From the mass difference between start and end of the measurement, the averaged growth rate could be calculated by Eq. 4.2.

$$G = \frac{L_1}{t} \left[\left(\frac{m_{end}}{m_{start}} \right)^{\frac{1}{3}} - 1 \right] \tag{4.2}$$

m_{start} is the crystal mass at the beginning of the experiment and m_{end} is the mass of the dried crystals after growth or dissolution. L_1 is the arithmetic average of the sieve fraction and t is the duration of the experiment. Detailed information for the derivation of Eq. 4.2 can be taken from literature (e.g. [Ste90] and [vBr92]).

The mass of the crystals after the drying process contains an error caused by adherent mother liquor or washing solution after the washing process and crystallization during the drying. Therefore a correction factor was introduced which was subtracted from the mass of the end m_{end}. This correction factor was determined by washing and drying 3 g of seed crystals (560-710 µm) and controlling the change in mass (average of 10 tests).

For each analyzed combination of solution properties (super- or undersaturation, concentration of impurities) one saturation test was made which means a run at 30 °C and after adjusting the correct super- or understauration three repetitions were carried out.

The results of the fluidized bed experiments are shown and discussed in Chapter 5.3.

4.4 Ultrasonic Speed Measurements

Within this work an ultrasonic speed measurement device was used to observe the effect of impurities on the metastable zone width (see Chapter 2.2.2) of ammonium sulfate. In former times the MZW was observed by the visibility method described e.g. by Mullin [Mul93]. This method had big disadvantages, namely that the observer has to monitor the experiment in order to detect and note the nucleation temperature and time of visible nucleation. In recent years different other methods were established to observe the MZW of various compounds. An example is the FBRM (Focused Beam Reflectance Method) technology which uses a light beam to detect nucleation and solubility [Bar02], other techniques observe changes in density or conductivity of the mother solution caused by nucleation (changes in concentration). The ultrasonic technology uses changes in the ultrasonic velocity induced by changes in concentration of the ammonium sulfate in solution. Fig. 4.3 shows the principle of the ultrasonic probe which is based on simple time-measuring.
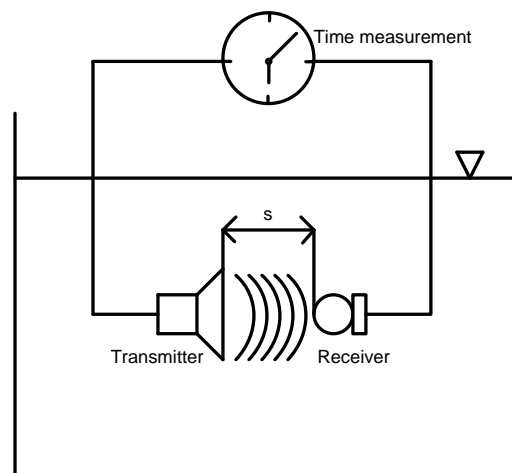
Fig. 4.3: Ultrasonic measuring principle [Sen10]

An ultrasonic signal is emitted by a piezo transmitter in periodic intervals. With a characteristic velocity the ultrasonic signal then passes the media and is detected by a receiver. From the duration of the passage and the known distance between transmitter and receiver the ultrasonic velocity could be calculated.

In liquids the ultrasonic velocity v_{US} is a temperature and concentration dependent physical property. Therefore it depends on the density ρ and the adiabatic compressibility β_{ad}. A very simple relationship was given by Urick [Uri48] and is shown in Eq. 4.3.

$$v_{US} = \frac{1}{\sqrt{\beta_{ad} \cdot \rho}} \qquad\qquad (4.3)$$

The precision of the system for ultrasonic velocity and temperature is ±0.01 m/s and ±0.01 °C, respectively.

Figure 4.4 shows the scheme of the setup used here for the determination of the MZW.
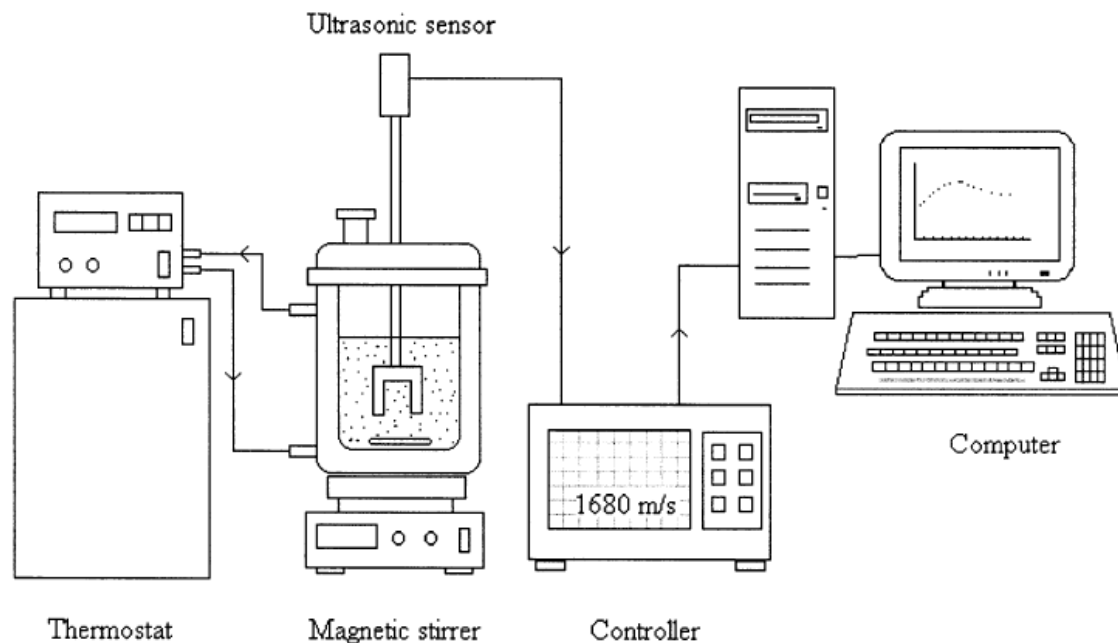
Fig. 4.4: Experimental setup of ultrasonic measurement device [Tit03]

A double-wall beaker with a volume of 300 mL (diameter 58 mm) was temperature-controlled by a thermostat. Cooling and heating rates were adjusted to 5 K/h. Stirring was realized by a magnetic stirrer (diameter 7 mm and length 30 mm) with a rotation speed of 500 rpm in each experiment. The ultrasonic probe was immersed into the AS solution and the signal was processed by a controller which is connected to a computer. The ultrasonic speed probe gives information on ultrasonic speed and temperature of the medium. Further information for this experimental setup could be achieved from literature [Tit02, Tit03].

The solution which should be observed concerning nucleation temperature and solubility and therefore MZW was prepared externally. A specific ammonium sulfate concentration was realized by adding appropriate amounts of ammonium sulfate to 100 g of distilled water, impurities were added based on the calculations of Eq. 4.1 and the pH value was set to a desired value by adding sulfuric acid or ammonium hydroxide, respectively.

After preparation the solution was transferred to the ultrasonic setup and the temperature profile was started. Before cooling down, the temperature of the solution was kept constant for 30 minutes in order to reach an equilibrium state for the metal ions in the solution (c.f. Chapter 5.1).

An example for a temperature profile is shown in Fig. 4.5 on the left side and the related results for nucleation and solubility are shown on the right side.
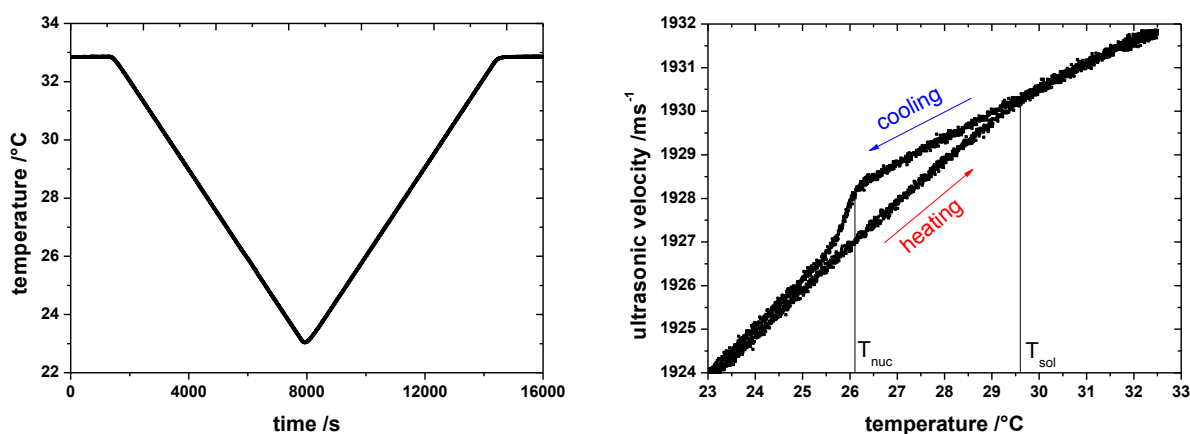
Fig. 4.5: Typical temperature profile for ultrasonic measurement (left) and the plot of the result including the nucleation temperature (T_{nuc}) and solubility temperature (T_{sol}) (right)

From this ultrasonic velocity – temperature – diagram the nucleation temperature T_{nuc} can be obtained which is located at the inflexion point of the cooling curve and the solubility temperature T_{sol} which is located at the intersection of the cooling and the heating curve. For every set of parameters (pH value, concentration of ammonium sulfate and impurity) at least three measurements were carried out and the average was taken for the interpretation of the experimental data which are shown in Chapter 5.4.

4.5 Batch Crystallization

Cooling batch crystallization was used to observe the effect of impurities on the morphology of ammonium sulfate crystals. A specific setup was designed which is shown in Fig. 4.6.
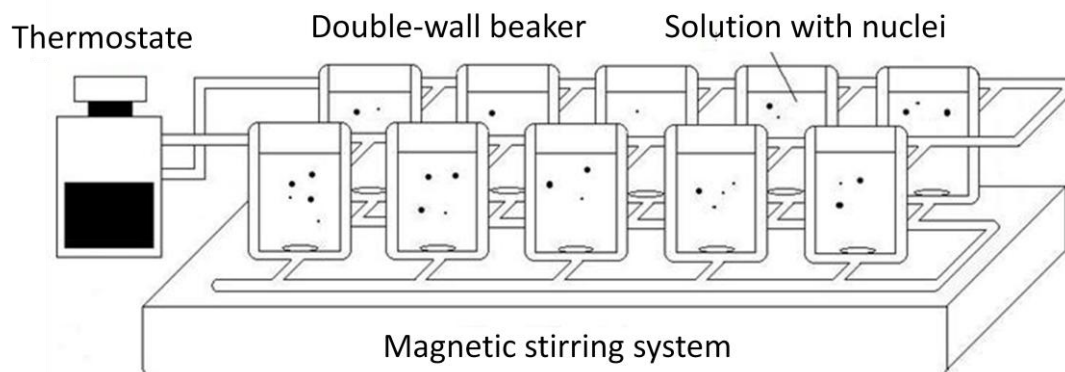
Fig. 4.6: Experimental setup for the batch crystallization

Ten double-wall beakers were connected to each other and could be temperature controlled by the help of one thermostat (Julabo MH). So it was possible to change several parameters like impurity concentration or pH value and observe their influence within only a few experiments. The solutions were stirred with magnetic stirrers (length 14 mm and diameter 6 mm) with a rotational speed of 400 rpm. A cooling profile was defined (cooling rate 5 K/h) to achieve supersaturation until the first nuclei appear in the solution. After a further time period of 20 min the crystals grow to a size which is investigable by optical microscopy. The results of these morphology experiments can be found in Chapter 5.6.

Also the integration experiments were performed with the batch crystallization setup. Therefore, the solutions were prepared externally with the desired concentration of impurities and pH values and an ammonium sulfate concentration of 800 gL^{-1}. After addition of the solutions into the small beakers a temperature profile was started (10 Kh^{-1}) until the temperature reached 2.5 °C. The solution was kept thereafter for two more hours at this temperature to achieve a sufficient amount of solids. After a solid- liquid separation via filtration (particle filter 413, VWR) the solid crystals and the mother liquor were observed by ICP-OES in terms of impurity concentration to examine the amount of impurities incorporated into the crystal lattice.

4.6 Metal ion concentration –ICP

The ICP-OES experiments were performed in cooperation with SKW Piesteritz who analyzed the samples by using a Cirros CCD (SPECTRO Analytic Instruments GmbH, Kleve). ICP-OES stands for "Inductively Coupled Plasma - Optical Emission Spectrometry" which is a very sensitive analyzing tool especially for metal ions in solution and therefore a very useful tool to observe the integration of impurity molecules into the lattice.

In both, industry and research, the ICP-OES became a standard analyzing tool and will not be explained further here. For detailed information concerning method, functionality or setup it is advised to go to the relevant literature (e.g. [Nöl02]).

4.7 Computer based Simulations

4.7.1 Hyss

Calculating the distribution of species in chemical equilibrium is an important feature for a wide variety of applications. For this work it is important to gain some information concerning complex formation of metal ions in aqueous solution. Certain computer-based programs like RAMESES [Leu89] or HYPHEN [Gan96] were established in recent years and for this work the program HySS (Hyperquad Simulation and Speciation) was chosen, which was developed based on the program HYPHEN [Ald99]. It can be used to simulate the distribution of metal-aquo-complexes depending on the pH value of the solution by using the hydrolysis constants taken from literature (see also Chapter 3.6). Detailed information concerning the structure of the used program can be taken from literature [Ald99] and the program can be downloaded as free ware from internet [Hys10].

4.7.2 Molecular Modeling

In recent years an increasing number of publications concerning molecular modeling of organic compounds can be found (see e.g. [Lu03], [Fie07], [Yür10]). Up to now, however, it is still impossible to predict the effect of impurities on the growth or crystal shape of inorganic crystal systems. This work does not claim to improve existing ideas of molecular modeling of inorganic compounds, but some basics of molecular modeling are already useful tools to help to understand and describe

observed phenomena. Two commercially available computer programs for molecular modeling were used within the scope of this work. The first program is GAUSSIAN and the second is SERIUS[2].

5. Results

5.1 Interactions Impurity – pH Value

As already explained in Chapter 2.6, the pH value of a solution is changed by adding metal ions like Fe^{3+} or Cr^{3+} caused by the hydrolysis reactions of the metal-aquo-complexes. For a first understanding in terms of the pH shift concerning magnitude of the change and the kinetics of the hydrolysis reactions, Figure 5.1 A shows the pH value of the solution over time. In defined time intervals defined concentrations of Fe^{3+} ions were added to the solution and the pH was measured by a pH probe (Dulcotest/ProMinent) connected to an Almemo. It can be clearly seen, that the hydrolysis reactions proceeds really fast and the equilibrium state is reached within the first 30 minutes. These could be observed for all of the investigated impurities. Based on these results, for all performed experiments the solution was kept 30 min at a constant temperature before starting to reach an equilibrium state of the complexes in solution.
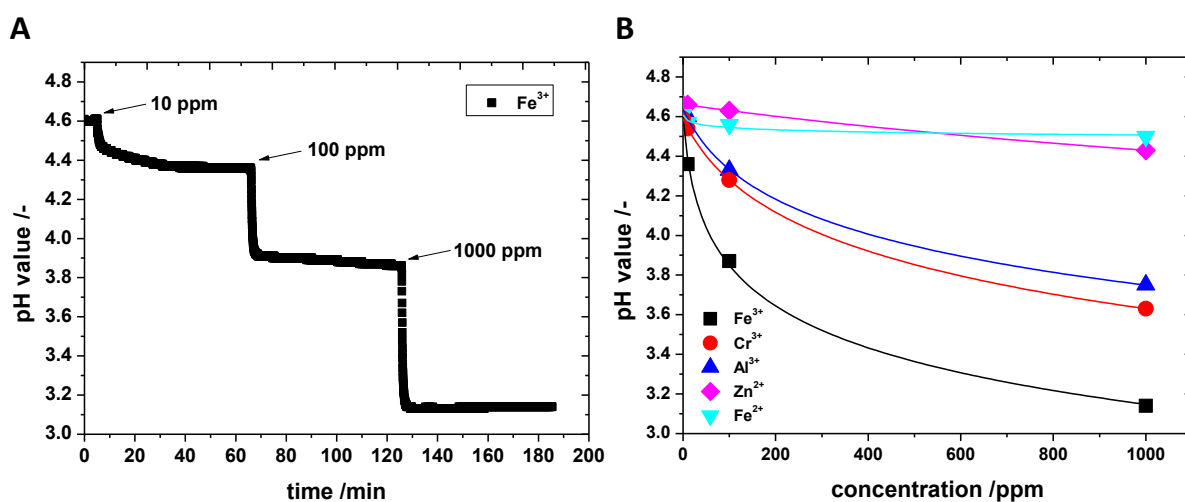
Fig. 5.1: A) Kinetics of pH shift caused by the addition of different concentrations of Fe^{3+}
B) Effects of different impurities on the pH value of AS solutions (c_{AS}=760 gL^{-1})

Figure 5.1 B shows the effect of different impurities on the solution pH value. The solution pH value of a pure ammonium sulfate solution is around 4.6. It can be clearly seen, that Fe^{3+} has the strongest impact on the solution pH since the pH decreases to 3.1 after adding 1000 ppm. The effect of Cr^{3+} and Al^{3+} is similar, because 1000 ppm reduces the pH value to 3.6 and 3.75, respectively. Only a small effect could be detected in case of the divalent metal ions Zn^{2+} and Fe^{2+} which reduces the solution pH to 4.4 and 4.5, respectively. These results are in agreement with the ratios of the

hydrolysis constants of the different metal ions (see Chapter 2.6). The monovalent metal ions Na^+ and K^+ do not cause any change in the pH value of an ammonium sulfate solutions even up to concentrations of 1000 ppm.

5.2 Morphology – Microscopy Cell

As already explained in Chapter 4.2 the microscope cell is one possible experimental method to detect changes in crystal morphology caused by the addition of different additives/impurities. To give a first idea about the results of the microscope cell, Fig. 5.2 shows the growth of a crystal in pure ammonium sulfate solution at pH 4 at a supersaturation level of 2.5 K. Thereby for all the pictures the length and width over time was analyzed by the program Analysis and based on this growth velocities could be calculated. These then could be combined to the ratio between growth into the length G_L and growth into the width G_W.
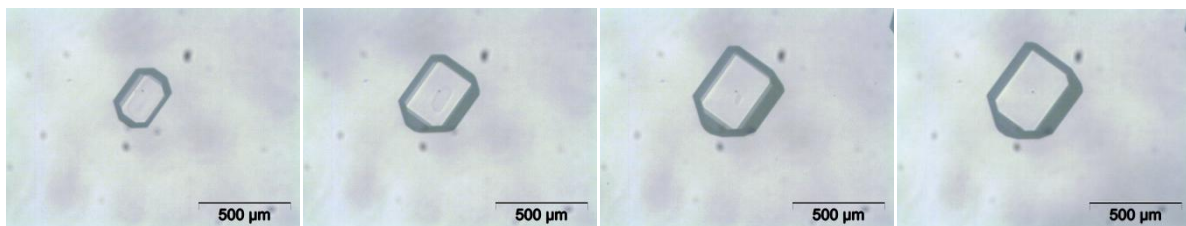
Fig. 5.2: Crystal growth of ammonium sulfate in the microscopy cell (0, 20, 40 and 60 min)

A big disadvantage of the used microscopy cell is the stagnant solution. It is not possible to stir the solution within the cell because the unfixed crystal would change its position and no crystal images could be taken over time. Therefore the solution surrounding the crystal will get desupersaturated during crystal growth, if the diffusion is too slow to transport growth units from the bulk to the crystal surface. This phenomenon is shown exemplary in Fig. 5.3 (left) which shows the growth of three crystals into length direction under different supersaturation levels (pH 4 and pure ammonium sulfate solution). For 1 K supersaturation the curve progression is linear over the complete time range of 60 min. For higher supersaturations like 1.5 or 3 K the slope of the curves decrease with time and so only the first linear parts could be used to calculate the growth rate.
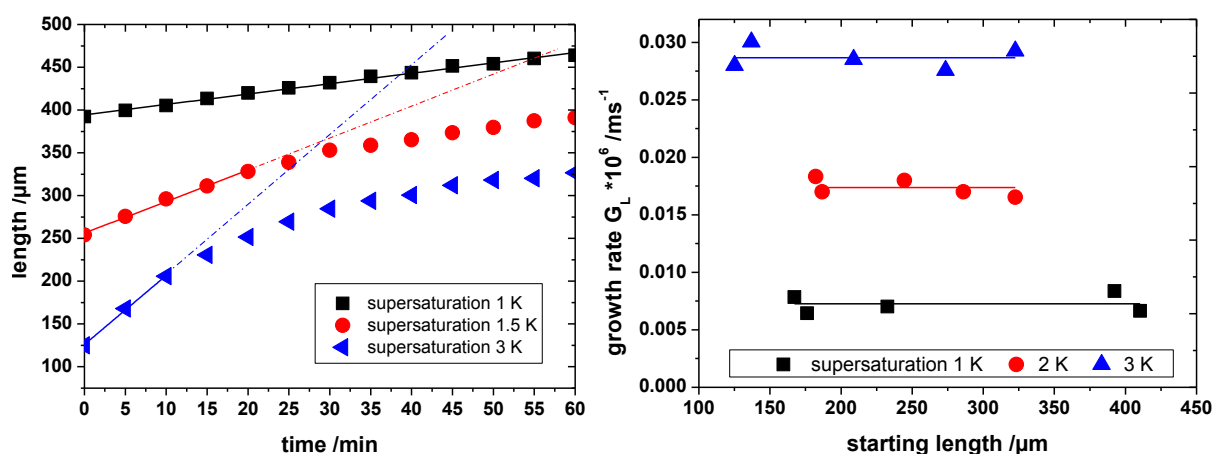
Fig. 5.3: Desupersaturation effects at the crystal-liquid-interface caused by crystal growth (left) and the effect of starting size of the crystals on the crystal growth rate (right)

Figure 5.3 (right) shows that the initial sizes of the seed crystals do not have any influence on the growth rate of the crystals.

However, with the help of the microscopy cell several impurity concentrations were observed and Fig. 5.4 shows the results for the effect of Fe^{3+} on the growth of ammonium sulfate crystals into length and width direction. At least five crystals were observed and the average was taken to illustrate the data.
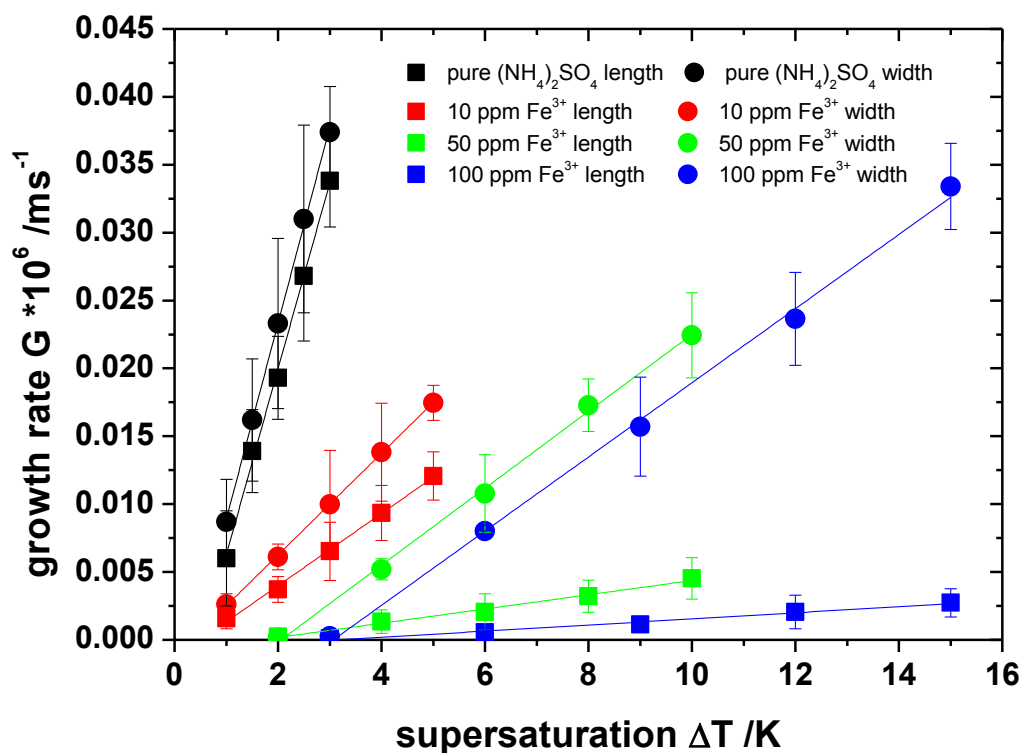
Fig. 5.4: Growth rates into length and width direction depending on supersaturation level and concentration of Fe^{3+} at pH 4

It can be concluded that Fe^{3+} has a strong effect on the growth rates of ammonium sulfate crystals, both into length and into width direction, even at low concentrations of 10 ppm. This is absolutely in accord with the results of fluidized bed results, which are summarized in Chapter 5.3.

But the key information of Fig. 5.4 is that Fe^{3+} affects the growth rate of ammonium sulfate crystals into length and into width in different ways. While in the pure solution G_L and G_W are nearly parallel curves over the observed range of supersaturation, with increasing Fe^{3+} concentration the angle between both curves increases. This means the crystal morphology changes from compact cubic crystals to needle-like crystals. In Chapter 5.5 some vivid pictures of crystals grown under different Fe^{3+} concentration will emphasize these results. 50 ppm Fe^{3+} nearly stops the growth of the crystals into the width direction (see Fig. 5.4) even at high supersaturation levels.

There are two reasons for the different ranges of supersaturation used during these experiments. The first is the small metastable zone width of pure ammonium sulfate solutions which does not allow adjusting higher supersaturation without inducing primary nucleation along with fast desupersaturation within the microscope cell. The metastable zone width is increased by impurities (e.g. Fe^{3+}) as can be seen in Chapter 5.4 which opens the possibility to set higher supersaturations and therefore reach faster growth rates.

After calculating the ratio between growth into length G_L and width G_W over the complete range of supersaturation a comparison between the different metal ions according to their effect on the morphology can be done (see Fig. 5.5).

The clear trend of the effect of Fe^{3+} on the morphology of ammonium sulfate from Fig. 5.4 is shown again vividly in Fig. 5.5. There is a steep increase in the ratio G_L/G_W from the pure solution (around 1.2) to 13 at a concentration of 100 ppm Fe^{3+}. Al^{3+} has a similar influence on the crystal morphology of ammonium sulfate, although the effect is less. The ratio G_L/G_W is increased to 3.5 by 100 ppm of Al^{3+}. For the monovalent metal ions Na^+ and K^+ and the divalent metal ion Zn^{2+} no influence on the morphology of ammonium sulfate could be observed even at higher concentrations up to 1000 ppm.
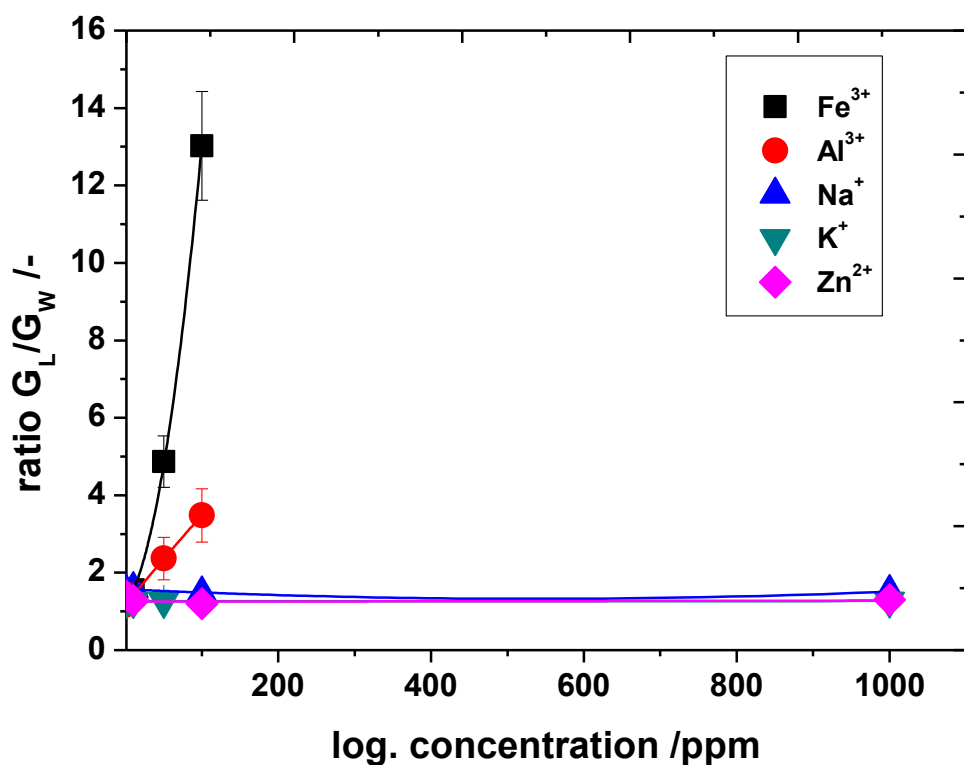
Fig. 5.5: Effect of impurities on the ratio G_L/G_W at pH 4

It was not possible to perform microscope cell experiments for the impurity Cr^{3+}. The seed crystals were not growing even at high supersaturation levels, but at a certain supersaturation a new crystal was growing from the surface of the seed crystal as shown in Fig. 5.6 at the top which shows the effect at a concentration of 10 ppm Cr^{3+}. At a Cr^{3+} concentration of 50 ppm a no more well-shaped crystal is growing from the original seed crystal (see Fig 5.6 at the bottom) and the shape is comparable to the results of batch crystallization (see Chapter 5.5).
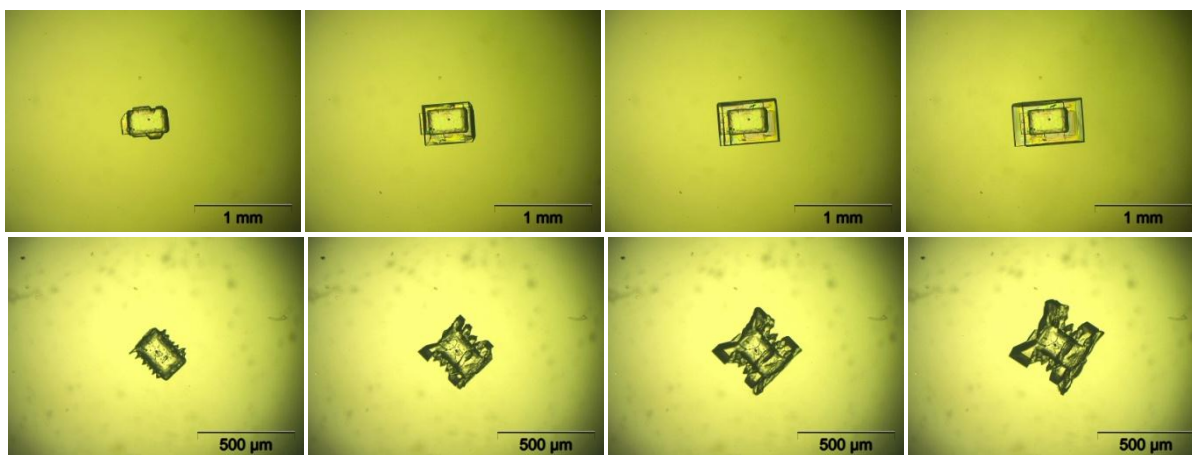
Fig. 5.6: Growth phenomenon of ammonium sulfate from Cr^{3+} contaminated solutions at pH 4 after 0, 20, 40 and 60 min (10 ppm Cr^{3+} upper part and 50 ppm Cr^{3+} bottom part)

5.3 Metastable Zone Width

5.3.1 Effect of Impurities on the MZW (pH 4)

The metastable zone width was observed as described in Chapter 4.3 by using the ultrasonic speed measurement. Figure 5.7 shows the effect of Fe^{3+} on the phase diagram of ammonium sulfate at a solution pH value of 4.
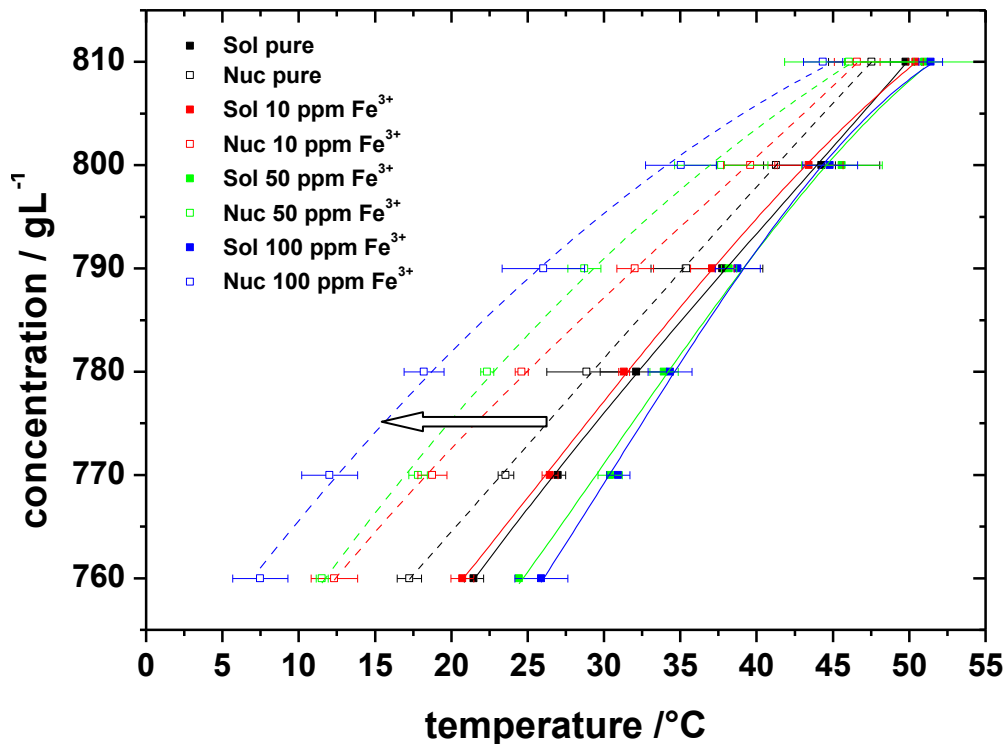
Fig. 5.7: The effect of Fe^{3+} on the phase diagram of ammonium sulfate (pH 4)

After adding even small amounts of Fe^{3+} into an ammonium sulfate solution, the nucleation curve is shifted to lower temperatures as marked by the arrow in Fig. 5.7. For a crystallization process this means that a much higher supersaturation is needed to obtain nucleation within the system. The solubility curve, however, shifts only a little to higher temperatures. This shift can be explained by the addition of ammonium and sulfate ions due to impurity adding and pH adjustment. As a consequence of these shifts the MZW of ammonium sulfate is widened very strong under the effect of Fe^{3+}. Figure 5.8 A shows the combined results for the effect of all observed trivalent impurities on the MZW. Thereby the average of the change in MZW caused by the impurities was taken over the complete observed range of ammonium sulfate concentrations from 760 to 810 g/L at pH 4.
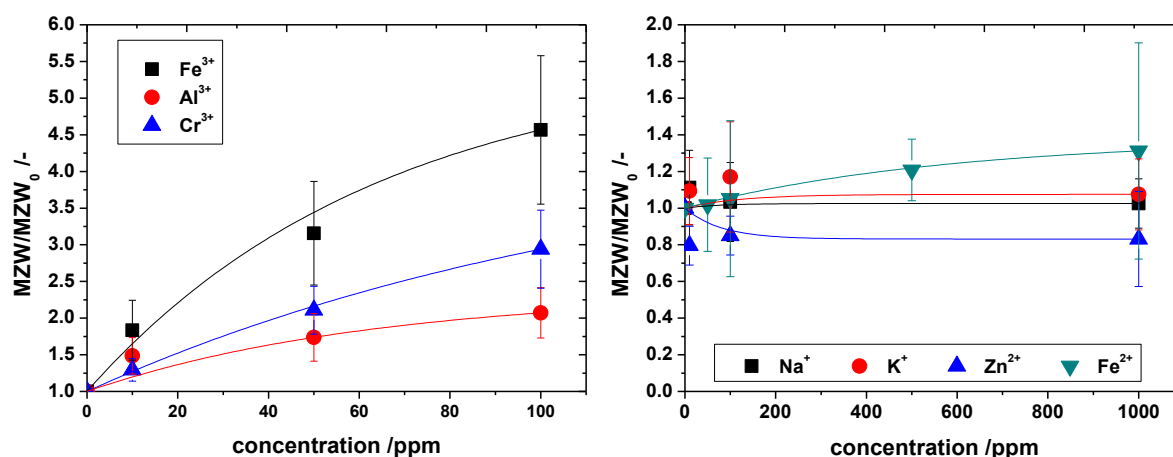
Fig. 5.8: A) Effect of trivalent metal ions on the MZW of ammonium sulfate at pH 4

B) Effect of di- and monovalent ions on the MZW of ammonium sulfate at pH 4

There is a very clear trend that all of the observed trivalent metal ions widen the MZW of ammonium sulfate. Fe^{3+} showed the strongest effect and the MZW was widened up to 4.5 times by addition of 100 ppm Fe^{3+} compared to the pure AS solution. Adding 100 ppm of Cr^{3+} showed a moderate effect with an increasing MZW of factor 3 and the smallest effect could be observed at a concentration of 100 ppm Al^{3+} when the MZW increased only about 2 times compared to the pure AS solution.

In Fig. 5.8 B the results for the di- and monovalent ions are shown. For the monovalent ions K^+ and Na^+ no effect on the MZW could be observed even at concentrations up to 1000 ppm. Different trends were found in case of the divalent ions. Fe^{2+} on the one hand slightly increases the MZW at higher concentrations even though the effect is very small (a 1.3 times higher MZW at a concentration of 1000 ppm compared to the pure solution) compared to the trivalent metal ions. In contrary, Zn^{2+} reduces the MZW of ammonium sulfate to 80 % of the original MZW of the pure solution. Here it is conspicuous that this value is already reached at 10 ppm of Zn^{2+} and a further increase does not show an increasing effect. This can be explained by the precipitation of the Zn^{2+} which will be further discussed in Chapter 6. It can be concluded that especially the trivalent metal ions show an effect on the MZW of ammonium sulfate and these results correspond to the results of Chapter 5.4 concerning the growth rate of ammonium sulfate crystals in the presence of trivalent metal ions. An arising question deals with the reasons for the different strength of the effects of Fe^{3+}, Cr^{3+} and Al^{3+}. A first approach will be shown and discussed in the following Chapter 5.3.2.

5.3.2 Influence of the pH Value on the Effect of Trivalent Metal Ions on MZW

Based on the knowledge of the pH value dependent distribution of various metal-aquo-complexes in aqueous solutions (Chapter 3.4) the effect of the trivalent metal ions on the MZW of ammonium sulfate was observed over a wide pH range from pH 2 to 6.5. The aim was to identify an active complex in widening the MZW. Fig. 5.9 shows the influence on the effect described in Chapter 5.3.1, namely that trivalent metal ions widen the MZW of ammonium sulfate at pH 4. The pH value has a strong impact on this effect. It can be seen in Figure 5.9 that there are some different curve progressions for all of the trivalent metal ions. The effect of Fe^{3+} at first increases then shows a maximum at pH 4 and then there is a sharp decrease of the effect between pH 4 and 4.5 until the effect disappears at around pH 5.5 when the curve converges to $MZW/MZW_0 = 1$. In case of Cr^{3+} and Al^{3+} there is a similar progression but the curves are shifted to higher pH values.
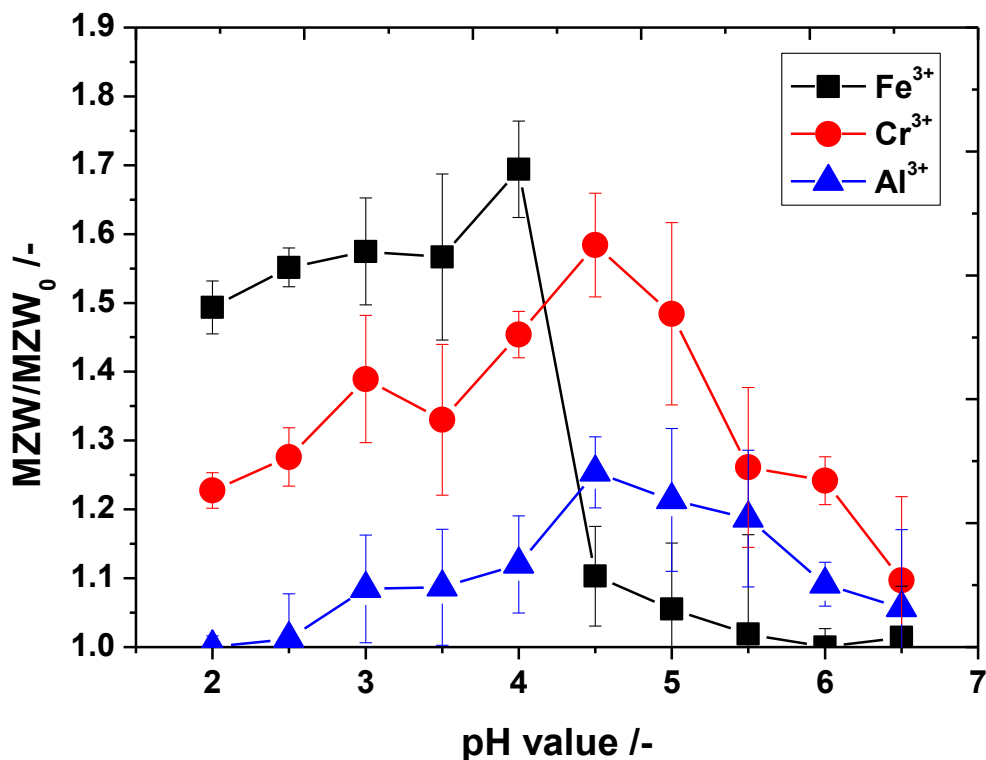
Fig. 5.9: Normalized influence of the pH value on the widening of the MZW by trivalent metal ions (impurity concentration 10 ppm)

These curve progressions were compared to the distribution of the different metal-aquo-complexes simulated by the program HySS (see Chapter 4.7) using hydrolysis constants taken from literature (Chapter 2.6). The Figures 5.10 to 5.12 give an overview of the interrelation between the distributions of the various complexes and their effect on the MZW of ammonium sulfate. It can be clearly seen that the first hydrolysis product $[Me(H_2O)_5]^{2+}$ (Me in this case stands for Fe, Cr and Al) is responsible for the effect of the metal ion on the metastable zone width of ammonium sulfate. The pH depending distribution of the first hydrolysis products fit the data for the increase in MZW achieved from ultrasound velocity measurements over a wide range of solution pH values. This behavior will be further discussed in Chapter 6 by using aspects in a molecular level.
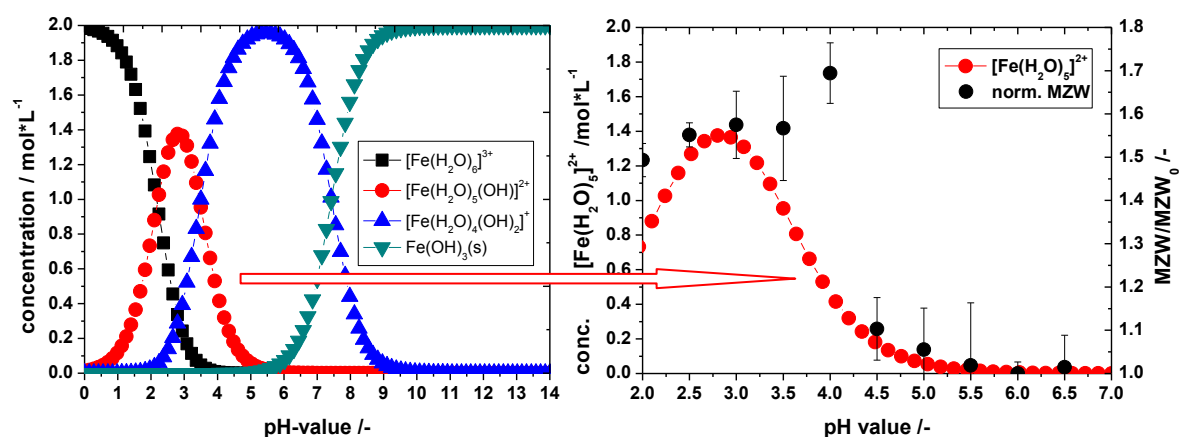
Fig. 5.10: Normalized influence of the pH value on the widening of the MZW by Fe^{3+} (impurity concentration 10 ppm)
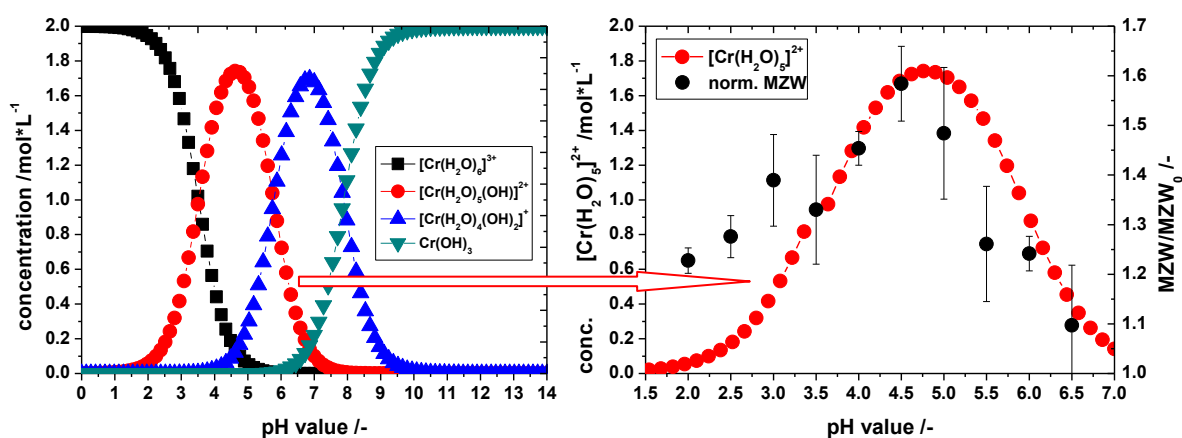
Fig. 5.11: Normalized influence of the pH value on the widening of the MZW by Cr^{3+} (impurity concentration 10 ppm)
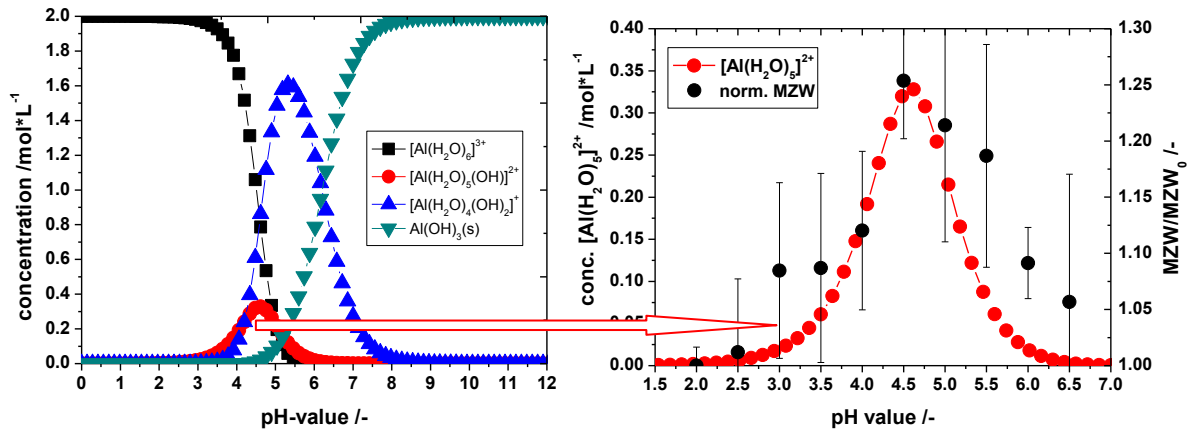
Fig. 5.12: Normalized influence of the pH value on the widening of the MZW by Al^{3+} (impurity concentration 10 ppm)

5.3.3 Synergy Effects of Fe^{3+} and Al^{3+} Ions on MZW

Up to now the effect of one single impurity on the MZW of ammonium sulfate was observed, but it is important to gain some information on possible synergy effects. This means how does one impurity like Al^{3+} (low effect) influences the effect of another impurity like Fe^{3+} as the strongest enhancer for the MZW of ammonium sulfate. These synergy effects are shown exemplary in Fig. 5.13 in a concentration range from 0 to 50 ppm Fe^{3+} and Al^{3+}.
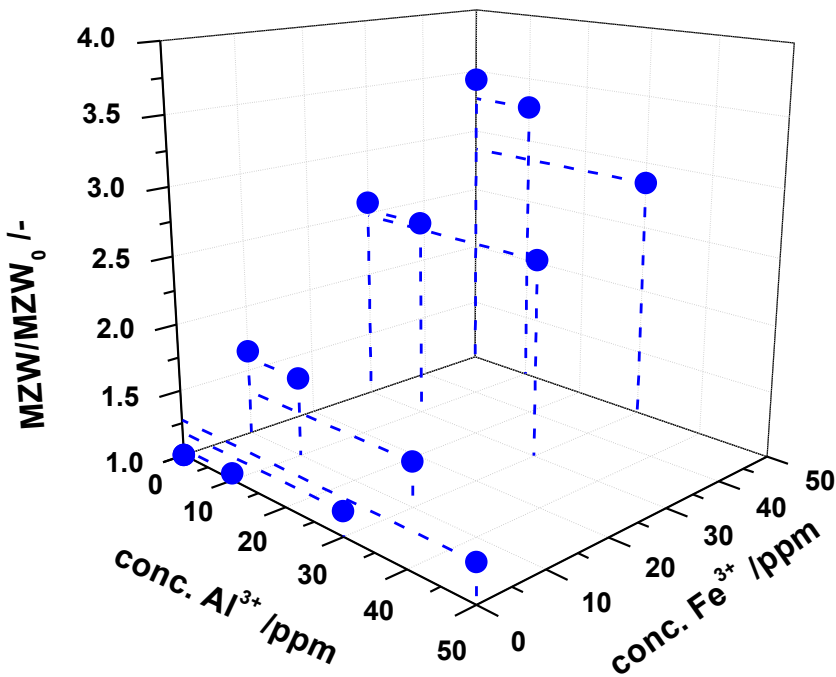
Fig. 5.13: Synergy effects of Fe^{3+} and Al^{3+} concerning widening MZW

Before, it was expected that the effects of both impurities (Fe^{3+} and Al^{3+}) will superimpose each other which means the total effect is the sum of the individual effects. In reality, the effect of the impurity with the stronger influence on the MZW, here Fe^{3+}, is decreased by adding several amounts of a weaker impurity, here Al^{3+}, as shown by the performed experiments and Fig. 5.13. For a further discussion a reference is made to Chapter 6.

5.3.4 Removing Effect of Oxalic Acid

Already about 50 years ago, a paper was published which describes the effect of oxalic acid [Sei55] on the crystallization of ammonium sulfate. The effect of e.g. Fe^{3+} ions can be neglected if oxalic acid is added in an appropriate amount. This effect should be validated within this work and the mode of action should be identified. Therefore ultrasonic velocity measurements were carried out. Different amounts of oxalic acid were added to Fe^{3+} and Cr^{3+} contaminated solutions (50 ppm impurity) at a solution pH value of 4. Figure 5.14 shows the results of these measurements. Thereby the results were normalized to the metastable zone width of a solution with 50 ppm of impurity and without oxalic acid at pH 4.
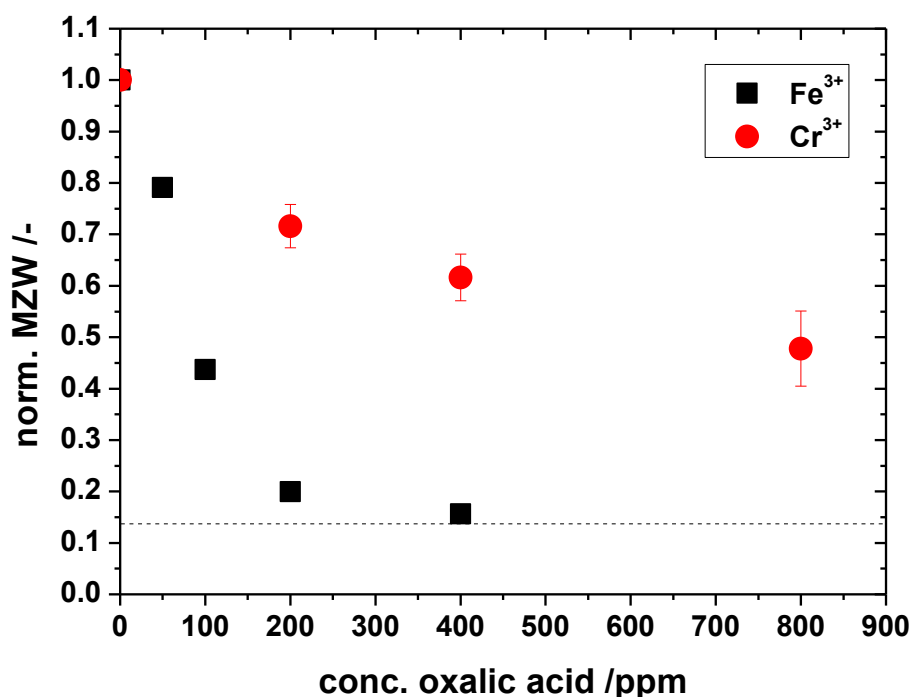
Fig. 5.14: Normalized influence of oxalic acid on the widening of MZW caused by 50 ppm of trivalent metal ions at pH 4 (dashed line)

The oxalic acid reduces the effect of the trivalent metal ions Fe^{3+} and Cr^{3+} on the MZW of ammonium sulfate. 400 ppm of oxalic acid is enough to remove the effect of 50 ppm Fe^{3+} completely (mass ratio 1:8). In contrast, 800 ppm of oxalic acid reduces the effect of 50 ppm Cr^{3+} to about 50% of the original value. This conspicuous difference in the effect of oxalic acid speaks for different modes of action of the oxalic acid concerning the two observed trivalent metal ions. A detailed discussion of this context could be found in Chapter 6.

5.4 Crystal Growth and Dissolution Rate

The effect of different metal ions on the crystal growth and dissolution rates of ammonium sulfate was observed by using a fluidized bed apparatus as described in Chapter 4.3. Figure 5.15 shows the effect of the trivalent metal ion Fe^{3+} on the crystal growth and dissolution rates of ammonium sulfate at a solution pH of 4 and in a super- or undersaturation range from 0 to 2 K, respectively.
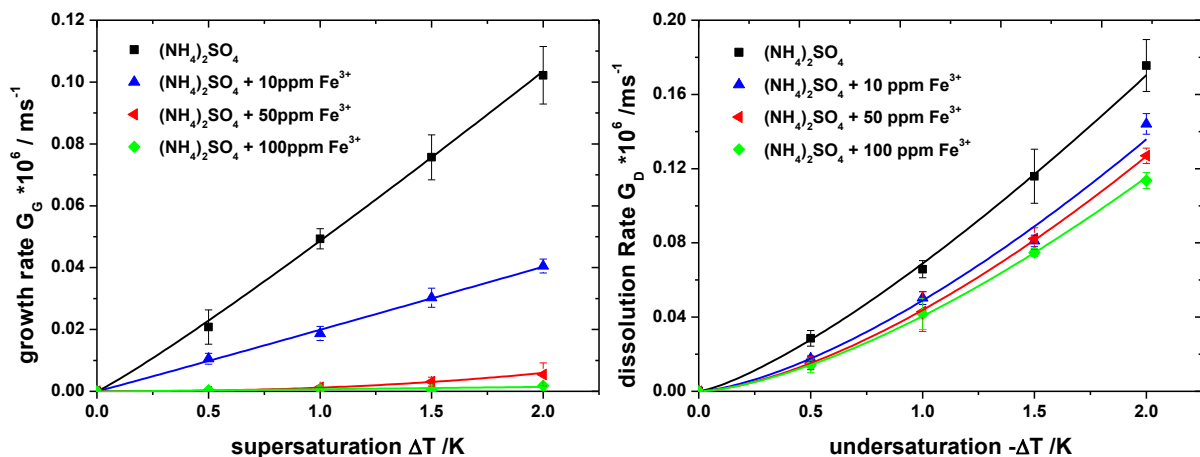
Fig. 5.15: The effect of Fe^{3+} on the growth rates (left side) and dissolution rates (right side) of ammonium sulfate at pH 4

Fe^{3+} has a strong influence on the growth rate of ammonium sulfate. The growth is almost stopped at an iron concentration between 50 ppm and 100 ppm at the investigated supersaturation level. The dissolution rates are also suppressed by the iron ions in the solution, even though the effect is much less than in case of the growth rates.

These measurements were also performed for other trivalent metal ions and the combined results for the effect on the growth rates are shown in Figure 5.16. Thereby the average of the decrease in growth and dissolution rates over the complete observed super- and undersaturation range was used. The achieved data points were

fitted to the Kubota-Mullin-model, which was already explained in Chapter 2.2.1 and is shown again in Eq. 5.1 [Kub95]. The fitting parameters are shown in Table 5.1.

It can be clearly seen, that the trivalent metal ions have a huge effect on the crystal growth rate of ammonium sulfate crystals at a solution pH value of 4. This is a similar trend compared to the observed effect of trivalent metal ions on the MZW of ammonium sulfate (see Chapter 5.3). Fe^{3+} has the biggest effect on the crystal growth rate followed by Cr^{3+} and again Al^{3+} shows the smallest effect of all three observed trivalent metal ions. Based on the fitting, critical impurity concentrations could be determined theoretically at which the growth of ammonium sulfate will be stopped completely. The critical value for Fe^{3+} is 86.5 ppm, for Cr^{3+} 138.5 ppm and for Al^{3+} no value could be calculated because $\alpha < 1$ and therefore $G/G_0 > 0$. One has to keep in mind that this is only valid for the observed range of supersaturation.
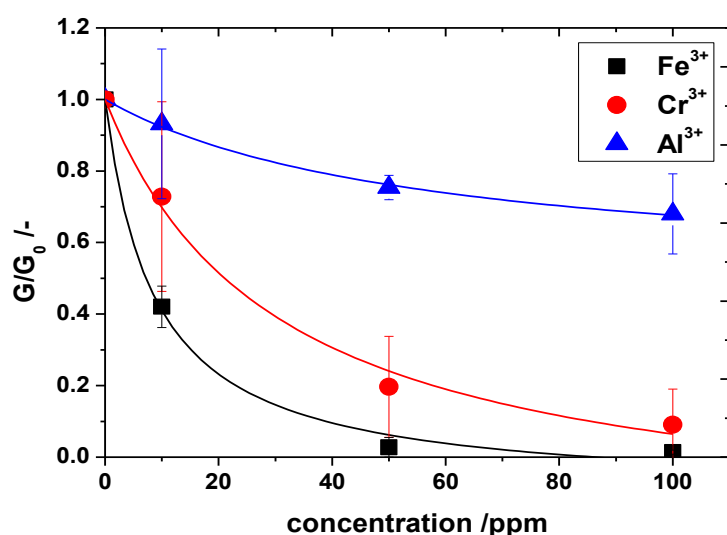
Tab.5.1. Fitting parameters of the Kubota-Mullin-model (Fig. 5.16)

	Fe^{3+}	Cr^{3+}	Al^{3+}
R^2	0.997	0.995	0.997
α	1.1002	1.2183	0.5044
K	0.1155	0.0331	0.0179

$$G = G_0 \left(1 - \alpha \cdot \frac{K \cdot c_i}{1 + K \cdot c_i}\right) \quad (5.1)$$

Fig. 5.16: The effect of trivalent metal ions on the crystal growth rate of ammonium sulfate (pH 4)

The Kubota-Mullin model [Kub95a] fits the data very well as can be derived from the coefficient of determination R^2 (see Table 5.1). This model contains two different parameters. On the one hand there is α, the impurity effectiveness factor, which stands for the quality of the adsorbed impurity molecules and describes the strength of the effect of an impurity and on the other hand K, the adsorption constant of the adsorption isotherm (Langmuir) which stands for the quantity of adsorbed impurity. From the determined parameters (see Table 5.1) it can be concluded that Cr^{3+} shows the highest efficiency concerning crystal growth retardation of ammonium sulfate.

This seems to stand in contradiction to the obtained results, but the reason could be find in the adsorbed amount of impurity molecules which is over three times higher in case of Fe^{3+} compared to Cr^{3+}. Al^{3+} shows a small efficiency in blocking crystal growth and also the adsorbed amount is smaller compared to Fe^{3+}, and Cr^{3+}.
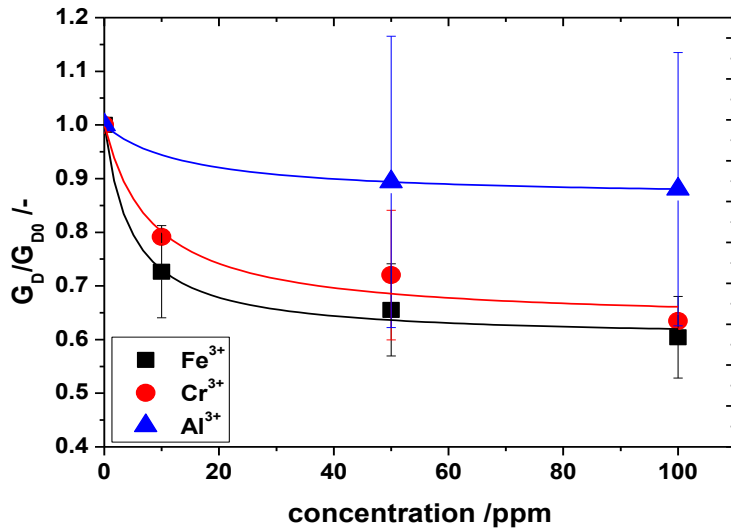
Tab.5.2. Fitting parameters of the Kubota-Mullin-model (Fig. 5.17)

	Fe^{3+}	Cr^{3+}	Al^{3+}
R^2	0.993	0.972	1
α	0.3985	0.3677	0.1369
K	0.2094	0.1183	0.0691

Fig. 5.17: The effect of trivalent metal ions on the crystal dissolution rate of ammonium sulfate (pH 4)

Similar results could be obtained from the dissolution experiments shown in Fig. 5.17. The Kubota-Mullin model also fits these effects very well and similar ratios for the α- and K-values of the observed trivalent metal ions were detected as shown in Tab. 5.2. It can in general be stated that the dissolution is not affected as strong as the crystal growth by trivalent metal ions. In case of Fe^{3+} the growth was nearly stopped at 100 ppm within the observed supersaturation level, the dissolution rate was only decreased to 60 % compared to the pure solution. Also 100 ppm of Cr^{3+} stopped the growth nearly completely meanwhile the dissolution was reduced only to around 65 % of the pure system. Whereas 100 ppm of Al^{3+} decreases the growth of ammonium sulfate to around 70 %, the dissolution rate, however, decreases only about 10 %. These trends are reflected by the fitting parameters α and K. In case of dissolution the α-values are smaller than one for all investigated impurities which means the dissolution will not be completely stopped even at higher concentrations. Fluidized bed experiments were also performed for di- and monovalent metal ions and the results are concluded in Fig. 5.18.
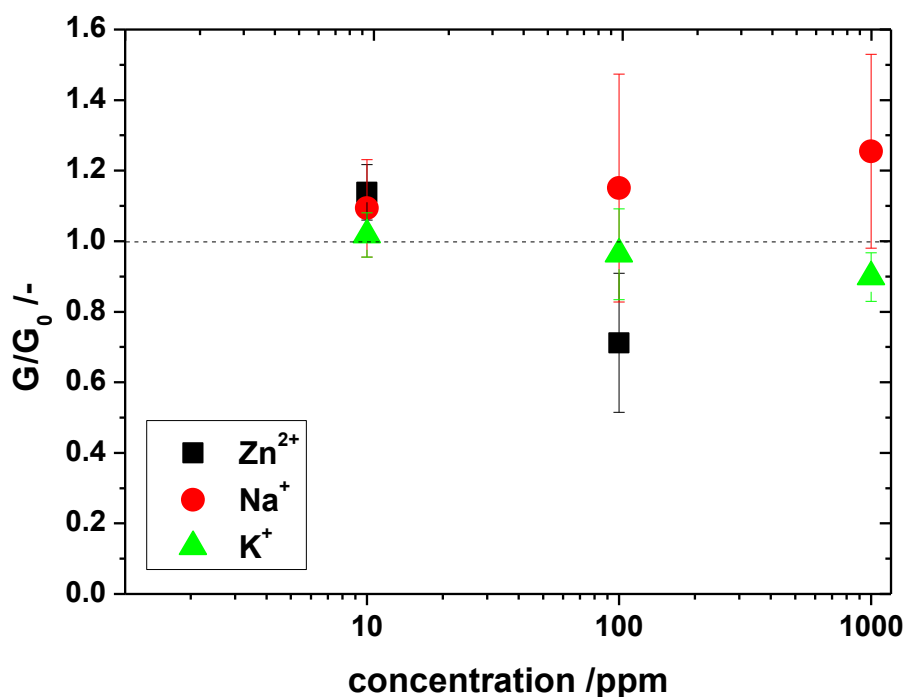
Fig. 5.18: The effect of mono- and divalent ions on the crystal growth rates of ammonium sulfate (pH=4)

It can be clearly seen that the monovalent ions Na$^+$ and K$^+$ do not show a strong effect on the growth rates of ammonium sulfate, albeit there is a small increasing effect of Na$^+$ at a high standard deviation.

Again, Zn^{2+} shows a special trend (Fig. 5.8 B) since at a concentration of 10 ppm the growth is enhanced and at a concentration of 100 ppm the growth rate is decreased. At this point again it should be referred to Chapter 6 where the precipitation of a chemical compound containing Zn^{2+} will be discussed. The same trends could be observed for the dissolution rates (data not shown here).

5.5 Morphology – Batch Crystallization

5.5.1 Effect of Metal Ions on the Morphology

The changes in crystal morphology caused by the addition of different metal ions were observed as already described in Chapter 4.5. Figure 5.19 shows the results for the effect of different concentrations of Fe^{3+} ions on the crystal morphology of ammonium sulfate.

Fig. 5.19: The effect of different concentrations of Fe^{3+} on the morphology of ammonium sulfate crystals at pH 4 (scale bar 100 μm)

It can be clearly seen that Fe^{3+} ions have a very strong effect on the morphology of ammonium sulfate crystals. At low concentrations up to 50 ppm the crystals were elongated and become more needle-like which stands in compliance with the results of the microscope cell experiments in Chapter 5.2. Concentrations higher than 50 ppm Fe^{3+} causes a rough surface which will be discussed later. A further increase of the Fe^{3+} concentration to 200 ppm changes the morphology to thin plate-like crystals with jagged borders. At concentrations of 500 ppm and 1000 ppm no nucleation could be observed at the investigated supersaturation level, because the metastable zone width increases with the concentration of Fe^{3+} in solution (see Chapter 5.3).

To verify the results of Chapter 5.3 concerning the effect of the pH value on the influence of Fe^{3+} ions on the metastable zone width of ammonium sulfate, in Fig. 5.20 the effect of the pH value on morphology is shown.

It becomes clear that the pH value changes the effect of Fe^{3+} on the morphology of ammonium sulfate crystals. At pH 2.7 very fine nuclei with a needle-like shape could be found in the solution and at pH 3.7 long needles with the rough surface as described before. The interesting point is that the effect of Fe^{3+} on the morphology could be completely removed by increasing the solution pH value to 6. This matches the results of Chapter 5.3.

pH 2.7 **pH 3.7** **pH 6**

Fig. 5.20: The effect of different solution pH values on the effect of 100 ppm Fe^{3+} on the morphology of ammonium sulfate (scale bar 100 μm)

The results of the effect of the other observed trivalent metal ions Cr^{3+} and the influence of solution pH value are shown in Figures 5.21 and 5.22, respectively.

Pure **10 ppm** **20 ppm**

50 ppm **100 ppm** **200 ppm**
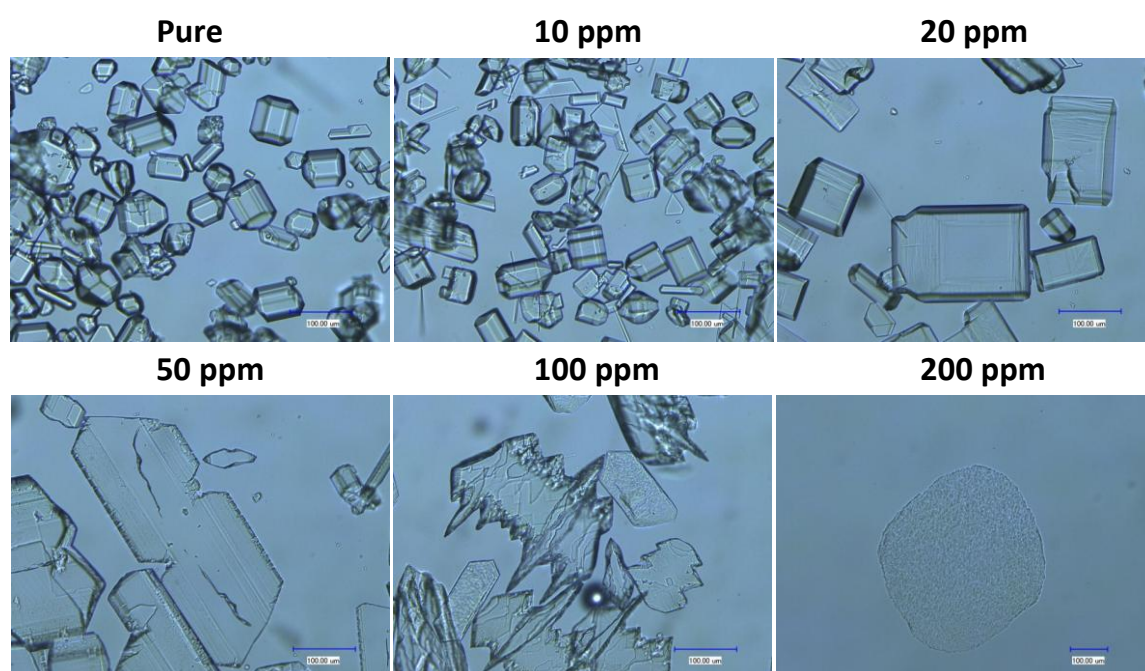
Fig. 5.21: The effect of different concentrations of Cr^{3+} on the morphology of ammonium sulfate crystals at pH 4 (scale bar 100 μm)

The morphology of ammonium sulfate crystals is not changed up to 20 ppm of Cr^{3+}, although there is a visible change in the surface structure of some faces which are full of steps at 20 ppm of Cr^{3+}. By a further increase of the Cr^{3+} concentration (50 ppm) the crystals first turned into some kind of needle-like crystals with jagged borders as already seen for the case of Fe^{3+} and at 100 ppm these effects become even more considerable (some kind of holes in the surfaces and pikes growing from some faces into the solution). In case of 200 ppm Cr^{3+} very thin plate-like crystals could be observed comparable to 200 ppm of Fe^{3+}. For higher concentrations also in case of Cr^{3+} no nucleation appeared at the used supersaturation level.

Especially, the picture of 100 ppm Cr^{3+} fits with the findings of the microscopy cell experiments (Fig. 5.6) and the growth of this "spikes" from the crystal surface.

| pH 2 | pH 3 | pH 6.3 |

Fig. 5.22: The effect of different solution pH values on the effect of 100 ppm Cr^{3+} on the morphology of ammonium sulfate (scale bar 100 μm)

If the roughness of the crystals is taken as the factor to describe the effect of Cr^{3+}, it can be concluded, that the effect of Cr^{3+} increases from pH 2 to pH 3, reaches some kind of maximum (really rough surfaces and notches in the surfaces) at pH 3-4 and decreases again at pH 6.3. This stands in agreement with the results of MZW (Chapter 5.3).The results for the effect of Al^{3+} and the influence of pH are shown in Figures 5.23 and 5.24.
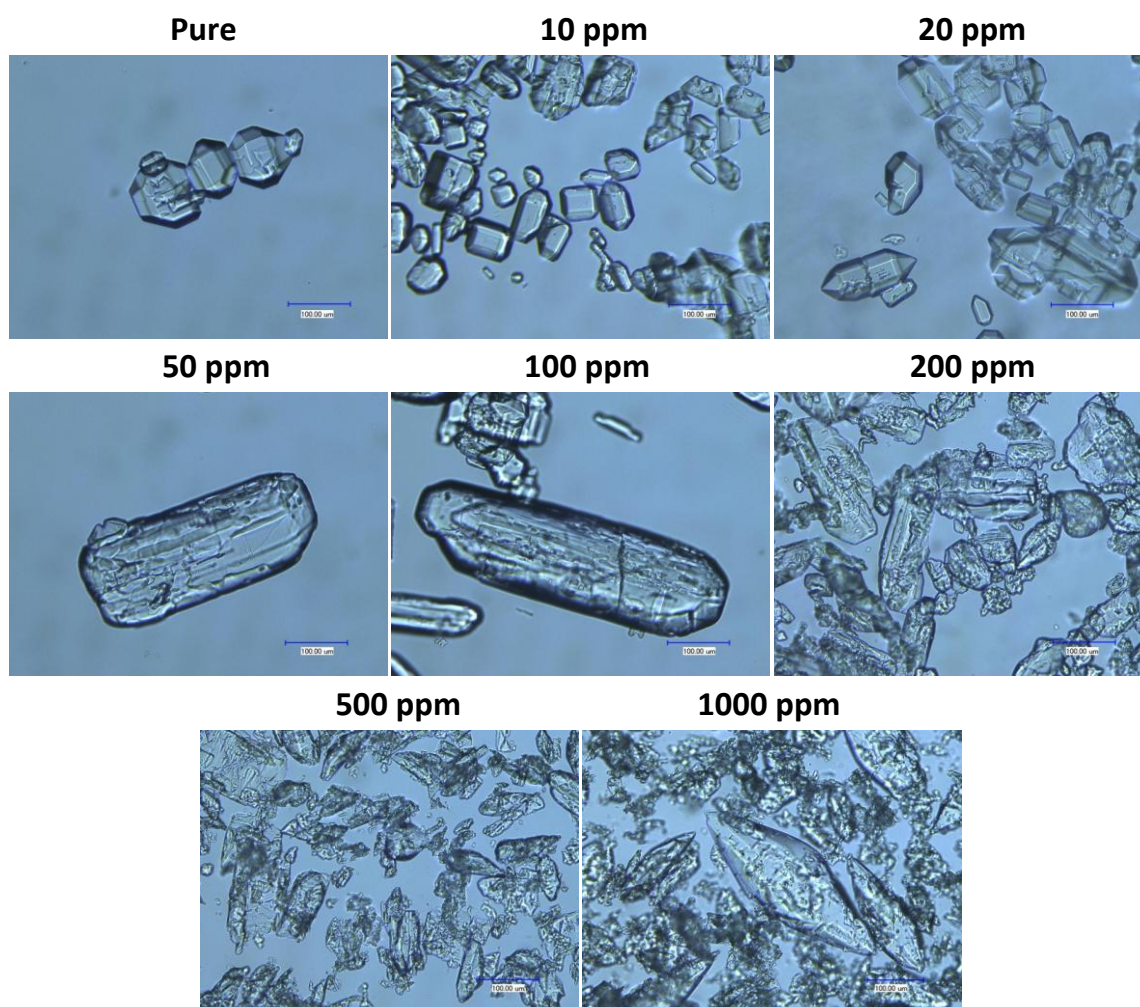
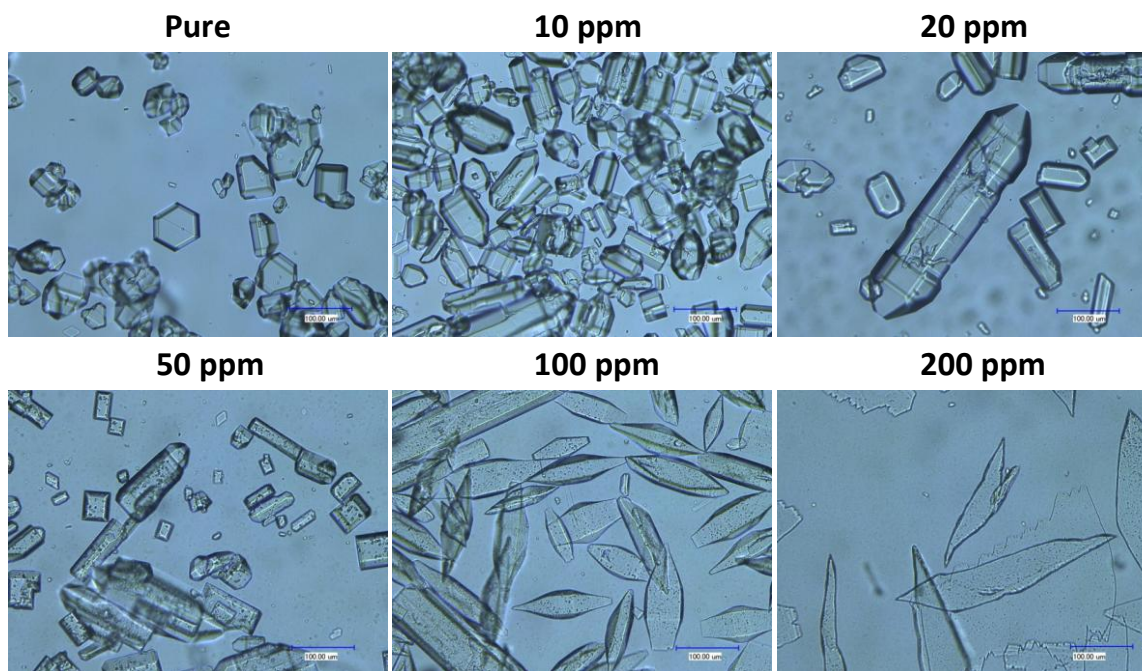**Fig. 5.23: The effect of different concentrations of Al^{3+} on the morphology of ammonium sulfate crystals at pH 4 (scale bar 100 µm)**

Al^{3+} shows a comparable behavior like Fe^{3+}, although higher concentrations are needed to achieve the same effect. So at 100 ppm the crystal morphology turns into a needle-like crystal as already shown by microscopy cell experiments (Chapter 5.2). In contrast to Fe^{3+} and Cr^{3+} also at Al^{3+} concentrations of 500 and 1000 ppm nucleation could be observed (smaller effect on MZW of ammonium sulfate see Chapter 5.3). Thereby the morphology changed into a double pyramid. Furthermore, a lot of very small crystals or crystal fragments can be seen next to the big double pyramids at the pictures of 500 and 1000 ppm.
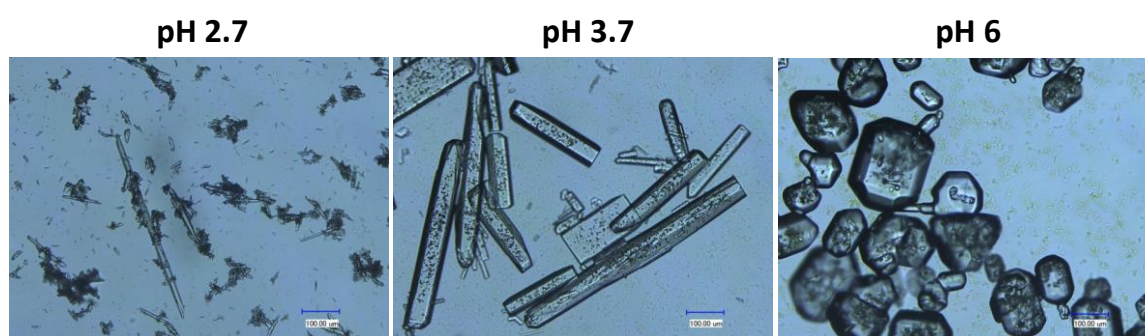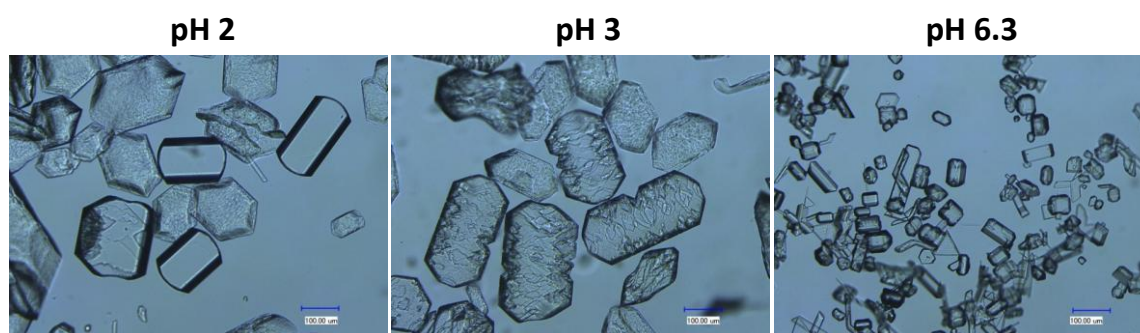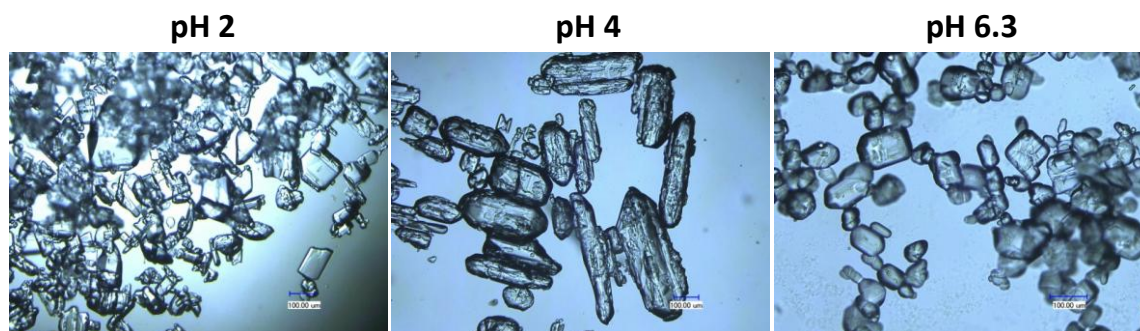
Fig. 5.24: The effect of different solution pH values on the effect of 100 ppm Al³⁺ on the morphology of ammonium sulfate (scale bar 100 μm)

The results concerning the influence of the pH value on the effect of Al^{3+} on the morphology confirm the trends of Cr^{3+} and Fe^{3+}, because at low pH values the shape of the crystals is comparable to pure ammonium sulfate crystals, at pH 4 the crystals change into needle-like morphology and at higher pH values the effect disappears again.

5.5.2 The Removing Effect of Oxalic Acid

As mentioned before the effectiveness of oxalic acid in removing the negative effects of Fe^{3+} should be evaluated. It was already shown in Chapter 5.3 that by adding oxalic acid the MZW of Fe^{3+} contaminated ammonium sulfate solutions can be decreased to the original level of pure solution.

Figure 5.25 proves the ability of oxalic acid to remove also the effect of Fe^{3+} on the crystal morphology. The first picture shows the crystal morphology of ammonium sulfate grown under the influence of 50 ppm Fe^{3+}. As already mentioned before these crystals have a needle-like shape, but after adding different amounts of oxalic acid the effect disappears.

To quantify the effect of oxalic acid in Fig. 5.26 the ratios G_L/G_W (as defined in Chapter 5.2) for the different Fe^{3+} and oxalic acid concentrations are shown. The data points were achieved by taking the average of the length and width of 15 crystals. It can be seen that with increasing Fe^{3+} concentrations the ratio increases, as it was described extensively in Chapter 5.2.

By adding oxalic acid this effect decreases very fast until a ratio of 1:1 of Fe^{3+} and oxalic acid and at a ratio of 1:8 the effect completely disappeared.
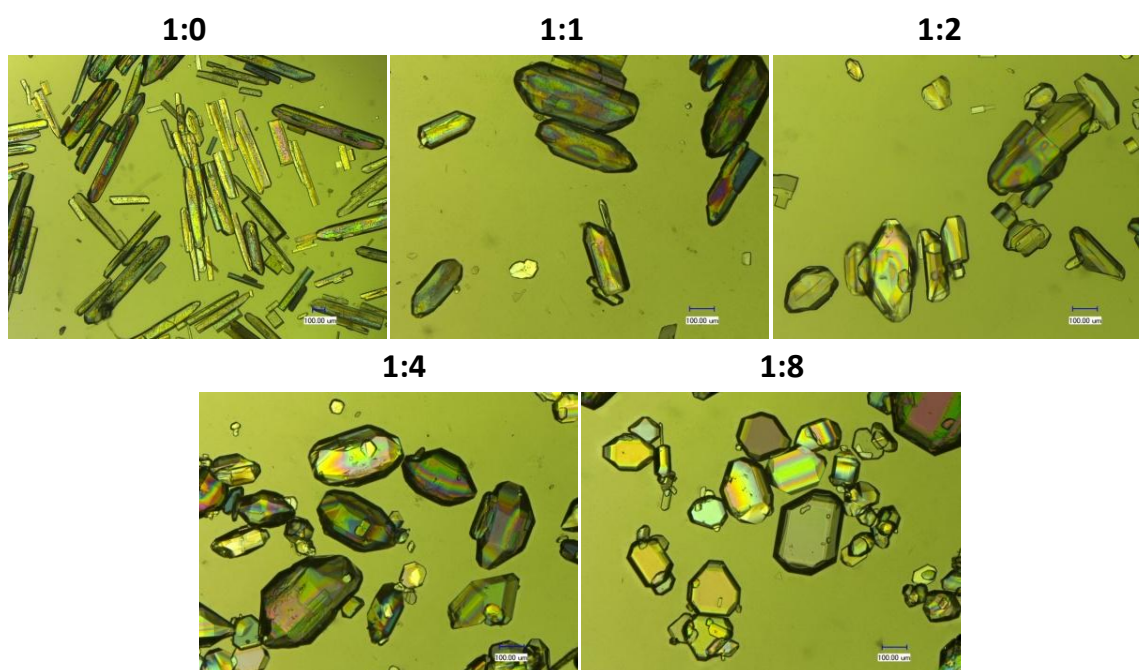
Fig. 5.25: The removing effect of different concentrations of oxalic acid at a Fe^{3+} concentration of 50 ppm and solution pH value of 4 (scale bar 100 μm)
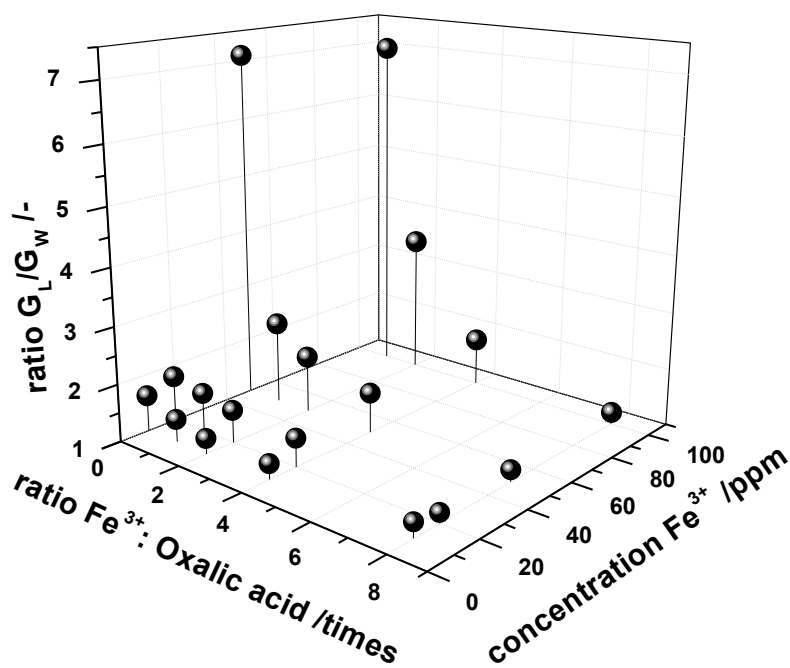
Fig. 5.26: The removing effect of different concentrations of oxalic acid at various Fe^{3+} concentrations at a solution pH value of 4

5.6 Integration Experiments

The integration of impurities into the crystal lattice is an important parameter for industrial crystallization processes and the quality of the obtained product. In order to produce an ultra pure product one should provide the integration of impurities. Whereas in some special cases the integration of impurities can guarantee stable continuous crystallization processes and impurity concentrations due to the removal of impurities enclosed in the product.

So a fundamental understanding in impurity integration is necessary to control the process on the one hand and the product quality on the other hand. Figure 5.27 shows the results for the integration of Fe^{3+}, Cr^{3+} and Al^{3+} into the crystal lattice of ammonium sulfate over a wide range of solution pH value. Here it has to be mentioned that the experiments were only carried out once and no statistical reliability can be guaranteed.
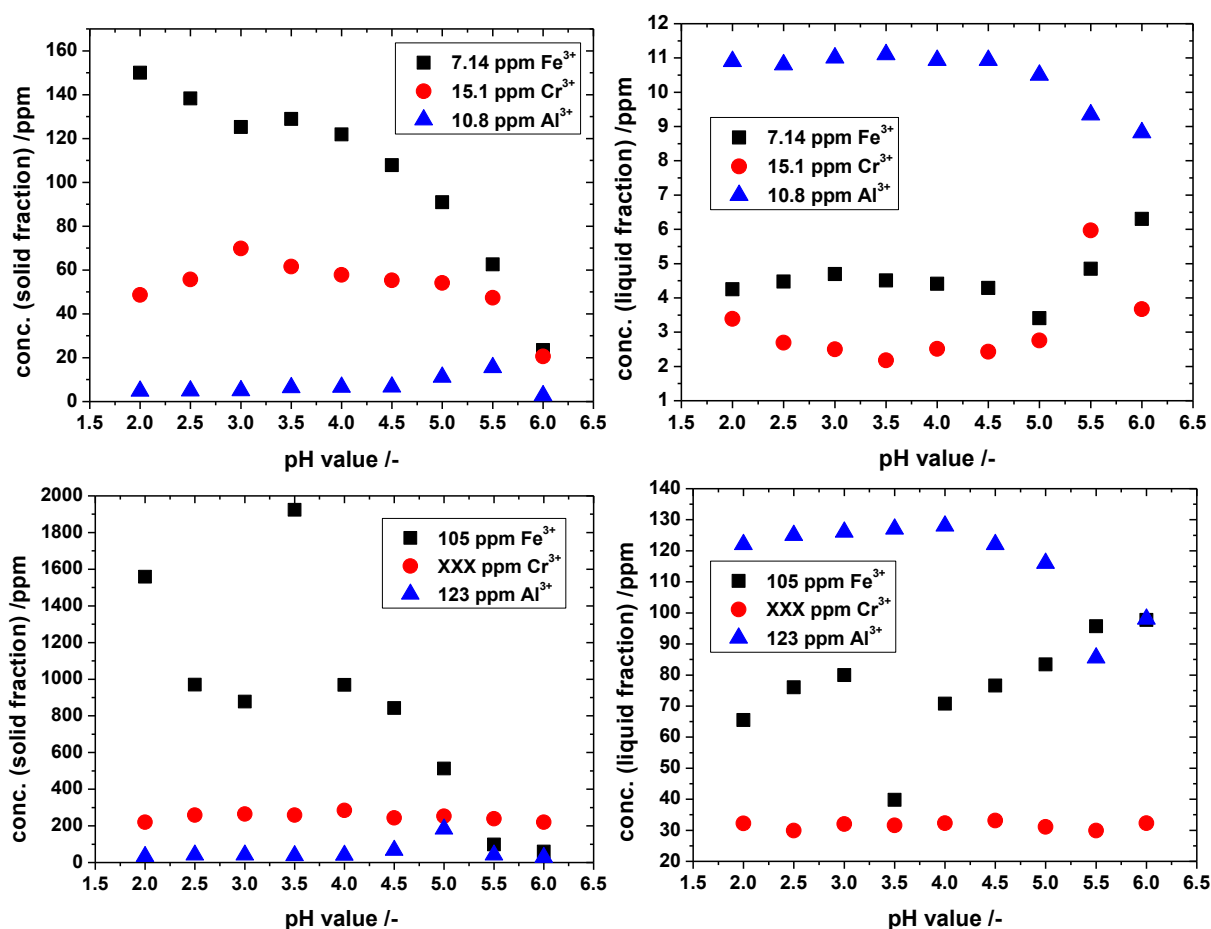
Fig. 5.27: Integration of trivalent metal ions into the crystal lattice of ammonium sulfate

On the first view the data shown in Figure 5.27 seem to be a little confusing but by taking a closer look some interesting trends get obvious. It can be clearly seen that the incorporation of impurity into the crystal lattice depends on the pH value of the solution. In general, it can be stated that Fe^{3+} gets incorporated very easily, Cr^{3+} is also incorporated, however, less then Fe^{3+}, and Al^{3+} is not integrated over a wide range of pH values. This is in absolute agreement with the results for the effects on crystal growth, MZW and crystal morphology ($Fe^{3+} > Cr^{3+} > Al^{3+}$). For all three trivalent metal ions again some kind of maxima for integration could be observed as already shown for the effect on the MZW depending on the solution pH value (c.f. 5.3.2). For Fe^{3+} there is a maximum at around pH 3.5, for Cr^{3+} at pH 4 and for Al^{3+} at pH 5. The reasons for this pH dependent integration behavior will be further discussed in Chapter 6.4 and an interrelation to the impurity adsorption will be given. Moreover, in Fig. 5.27 the correlation between the concentration of impurity in the solid and in the liquid fraction can be seen. With increasing impurity concentrations in the solid fraction the concentration in the liquid fraction decreases which is the "cleaning-effect" of the crystals for the mother liquor and will be subject of the discussion (Chapter 6).
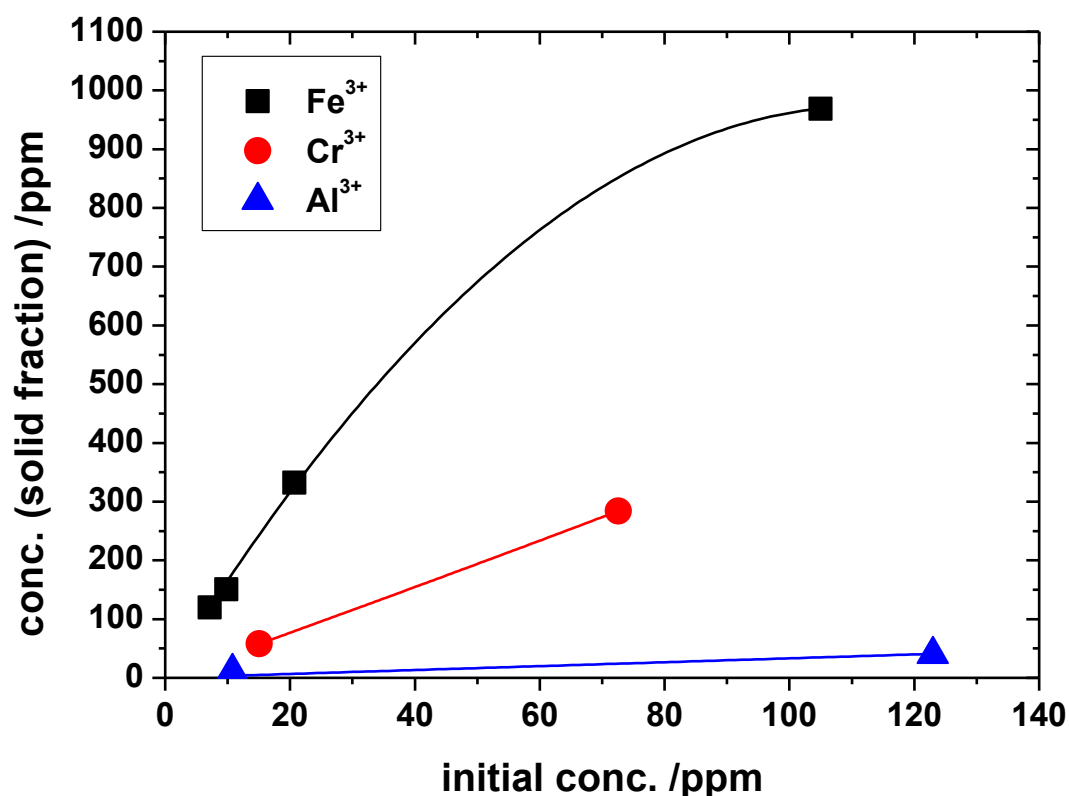
Fig. 5.28: Influence of initial impurity concentration on the incorporation (pH 4)

Increasing initial impurity concentrations in the mother liquor causes higher impurity concentrations in the solid fraction at a solution pH value of 4.

For Cr^{3+} and Al^{3+} only two data points are available, nonetheless the same trend can be seen as in case of Fe^{3+}. With a further increase of the initial impurity concentration the curve of Fe^{3+} in the solid fraction increases more and more slightly which indicates a saturation behavior. This can be explained by the adsorption isotherms of impurity molecules onto the crystal surface which will be discussed detailed in Chapter 6.3.

Another part of the systematic research implied the effect of oxalic acid on the incorporation of Fe^{3+} into the crystal lattice of ammonium sulfate which is shown in Fig. 5.29.
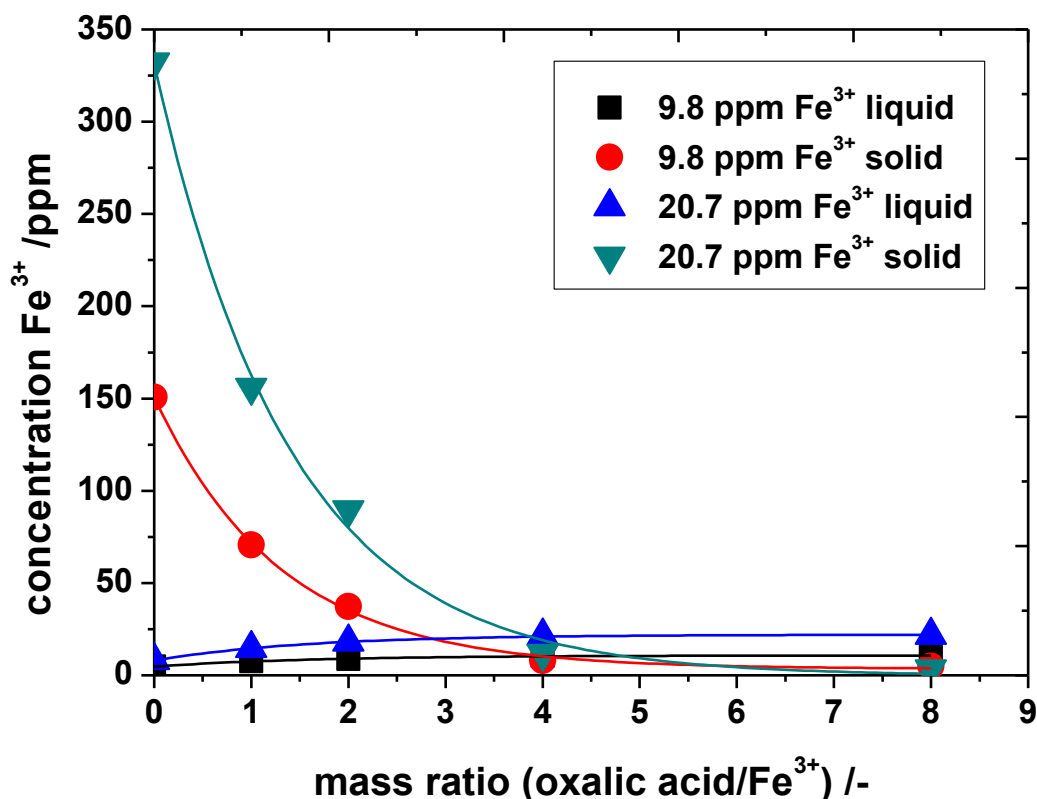
Fig. 5.29: "Removing effect" of oxalic acid in terms of incorporation of Fe^{3+} (pH 4)

By increasing the concentration of oxalic acid added to the contaminated solution, the amount of incorporated Fe^{3+} decreases. At mass ratios of 1:8 (Fe^{3+}:oxalic acid) the integration of Fe^{3+} is nearly completely stopped. This phenomenon will be further discussed in Chapter 6.3.

6.Discussion

In Chapter 5 the effects of different metal ions and the influence of the pH value on the crystallization parameters growth rate, metastable zone width and crystal morphology of ammonium sulfate were presented. Within the following discussion a comparison to the existing literature will be made, the reasons for the observed effects will be given and discussed, and the connection to an industrial crystallization process of ammonium sulfate will be shown.

6.1 Impurity Adsorption and Consequences

6.1.1 Changes in Crystal Growth Rate

In Chapter 5.4 the results for the effects of different metal ions on the growth and dissolution rates of ammonium sulfate were presented. For the pure ammonium sulfate–water system, growth rates in a magnitude of $0.5*10^{-7}$ m/s were detected at a undercooling of $1\,K$ which is a relative supersaturation of 0.0035. This is in agreement with the results of Kitamura et al. [Kit92] who observed similar growth rates of $1*10^{-7}$ to $1.5*10^{-7}$ m/s depending on the different faces at a supersaturation σ=0.003 (the small deviations can be contributed to a different experimental setup) [Kit92]. For the dissolution kinetics they observed dissolution rates of $1*10^{-7}$ to $2*10^{-7}$ m/s at a relative undersaturation of 0.003 [Kit92] which is similar to the results of this work ($0.7*10^{-7}$ m/s at a relative undersaturation of 0.003). Also the shape of the curves of growth and dissolution rates depending on relative super- or undersaturation are comparable, since they appear as nearly linear curves which indicates a linear relationship between driving force and growth or dissolution rates at the observed super- or undersaturation level.

The differences between crystal growth and dissolution rates which could be detected can be contributed to a theoretical approach which was already discussed in Chapter 2.4.1. In case of crystal growth the growth units face an additional resistance, namely the integration step of the growth unit into the crystal lattice. From the difference between growth and dissolution at comparable driving forces one can decide, if the growth is integration or diffusion controlled. If the diffusion resistance of growth is assumed to be equal to the diffusion resistance of the dissolution, the integration resistance could directly be calculated from the difference between growth and dissolution rates [Gar71].

In the case of ammonium sulfate the integration of growth units is the limiting factor as could be seen from Fig. 6.1 for the example Fe^{3+}, where the difference between growth and dissolution rates are shown. The difference increases with increasing driving force because the diffusion improves due to the driving force while integration of growth units remains constant. The Fe^{3+} impurity hinders the integration of growth units. The reverse effect between 50 ppm and 100 ppm (decreasing importance of integration step) is related to the complete growth stoppage.
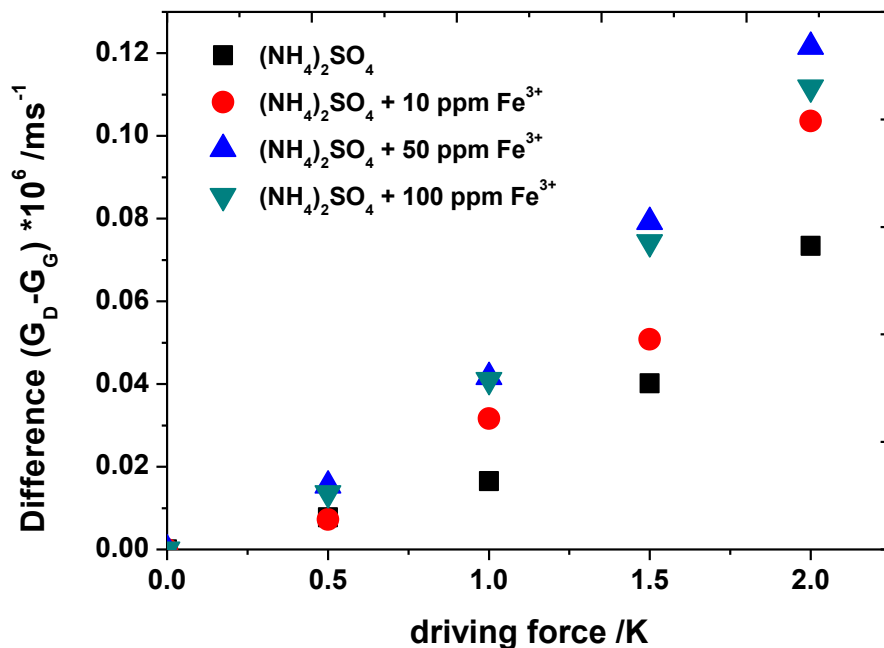
Fig. 6.1: Difference between growth and dissolution rates of ammonium sulfate under influence of Fe^{3+} at solution pH of 4

From Fig. 6.1 it can be derived that the effect of Fe^{3+} originates from the blockage of active growth sites due to adsorption at the crystal surface which increase the integration resistance for crystal growth.

Another evidence for this statement is the successful fitting of the results for the effect of trivalent metal ions on the growth rates of ammonium sulfate by the Kubota-Mullin-model (Chapter 5.4). The basis of this model is the adsorption of impurities including the use of adsorption isotherms like Langmuir (Chapter 2.4.2).

In literature there are high numbers of papers concerning the effect of different metal ions on crystal growth of various compounds, whether inorganic and organic. Table 6.1 shows a composition of effects of some impurities on the crystal growth rate of different compounds only to give an idea about the significance of the topic. It

is not possible to find a clear trend because trivalent as well as divalent metal ions were proven to show growth retardation effects on crystals of different compounds.

Tab. 6.1: Overview about literature - the effects of impurities on crystal growth rates

Nr.	Reference	Compound	Impurity	Effect
1	[AlJ01]	NaCl	Pb^{2+},Mg^{2+}	
2	[Dav74]	$(NH_4)_2H_2PO_4$	Fe^{3+},Cr^{3+},Al^{3+}	
3	[Gou09]	K_2SO_4	Cr^{3+}	
4	[Kit92]	$(NH_4)_2SO_4$	Cr^{3+}	Growth retardation
5	[Kub99]	K_2SO_4	Fe^{3+}	
6	[Kub00]	NaCl	Pb^{2+}	
7	[Mie04]	$(NH_4)_2C_2O_4*H_2O$	Co^{2+},Ni^{2+}	
8	[Ras97]	KH_2PO_4	Fe^{3+},Al^{3+}	

Some of these publications refer with their data to the model of Kubota and Mullin. For example the influence of $FeCl_3$ and $AlCl_3$ on the growth of ADP (ammonium dihydrogen phosphate) crystals was observed by Davey and Mullin [Dav74]. Later Kubota et al. [Kub95a] transferred these data to the Kubota and Mullin model. For $FeCl_3$ α was found to be 1.18 and K was assigned to be 25.5 $(kg\ m^{-3})^{-1}$. These are quiet similar results for α compared to this work, which means, that the impurity effect is nearly the same and the growth rate will asymptotically converge to zero (in the special case of α=1). If the unit of parameter K is changed to kg/kg the value changes to 0.02045 (kg/kg) which is also comparable to the obtained values of this study. In case of $AlCl_3$ they observed similar values for α (1.04) and K (40.6 $(kg\ m^{-3})^{-1}$) compared to the results of $FeCl_3$. These values are much higher than the parameters determined for the effect of Al^{3+} on ammonium sulfate within this study. Possible reasons for this will be discussed later within this Chapter.

The growth of potassium sulfate is affected in the same way by traces of Fe^{3+} ions [Kub99] as in the case of ammonium sulfate in this study. The two parameters α and K were calculated to be 690 and 312 dm³/mol, respectively. The value of α for the iron effect on potassium sulfate is very high in comparison to the others. Furthermore, Al-Jibbouri and Ulrich [AlJ01] studied the influence of Pb^{2+} and Mg^{2+} on the crystal growth rate of sodium chloride and they determined α-values of 0.86 for Pb^{2+} and 0.57 for Mg^{2+}. Kubota et al. [Kub00] examined the same system and found α-value between 1.8 and 3 depending on the supersaturation level [Kub00].

The dissolution rate as the second important part of Chapter 5.4 is not as well studied as the growth and consequently not so many papers were published in terms of the

dissolution kinetics (e.g. Fab96]. Another example which was observed by Omar and Ulrich [Oma97] is the effect of Fe^{2+} on the dissolution rates of KCl. The dissolution rate was increased from about $0.15*10^{-6}$ ms^{-1} in a pure solution to $0.25*10^{-6}$ ms^{-1} in a contaminated solution (50 ppm Fe^{2+}) [Oma97]. Another example is the effect of Al^{3+} on the dissolution of potassium sulfate reported by Sato [Sat88]. It was shown that the dissolution rate was decreased by traces of Al^{3+} (115 ppm) [Sat88]. Cr^{3+} shows the same effect decreasing effect on the dissolution kinetics of potassium sulfate [Kub95b]. This stands in good agreement with the results obtained in this work especially taking into account that the dissolution rates are less affected by the impurities than the growth rates (see [Sat88] and [Kub95b]).

The different effectiveness of different impurities with respect to growth retardation is an open question and this will be further discussed later with a focus on impurity adsorption in Chapter 6.1.4.

6.1.2 Changes in Metastable Zone Width

The effects of different metals ions on the MZW of ammonium sulfate were presented in Chapter 5.3. For the pure ammonium sulfate solution a MZW of 4.78 K was determined as an average value from 760 – 810 g/L ammonium sulfate concentration, at a solution pH value of 4 and at a cooling rate of 5 K/h. In the literature different values can be found for pure ammonium sulfate solutions depending on cooling rate, presence or absence of crystals and method of determination. So Nyvlt et al. [Nyv70] reported the MZW for many different inorganic compounds including ammonium sulfate. For a cooling rate of 5 K/h in absence of crystals a MZW of 3.6 K was determined by the visibility method [Nyv70]. The higher MZW of the pure solution in this work can be related to the different methods of determination, the different pH value of the solution and possible traces of impurities which are also present in "pure" solution (Chapter 4.1). Compared to crystal growth, the MZW is not that often in the focus of the research. Nonetheless there are some examples for the effects of various metal ions on different compounds. So Mullin et al. [Mul79] reported the effect of Cr^{3+} on the MZW of potash alum solutions. The MZW increases from 0.6 K to 1.1 K after adding 20 ppm of Cr^{3+}, but a further increase in Cr^{3+} leads again to a decrease in MZW and at a concentration of 50 ppm the MZW reaches the level of the pure solution (Mul79]. Cr^{3+} ions also increase the MZW of potassium sulfate, although no maximum for the increase in MZW could be detected [Oma03]. Titiz-Sargut and Ulrich [Tit02] observed the effect of different impurities

$(Mg^{2+}$, Cu^{2+} and Cr^{3+}) on the MZW of potassium alum. All of the investigated impurities increases the MZW and show a similar trend as observed by Mullin [Mul79] which means the MZW show a maximum at a specific impurity concentration and decreases afterwards to the MZW of the pure solution [Tit02].

For ammonium sulfate Rauls et al. [Rau00] reported an increase in MZW from 1K to 2.5 K after adding 500 ppm Al^{3+} in a seeded system. It is hard to compare data of seeded (data of [Rau00]) and unseeded experiments (this work), but Figure 6.2 shows the comparison of the inhibition of the effect of increasing Al^{3+} concentrations on the MZW of ammonium sulfate [Rau00] (left side) and the inhibition of the effect of the trivalent ions on the MZW of ammonium sulfate as shown before in Chapter 5.3.1.
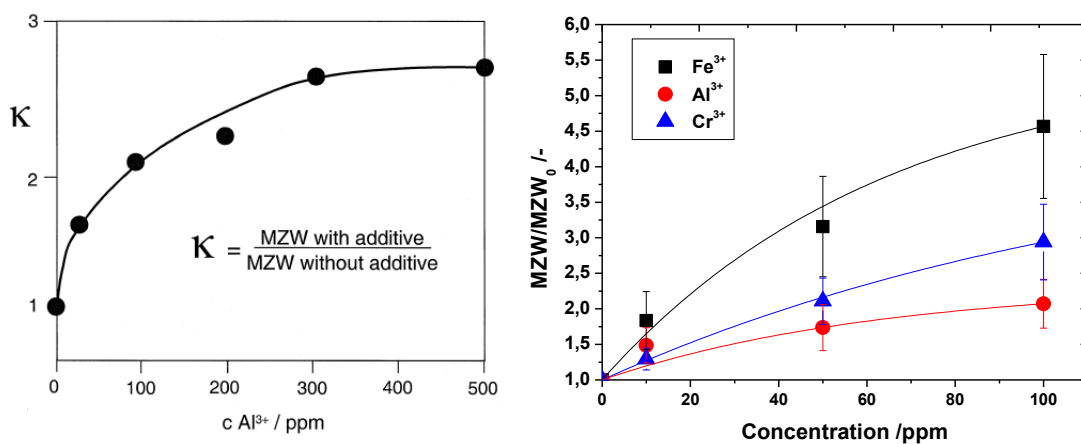
Fig. 6.2: Comparison of the data of [Rau00] (left) and the results of this work (right)

The ratios MZW/MZW_0 of Rauls et al. [Rau00] and of this study are similar since in both studies the MZW is doubled by adding 100 ppm of Al^{3+} and there is an inhibition of the effect with increasing impurity concentrations. Sayan and Ulrich [Say01] observed the effect of different divalent ions on the MZW of ammonium sulfate and Table 6.2 shows some characteristic results for a cooling rate of 4.8 K/h investigated by the ultrasound velocity method.

Tab. 6.2: Influence of divalent ions on the MZW of ammonium sulfate [Say01]

	pure	Cu^{2+}			Ni^{2+}			Mg^{2+}		
c_i /ppm	0	2.5	5	10	10	20	50	5	10	20
MZW /K	6.61	10.52	12.25	15.19	10.79	11.41	12.06	9.13	9.69	10.35

All of the observed divalent ions increase the MZW of ammonium sulfate. Nonetheless in both studies ([Rau00] and [Say01]) as well as in this study no reduction with a further increase in impurity concentration could be detected as in

the studies of Mullin [Mul79] and Titiz-Sargut [Tit02]. The possiblity that the maximum is not reached yet and will appear at even higher concentrations of impurities is unlikely due to the high concentrations compared to the literature which reports a maximum. Within these studies no reasonable explanation for the decrease in MZW at higher impurity concentrations was given.

The MZW is defined by the thermodynamic fixed solubility curve and the kinetic factor nucleation curve (Chapter 2.3.2). Both parameters could be affected in different ways by adding impurities to a system. Therefore it is not enough to talk only about the in- or decrease in MZW, rather the shift in both curves has to be distinguished which at the end leads to the change in MZW. As already mentioned in Chapter 5.3.1 the change in MZW of ammonium sulfate caused by the observed impurities is derived from a shift of the nucleation curve to lower temperatures (Fig. 5.7). However, there is also a small shift of the solubility curve to higher temperatures which could be related to the adding of further ammonium or sulfate ions due to impurity addition and pH adjustment. This behavior could be confirmed by Zhu et al. [Zhu08] who observed the effect of Fe^{3+} and pH value on the solubility of ammonium sulfate. They observed only a small decrease in solubility (shift of solubility to higher temperatures) by decreasing the pH value with sulfuric acid and nearly no change in solubility by adding 1.7 mol/mL Fe^{3+} as iron trioxide [Zhu08]. In literature many examples are shown in which impurities can change the solubility of different compounds. For example Kubota et al. [Kub88] showed that the solubility of potassium sulfate is decreased from 13 % (w/w) to 12.3 % (w/w) at a Cr^{3+} concentration of 150 ppm [Kub88]. Another example is given by Sangwal et al. [San07a] who investigated the effect of different di- and trivalent ions on the solubility of ammonium oxalate monohydrate. The solubility was increased by all of the ions Cu^{2+}, Mn^{2+}, Zn^{2+}, Fe^{3+}, Cr^{3+}, Ni^{2+} and Co^{2+} [San07a]. In a former study they showed that some of these ions do not have any influence on the MZW of ammonium oxalate monohydrate [San04]. So Cu^{2+}, Fe^{3+} and Cr^{3+} show only a negligible effect on the MZW of ammonium oxalate monohydrate and Mn^{2+}, Co^{2+} and Ni^{2+} are effective in widening the MZW [San04].

By taking a look back to Figure 5.8 it is noticeable that the divalent ion Zn^{2+} decreases the MZW of ammonium sulfate. A very useful overview about the effects of different impurities on the MZW of various compounds is given by a book of Nyvlt et al.

[Nyv85]. Therein it is shown that 0.1 % (wt/wt) Zn^{2+} reduces the MZW from 3.61 to 2.93 K at a cooling rate of 10 K/h which is in agreement with the data of this work.

By concluding all these examples and facts for the influence of different ions on the MZW of various compounds and comparing them to the data achieved during this study it is hard to see any clear trend. This makes the prediction for the effects on the MZW caused by different impurities nearly impossible without performing experiments.

If it is hard to predict the effect of one impurity, how complex is it then to predict the effects of two impurities or even a mixture of different impurities. In Chapter 5.3.3 the synergy effect of two impurities are shown. Thereby Fe^{3+} as the strongest enhancer in MZW and Al^{3+} as the trivalent impurity with the lowest effect on the MZW of ammonium sulfate were chosen. Before it was expected that the influences of both are simply added to each other to show an even higher effect on the MZW, but in reality another phenomenon is observed. Al^{3+} decreases the effect of Fe^{3+} and the only logical explanation could be the competition of both impurities for the limited adsorption sites at the surface of the crystal or the nucleus. In the literature there is a lack of information concerning the effects of impurity mixtures. Sangwal [San07b] made some theoretical approaches towards this topic and Equation 6.1 shows the growth rate from a solution containing two impurities A and B.

$$\frac{v}{v_0} = \frac{\sigma_1^0}{\sigma} \cdot \left(\frac{K_A \cdot c_A + \Theta_B}{1 + K_A \cdot c_A} \right) \qquad (6.1)$$

Therefore the effect of one impurity (A) is increased by the adsorption of another impurity as suggested before and shown clearly in Fig. 6.3.
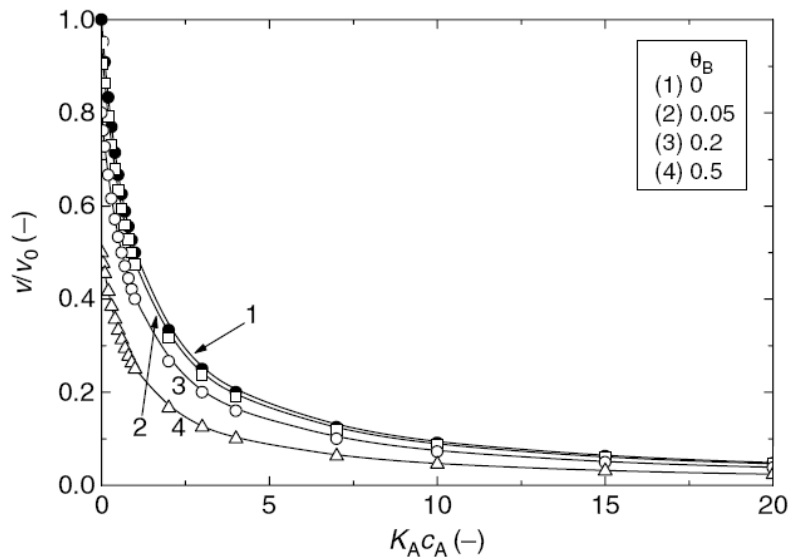
Fig. 6.3: The effect of the adsorption of a second impurity (taken from [San07b])

This model does not take into account, how the adsorption of a second impurity can decrease the adsorption of the first impurity since there is only a limited amount of available adsorption sites.

In Chapter 6.1.4 a general comparison and evaluation of the results concerning the effects on growth and dissolution rates, MZW and crystal morphology will be given.

6.1.3 Changes in Morphology

In Chapter 2.4 the theory of a change in crystal morphology caused by impurities was explained. Thereby the impurities adsorb in various amounts at the specific surfaces of a crystal like ammonium sulfate depending on their structures. It was shown in the Chapters 5.2 and 5.5 by two different experimental procedures, namely microscope cell and batch crystallization, that especially the trivalent metal ions Fe^{3+}, Cr^{3+} and Al^{3+} change the morphology of ammonium sulfate from a compact cubic to a needle-like habit at moderate impurity concentrations and some kind of plate-like crystals at higher impurity concentrations (Chapter5.5).

Before, similar results were reported in several publications for ammonium sulfate (e.g. [Sei55], [Nyv62], [Mes70], [Lar73], [Kit92], and [Rau00]). The results of Rauls et al. [Rau00] concerning the effect of Al^{3+} on the crystal morphology of ammonium sulfate are composed in Fig. 6.4.
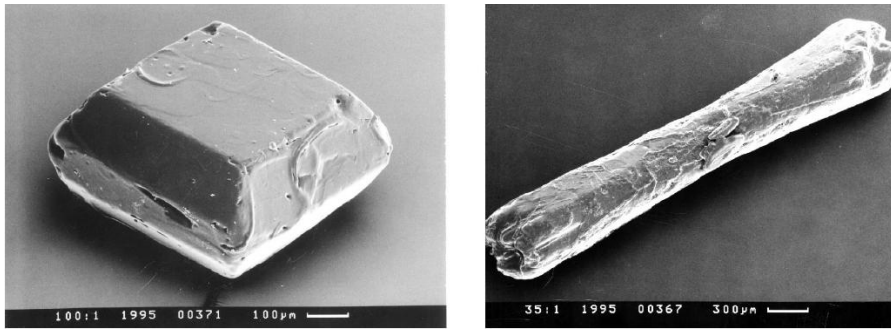
Fig. 6.4: SEM images of ammonium sulfate crystals grown from pure solution (left) and from Al^{3+} contaminated solution (100 ppm) (right) [Rau00]

Summarizing the literature it can be said that the observed change in morphology reported within this work could be confirmed. There are also an enormous number of other published papers concerning the effect of various impurities on the morphology of different inorganic salts including ammonium sulfate and a broad overview is given by Nyvlt and Ulrich [Nyv95].

An arising question is why do these impurities adsorb in different amounts at the specific faces of ammonium sulfate which at the end leads to a change in morphology?

Therefore the crystal habit and the surface structures for all of the specific faces of ammonium sulfate were simulated by "Material Studios" based on the unit cell. Figure 6.5 shows the characteristic crystal habit of ammonium sulfate including the faces with Millers indices as explained in Chapter 2.1. To prove the simulation an image of a crystal which was grown from pure ammonium sulfate solution is shown next to the simulated habit.
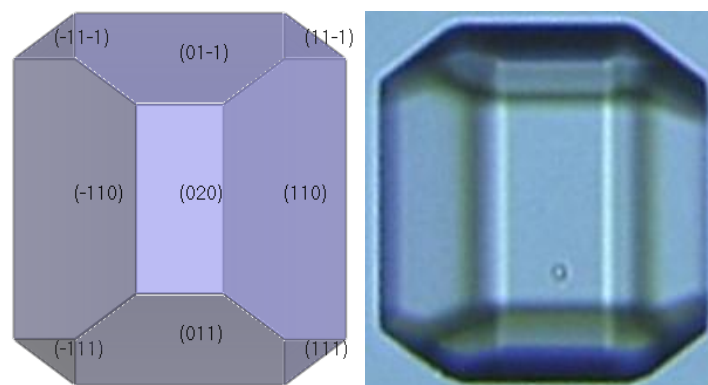
Fig. 6.5: Ammonium sulfate crystal with specific faces (Attachment Energy Model performed with Material Studios 4.0) (left) and ammonium sulfate crystal grown from pure solution at pH 4 (right)

The simulated crystal habit is similar to the crystal habit achieved by experiments because the same characteristic faces can be seen in the simulation as well as in the microscope image. Figure 6.6 summarizes the surface structures of the faces shown in Fig. 6.5. The ammonium sulfate crystal consists of four different faces, namely (011), (111), (020) and (110).

Here it has to be mentioned that e.g. all the small faces at the corners (111), (11-1), (-11-1) and (-111) have the same surface structure.

(011)

(111)

(020)

(110)
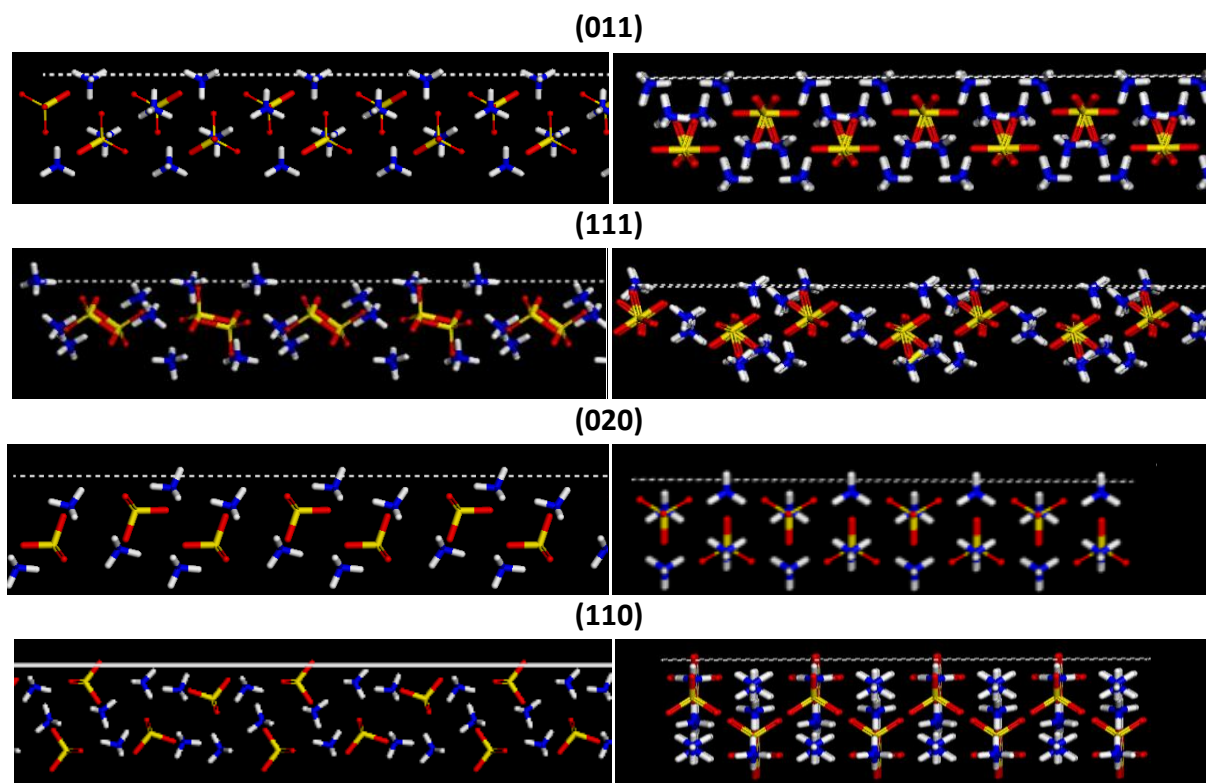
Fig. 6.6: Surface structure of the specific faces of ammonium sulfate on a molecular level (red/yellow = sulfate ion; blue/white = ammonium ion), left and right view are rectangular to each other), simulations made by the help of Material Studios 4.0

A comparison of the surface structures shown in Fig. 6.6 indicates the possible differences in the adsorption behavior of impurity molecules. Here only a qualitative discussion is made to explain the effect of trivalent metal ions on the morphology of ammonium sulfate crystals. Since the charges of the metal ions in solution (also as metal-aquo-complex) are positive, electrostatic effects may cause the main interaction forces between crystal surface and an impurity molecule close to the solid-liquid interface. The crystal lattice consists of ammonium (NH_4^+) and sulfate (SO_4^{2-}) ions which are arranged periodically as shown in Fig. 6.6. Depending on the amount of ammonium or sulfate ions at the surface, the charge of the surface will be

more or less negatively or positively charged and therefore more or less attractive for the adsorption of impurity molecules. Taking this into consideration, the (110) face is very attractive for adsorption due to its available sulfate ions at the surface. The face (020) also offers free available double bonds of the sulfate ions close to the crystal surface which makes it favorable for the adsorption of positively charged impurity molecules. The (011) and (111) faces, however, are almost completely covered by ammonium ions which makes them unattractive for the adsorption. Since adsorbed impurity molecules block active growth sites at the crystal surface, the growth rate of these faces is decreased (see Chapter 2.4.2). Consequently, face specific adsorption behavior causes various face growth rates into the different dimensions and therefore a change in the crystal morphology as already explained in Chapter 2.5. In case of ammonium sulfate the growth of (110) and (020) is more blocked than growth of the (111) and (011) faces and therefore a needle-like shape will appear for the crystals grown under the influence of trivalent metal ions.

A similar approach was made by Asakuma et al. [Asa08] who observed the effect of trivalent metal ions on the growth of potassium dihydrogen phosphate crystals. Figure 6.7 shows this context illustratively. In case of face (101) the surface is predominantly covered by potassium ions which are positively charged and the face (100) is negatively charged due to the dihydrogen phosphate ions. Therefore the impurities will adsorb at the (100) face and the crystal shape will change into a needle-like one [Asa08].
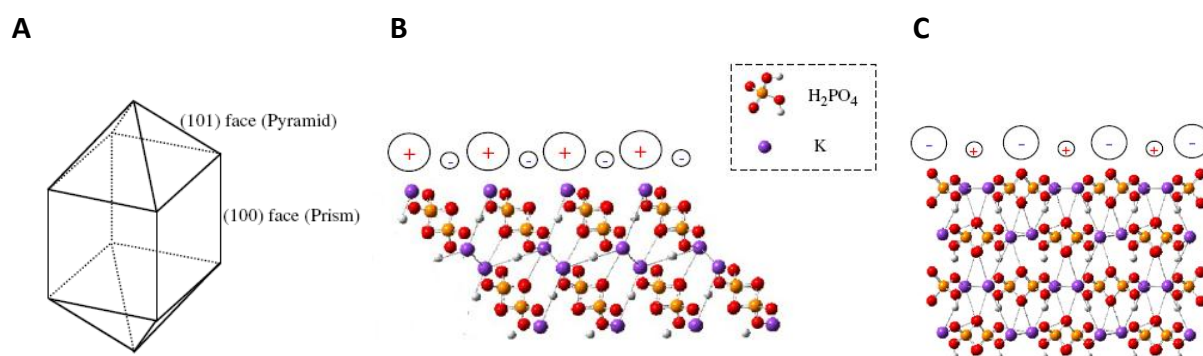
Fig. 6.7: Explanation for the face specific effect of impurities on KDP crystals; A: scheme of a KDP crystal; B: surface structure of (101) and C: surface structure of (100) [Asa08]

From these explanations it can be concluded that the changes in morphology are caused by a specific adsorption of impurity molecules on the different crystal surfaces depending on the surface structure and the interactions between surface and

impurity molecule close to the solid-liquid interface. It is common to observe adsorption kinetics of impurities onto crystal surfaces (e.g. [Guz98], [Kub00]) but up to now the adsorption isotherms of impurities onto specific crystal surfaces (e.g. only (101) are hard to investigate experimentally. A possible solution for this lack of information can be given by the establishment of molecular modeling. It was not the task of this work to establish molecular modeling as a tool to predict the crystal morphology of inorganic compounds, but during the work the need for quantitative analysis of interactions between surface and impurity was increasing due to give a useful discussion about this topic.

6.1.4 Concluding Focus on Impurity Adsorption

The previous Chapters 6.1.1 to 6.1.3 showed the effects of the observed impurities on the different crystallization parameters separately and gave a comparison to the existing literature. Comparing all of the observed effects of impurities, it is obvious that the adsorption of impurity on the crystal surface is the main factor for the impurity effect. In Fig. 6.8 the effects of the trivalent impurities on the growth rates and MZW of ammonium sulfate are compared.
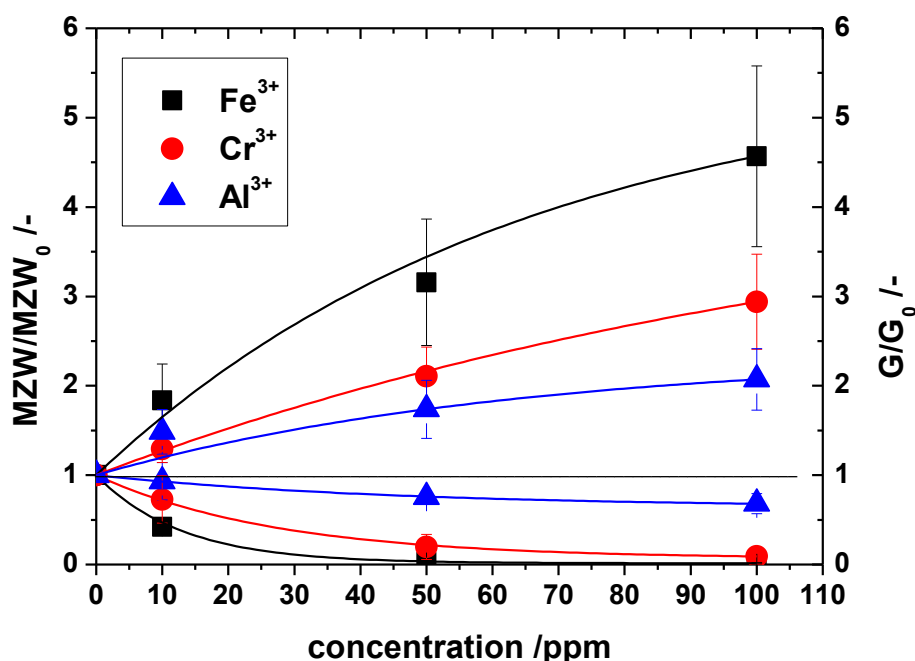
Fig.6.8: Comparison of the effects of trivalent metal ions concerning their effect on the growth rates and MZW of ammonium sulfate

The similarities can be clearly seen between the effects on growth rates and MZW of ammonium sulfate which indicates an equal mechanism of impurity effect of growth

inhibition and widening the MZW. It is assumed here that the adsorption of impurity molecules on the crystal surface causes the growth inhibition and an adsorption at the subcritical nuclei causes the widening of the metastable zone. As already mentioned before the adsorption at crystal surfaces reduces the growth of these crystal faces which could be mathematically described by the Kubota-Mullin model (Chapter 2.4.2).

For nucleation a similar approach can be made since the Equation to define the nucleation rate J (Chapter 3.3.1) could be extended by an adsorption term (see Eq. 6.2) like it is done for the Kubota-Mullin-model in case of crystal growth.

$$J = \frac{A_1}{(1+K \cdot c_i)} \cdot e^{\left[-\frac{16\pi \cdot \gamma^3 \cdot \Omega^2}{3k^3 \cdot T^3 \cdot (\ln \sigma)}\right]} \qquad (6.2)$$

This means the nucleation is suppressed by the decrease in the value A_1 and only by increasing the supersaturation σ, this inhibition can be overcome which at the end stands for the increase of the MZW. An open question is, of course, why some impurities can decrease the MZW (e.g. in case of Zn^{2+}). In such a case it is assumed that the solid-liquid interfacial tension γ is decreased, while the A_1 keeps constant and therefore the nucleation rate J increases [Kas02].

For the crystal growth there are similar coherences since in literature often a critical relative supersaturation was reported which is needed to overcome an existing impurity effect caused by adsorption on the crystal faces. Kubota et al. [Kub97] introduced a model for the critical supersaturation based on the model of Kubota and Mullin (Capter 2.4.2). Thus, the critical supersaturation needed to overcome the impurity effect can be calculated by Equation 6.3:

$$\sigma_c = \frac{\gamma \cdot a \cdot K \cdot c_i}{k \cdot T \cdot L \cdot (1+K \cdot c_i)} \qquad (6.3)$$

Similar to the previous discussion concerning the nucleation rate J, the critical supersaturation increases with an increasing impurity adsorption (represented by the Langmuir adsorption isotherm) and decreases with a decreasing solid-liquid interfacial tension.
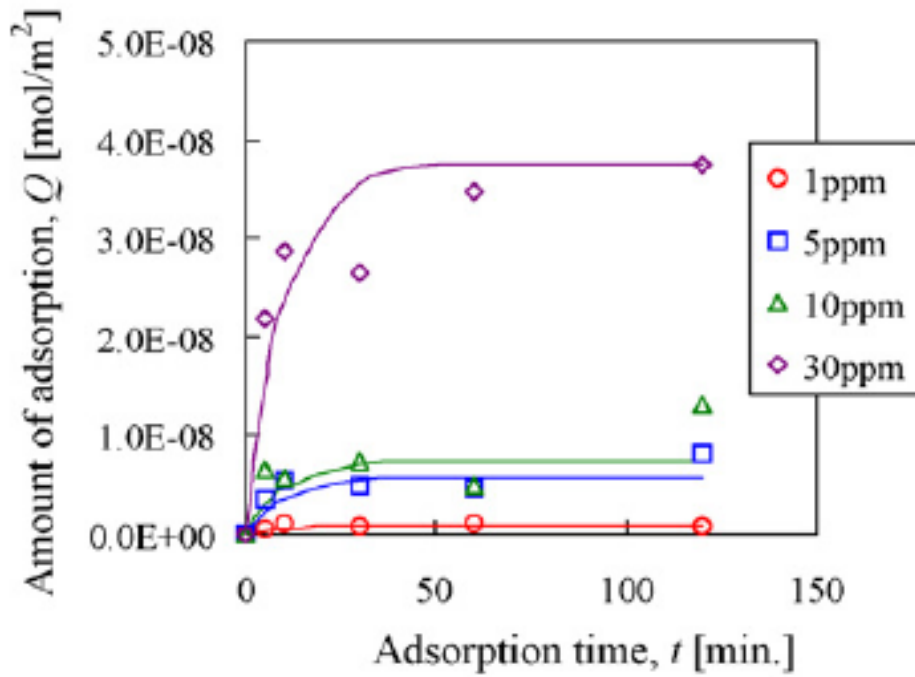
Fig. 6.9: Kinetics of adsorption of Cr^{3+} on the surface of potassium dihydrogen phosphate [Asa09]

$$Q_{eq} = N \left\{ \frac{K_{1e}c}{1 + K_{1e}c} + \frac{K_{2e}c}{1 + K_{2e}c} \right\}$$

$$N = 4.5e\text{-}8 \ [\text{moldm}^2]$$
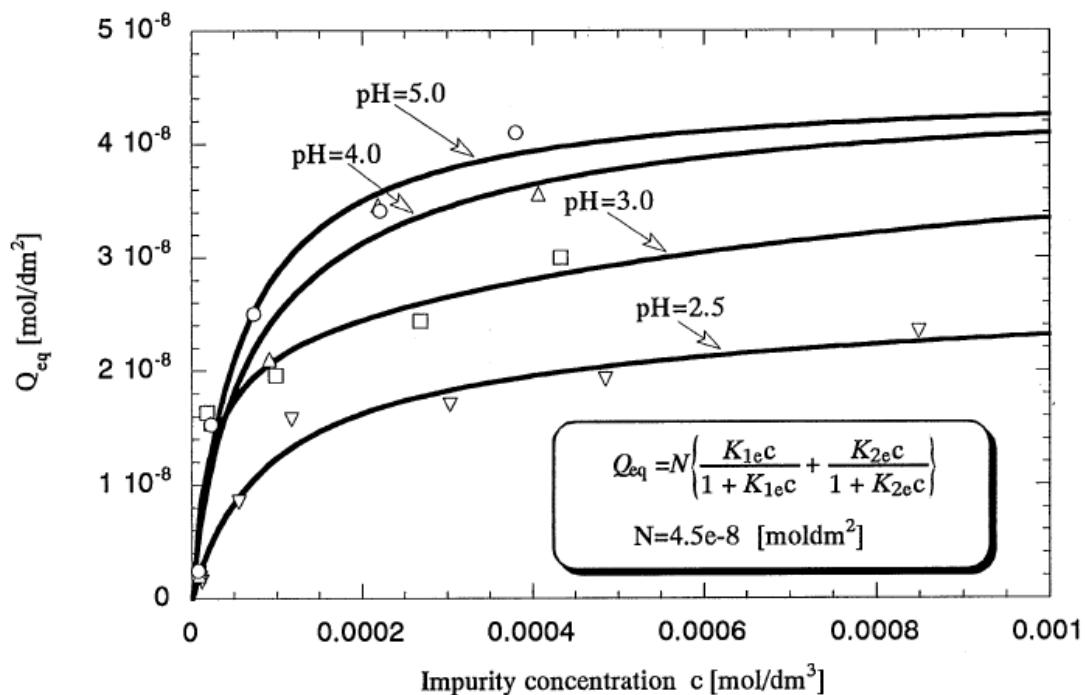
Fig. 6.10: Adsorption of Cr^{3+} on the surface of potassium sulfate [Guz98]

The progression of the curves (saturation with increasing impurity concentration) in Figure 6.8 can be explained by the characteristics of the adsorption isotherm of the impurities. Figures 6.9 and 6.10 show two examples of adsorption isotherms taken from literature.

It can be clearly seen that the impurity adsorption proceeds quiet fast (Fig. 6.9), but the more important fact is the increasing coverage of the surface by adsorbed impurity molecules which is shown in Fig. 6.10. This means at a specific impurity concentration the surface is covered completely and all the available adsorption sites are already blocked by impurity molecules. In this case an increase of the impurity concentration would not automatically cause an increase of the adsorbed amount of impurities and therefore an increase in impurity action. Figure 6.9 (right side) later will be also important to explain the pH dependence of the impurity action (Chapter 6.2).

But before discussing the influence of the pH value, it has to be understood where the huge differences in the effects of the various impurities, even in trivalent impurities, arise.

Referring to Chapter 5 it could be concluded that the trivalent metal ions Fe^{3+}, Cr^{3+} and Al^{3+} have the strongest impact on the growth rates, MZW and morphology of ammonium sulfate compared to a negligible effect of Fe^{2+}, Na^+ and K^+ and the reverse influence caused by Zn^{2+}. The first consideration deals with a "pseudo" impurity concentration which means the total concentration of impurity does not have to be the concentration of the active component in suppressing the growth or widening the MZW. This approach will be further discussed in Chapter 6.2.

Figure 6.11 shows the relationship between the hydrolysis constants of some metal ions and their effects on the MZW of ammonium sulfate. For a better understanding the data of Sayan and Ulrich [Say01] was added into the considerations. The hydrolysis constants for the divalent ions were taken from the following references: Cu^{2+} [Lin79], Ni^{2+} [Lin79] and Mg^{2+} [Bae76].
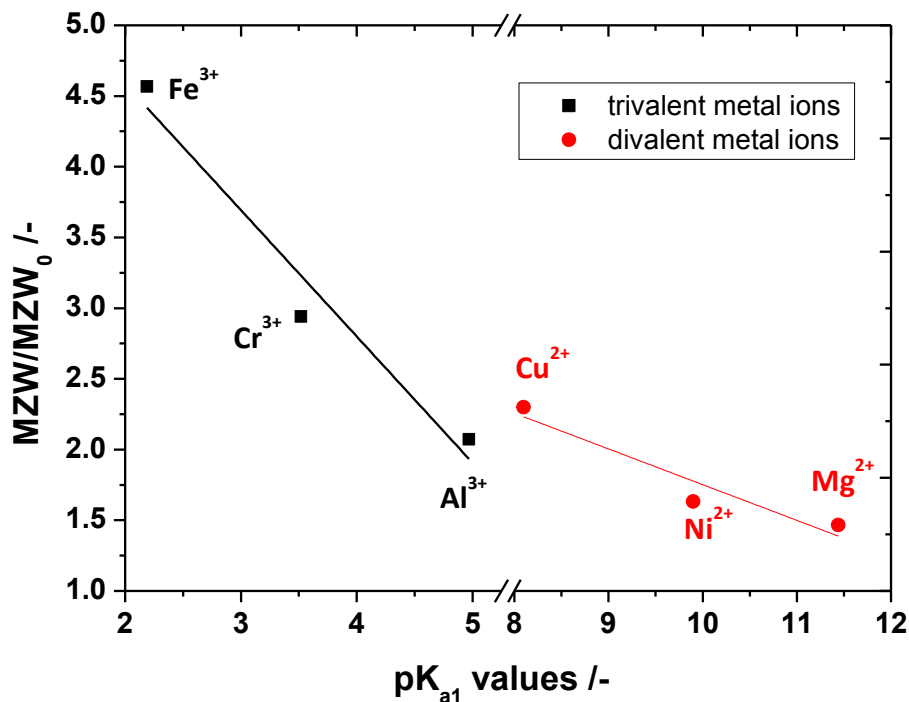
Fig. 6.11: Interrelation between the hydrolysis constant pKa1 of different ions and their effect on the MZW of ammonium sulfate (data of divalent metal ions taken from [Say01])

It is obvious that with decreasing pKa_1 values the effect of the metal ions on the MZW of ammonium sulfate increases. The effect of divalent Cu^{2+} is higher than the effect of trivalent Al^{3+} which can be explained with the different pH values used for the determination. Within this study a solution pH value of 4 was adjusted and in the work of Sayan and Ulrich [Say01] no pH value was mentioned (natural pH value of ammonium sulfate).

The pKa value depends, however, again on other characteristics of the specific metal ions. There is e.g. a global relationship between the hydrolysis constants and structural stability in hexa-aqua metal complexes as shown by Chang et al. [Cha97]. They observed a linear interrelation between pKa and the binding energy E_B which is shown in Equation 6.4 [Cha97].

$$pK_a = -16.824 + 0.0205 \cdot E_B \qquad (6.4)$$

6.2 Influence of the pH value

As shown in Chapters 5.3.2 and 5.5.1 the pH value of the mother liquor can affect the influence of trivalent metal ions on MZW and crystal morphology of ammonium sulfate. Furthermore, the adsorption of impurity molecules on the crystal surface was identified to be responsible for the effects caused by trivalent metal ions (Chapter 6.1). By combining both facts, a theory for the influence of the pH value on the effects of trivalent metal ions should be compiled.

One possible reason for the effect of the solution pH was already mentioned in Chapter 2.5. Metal ions do not exist as bare ions in aqueous solution, but in reality, they always form complexes e.g. with water molecules. Depending on the pH value, an equilibrium of different species can be found in a solution contaminated by trivalent metal ions. Figures 5.10 to 5.12 in Chapter 5.3.2 gave a relationship between the distribution of different metal-aqua-complexes in solution and their effect on the MZW of ammonium sulfate. Thereby the second hydrolysis product $[Me(H_2O)_5OH]^{2+}$ could be identified to be active in widening the MZW. What are the differences in the structure of the various metal-aqua-complexes? As mentioned before, the trivalent metal ions are surrounded by 6 water molecules as ligands at very low pH values. If the pH is increased, some of the water molecules get dehydrated and form hydroxyl groups. So e.g. the surface charges of the impurity molecule changes over the observed pH range (from 2 to 6). Figure 6.12 shows the surface charges of the metal-aqua-complexes $[Fe(H_2O)_3]^{3+}$, $[Fe(H_2O)_5OH]^{2+}$ and $[Fe(H_2O)_4(OH)_2]^+$ simulated by the software GAUSSIAN. The hexa-aqua-iron-complex $[Fe(H_2O)_3]^{3+}$ is positively charged all over its surface, but by dehydration the surface gets more negative close to the appearing hydroxyl group ($[Fe(H_2O)_5OH]^{2+}$). The second hydrolysis product $[Fe(H_2O)_4(OH)_2]^+$ is even less positively charged. This has a major influence on the adsorption of the complexes on the ammonium sulfate crystal surfaces as explained in Chapter 6.1.
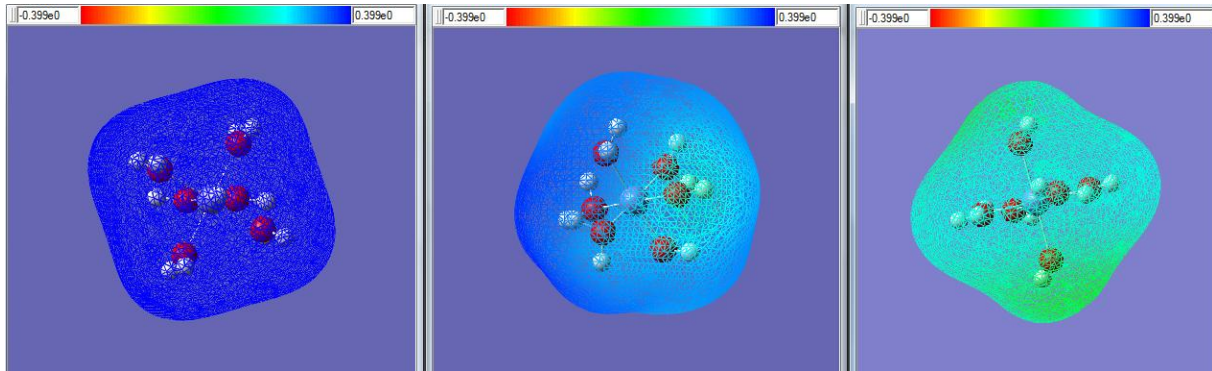
Fig. 6.12: Surface charges of the different metal-aquo-complexes simulated by GAUSSIAN

Guzman et al. [Guz97] observed the effect of Cr^{3+} on the crystallization kinetics of potassium sulfate. Furthermore, they studied the influence of the pH value on the effect of Cr^{3+}. At pH 10 the growth rate of potassium sulfate with 2 ppm Cr^{3+} was equal to the growth rates under pure conditions and precipitation could be observed during the experiment (solid $Cr(OH)_3$). With a decreasing pH value (until pH 3) the effect of Cr^{3+} increased until the growth was completely stopped (see Fig 6.13 A) [Guz97].

Kubota et al. [Kub99] investigated the effect of Fe^{3+} on the growth rates of potassium sulfate and they could observe similar results compared to Guzman et al. [Guz97] and this work which are shown in Fig. 6.13 B.
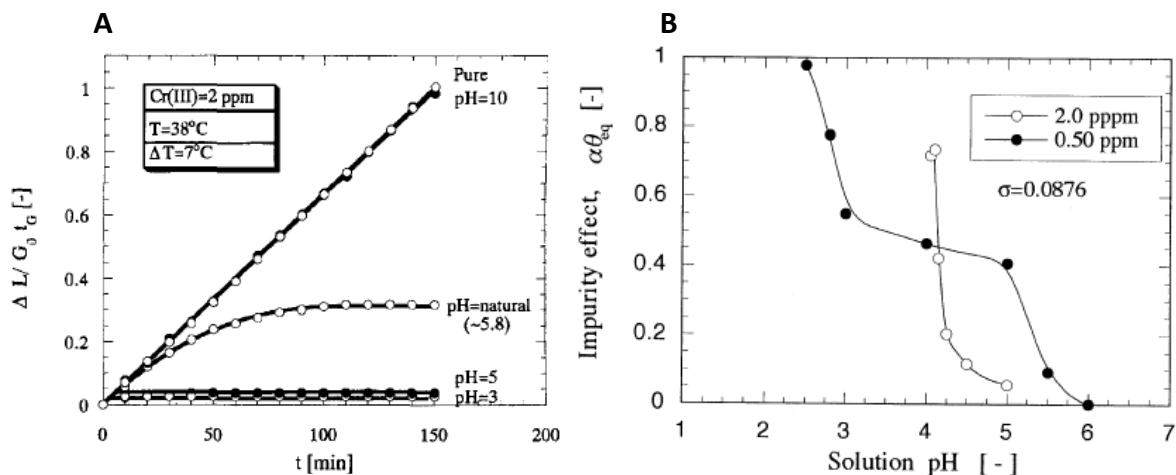
Fig.6.13: Influence of solution pH value on the effect of 2 ppm Cr^{3+} (A) [Guz97] and Fe^{3+} [Kub99] on the crystal growth of potassium sulfate crystals (B)

At a solution pH value of 6 the impurity effect defined as $\alpha\Theta_{eq}$ (see also Chapter 3.2.1) is nearly 0 which means, the impurity effect disappears and the growth rate is equal to the pure solution. By decreasing the pH (until pH 2.5) the effect of Fe^{3+} increases.

The disappearing effect at higher pH values observed in this study on the one hand and also observed by Guzman et al. [Guz97] and Kubota et al. [Kub99] can be contributed to the precipitation of solid metal hydroxide. This precipitation depends on the solution pH value and the hydrolysis constants of the system and was simulated by HySS (see Figures 5.10 to 5.12).

Figure 6.14 illustrates this precipitation. On the left side, Fe^{3+}-containing ammonium sulfate solutions (c = 800 g/L) are shown after preparation and on the right side the same samples are shown after 12 hours in the oven temperate at 50 °C.
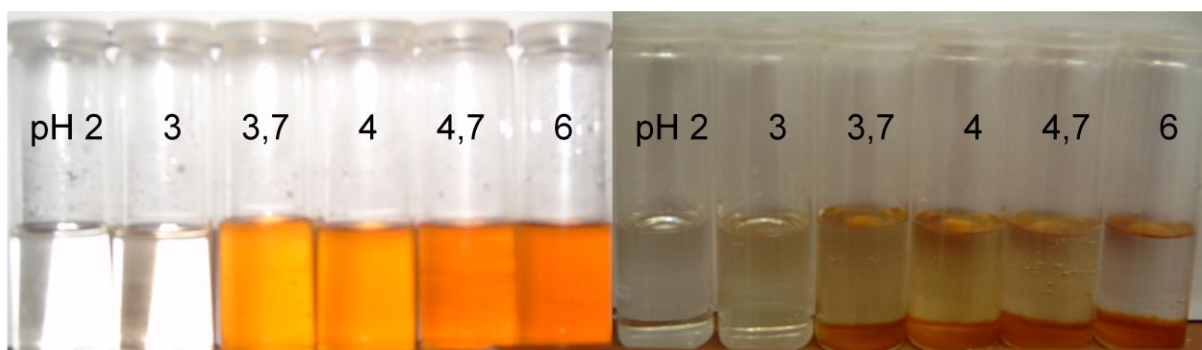
Fig.6.14: Precipitation of iron hydroxide from an ammonium sulfate solution (c = 800 g/L) containing 100 ppm of Fe^{3+}

It can be seen that immediately after preparation and pH adjustment the color of the solution changes depending on the pH value. At low pH values (pH 2) the solution is clear and colorless, with increasing pH value the color of the solution turns into yellow and above pH 3.7 a precipitation can be observed. The precipitates sediment after 12 hours and afterwards different tones of yellow color can be seen. The solution with pH 6 is colorless after sedimentation which means the complete Fe^{3+} is precipitated as $Fe(OH)_3$. This is the reason for the disappearing impurity effect at high pH values and it is comparable to all of the other used metal ions. The question for the different effects of the metal-aqua complexes seems to be a bit more complicated. By taking a look at the charges of the different complexes one would expect the highest effect for the hexa-aqua-metal complexes due to the highest charge and therefore strongest adsorption at the crystal surfaces, but this could not be verified within this study.

Referring to Fig. 6.12 it can be stated that the adsorption of impurity (Cr^{3+}) to the crystal surfaces (potassium sulfate) also depends on the pH value [Guz98]. With increasing pH values from 2 to 6 the adsorbed amount increases [Guz98] while the

effect decreases with increasing pH values (from pH 3 to pH 10) as shown before in Fig.6.13 A [Guz97]. On the first view this seems to be in contradiction to each other, but by taking a closer look to the distribution of the complexes of Cr^{3+} shown in Fig. 5.11 it supports the phenomenon observed in this work. The maximum in the active complex $[Cr(H_2O)_5OH]^{2+}$ is at around pH 5 and it is conceivable that the absorbed amount will decrease again by increasing the pH about pH 5. Furthermore, both, pH 3 and 5 lead to a complete growth stoppage (Fig 6.10) and so it is hard to distinguish the effects at both pH values since at pH 3 there is still a high enough concentration of the active complex (Fig.5.11).

It is necessary to observe adsorption kinetics of different metal ions over a wide range of pH values and compare them to the distribution of the different metal-aqua complexes in aqueous solution. A first relationship can be defined by taking the performed integration experiments into consideration which are shown in Chapter 5.6.

6.3 Removing Effect of Oxalic Acid

In Chapters 5.3.2 and 5.5.2 the so-called removing effect of oxalic acid was shown for the case of trivalent ions on MZW and crystal morphology of ammonium sulfate, respectively. As already mentioned, this effect is known for a long time, since a publication reported this effect in 1955 [Sei55]. It was reported that oxalic acid reduces the effect of Fe^{3+} by the formation of complex Fe^{3+}-oxalate-complexes which do not show the same effect [Sei55]. For industrial crystallization processes this seems to be a promising tool (additive) to avoid undesired effects of trivalent metal ions during crystallization which will be discussed controversially later.

But up to now there are no more information about the exact mechanism behind the effect of oxalic acid. In this Chapter possible mechanisms will be shown and discussed.

Figure 5.14 showed the effect of different amounts of oxalic acid on the effect of 50 ppm Fe^{3+} and Cr^{3+} on the MZW of ammonium sulfate. It could be clearly seen, that the oxalic acid reduced the effect of both trivalent metal ions. Noticeable are the strong differences in the efficiency. For Fe^{3+} the effect completely disappeared at a mass ratio of 4:1 to 8:1 (oxalic acid:Fe^{3+}) and for Cr^{3+} the effect only could be reduced to half at a ratio of 16:1. The open question is about the origin of these obvious differences. One possible explanation is a different mechanism behind the effect on both metal ions, Fe^{3+} and Cr^{3+}. It is well known from literature that oxalic acid is a

quiet strong reducing agent. So the preferred mechanism for the effect of oxalic acid on Fe^{3+} would be the reduction from Fe^{3+} to Fe^{2+} as shown in Eq. 6.7:

Reduction: $2Fe^{3+} + 2e^- \leftrightarrow 2Fe^{2+}$ E^0 = +0.77 V   (6.5)

Oxidation: $H_2C_2O_4 + 2H_2O \leftrightarrow 2CO_2 + 2e^- + 2H_3O^+$ E^0 = -0.47 V   (6.6)

$$2Fe^{3+} + H_2C_2O_4 + 2H_2O \leftrightarrow 2Fe^{2+} + 2H_3O^+ + 2CO_2 \qquad (6.7)$$
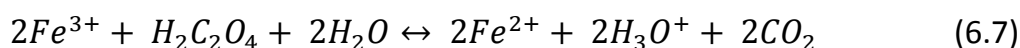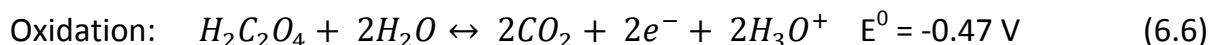
By adding oxalic acid to an ammonium sulfate solution contaminated by Fe^{3+} ions, the color of the solution changes from yellow/pale orange to pale green which is a further evidence for the reduction. It was already shown in Chapter 5.3.1 that Fe^{2+} ions have only a negligible influence on the MZW of ammonium sulfate even at high concentrations up to 1000 ppm (Fig 5.8 B). Summarizing these facts it can be said that the effect of oxalic acid on the effect of Fe^{3+} is caused by a reduction.

But this is not a sufficient prove for the effect of oxalic acid on Cr^{3+} since there is no possible reduction of Cr^{3+} ions. Consequently, another mechanism has to be responsible. In the literature a ligand exchange reaction as shown by Equations 6.8 and 6.9 (taken from [Ham53] was reported by several authors (e.g. [Ham53] and [Ban66]).

$$Cr(H_2O)_6^{3+} + C_2O_4^{2-} \leftrightarrow Cr(C_2O_4)(H_2O)_5^+ + H_2O \qquad (6.8)$$

$$Cr(H_2O)_6^{3+} + H_2C_2O_4 \leftrightarrow Cr(C_2O_4)(H_2O)_5^+ + 2H^+ + H_2O \qquad (6.9)$$
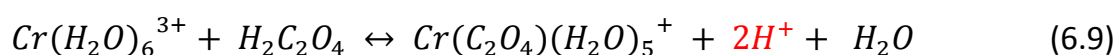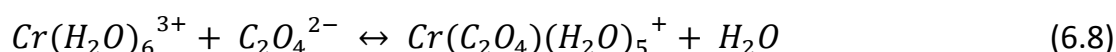
Thereby one water ligand is exchanged by an oxalate ion and a so-called mono-oxalato-penta-aquo-chromium complex is built. This reaction is accompanied with a color shift from green to reddish-purple [Ham53]. A look at Equations 6.9 to 6.11 indicates the equilibrium to be pH value dependent due to the two H^+ ions on the right side of the equation. It is also possible that more water molecules are exchanged by an oxalate ion and a bis-oxalato-chromium complex (see Eq. 6.10) or a tris-oxalato-chromium complex is built (Eq. 6.11):

$$Cr(C_2O_4)(H_2O)_5^+ + H_2C_2O_4 \leftrightarrow Cr(C_2O_4)_2(H_2O)_2^- + 2H^+ + 3H_2O \quad (6.10)$$

$$Cr(C_2O_4)_2(H_2O)_2^- + H_2C_2O_4 \leftrightarrow Cr(C_2O_4)_3^{3-} + 2H^+ + 2H_2O \qquad (6.11)$$
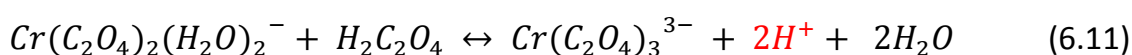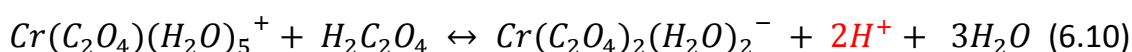
Here it is not possible to give the exact oxalate complex which is responsible for suppressing the effect of the Cr^{3+} ions because the effect was only observed at pH 4. The relatively small effects (half of the effect) of high concentrations of oxalic acid (ratio of 16:1) can be explained by the equilibrium between the hexa-aquo-chromium complexes and the different aquo-oxalato-chromium complexes depending on the pH value. A further research should be performed on the effect of the pH value on the effect of oxalic acid. Curve progressions with a maximum in the effect like in Figures 5.10 to 5.12 can be expected depending on the active complex and its distribution depending on the solution pH value. So also the effect of trivalent metal ions which cannot be reduced by reducing agents like oxalic acid can be diminished due to a complex ligand exchange reaction. This can be explained by strong change in the properties of the impurity complex concerning charge, size and steric composition.

On the first view this seems to be in contradiction to the results of Sangwal et al. (e.g. [San02], [San07]) who observed the effect of different metal ions (including Fe^{3+} and Cr^{3+}) on the growth rates of ammonium oxalate monohydrate. With an increasing Cr^{3+} concentration the growth rates of ammonium oxalate monohydrate crystals is decreasing [San02] similar to the growth rates of ammonium sulfate. Normally it could be expected that the Cr^{3+} ions would also be "inactivated" by the oxalate ions as shown before for the ammonium sulfate system. From the chemical point of view the same complexes are built also in case of an ammonium oxalate solution as shown by Sangwal et al. [San07]. The main difference between the ammonium oxalate monohydrate and the ammonium sulfate system concerning the "inactivating effect" of oxalate ions is the fact that oxalate ions for the one system is a part of the crystal lattice and in the other case not. Therefore the steric hindrance cannot be the reason for the observed effects because as in case of tailor-made additives on part of the impurity complex is similar or equal to the lattice units and the other side is not offering the perfect fit for an incorporation of new growth units.

Another example for a recovery mechanism was shown by Asakuma et al. [Asa07] who studied the effect of the chelating agent EDTA on the effect of the trivalent metal ion Al^{3+} on the growth of potassium dihydrogen phosphate. It could be proven that the EDTA decreases the effect of Al^{3+} on the growth rate of (100) face as shown in Fig. 6.15.

This mechanism can be compared to the effect of oxalic acid on Cr^{3+}, because special Al^{3+}-EDTA complexes are built which do not show the same effect on the crystal growth as the metal-aquo complexes of Al^{3+} do [Asa07].
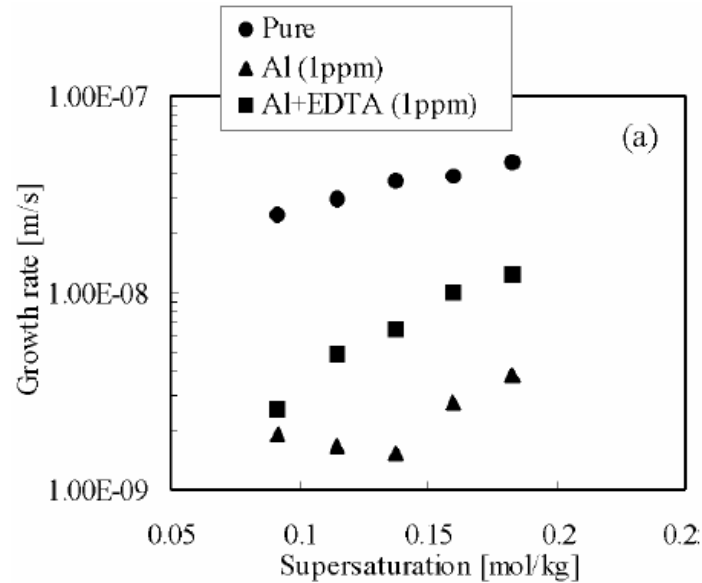
Fig.6. 15: Removing effect of EDTA on the growth inhibition of KPD induced by Al^{3+} (taken from [Asa07])

It could be proven, however, that the effect of trivalent metal ions can be removed partly or completely by adding specific amounts of oxalic acid. It will be discussed if here is a promising tool to optimize existing crystallization processes of ammonium sulfate concerning the negative effects of these impurities. As already mentioned continuous crystallization processes (e.g. FC crystallizers) are usually used to produce mass products like ammonium sulfate. Such processes accumulate impurities during their operation. In Chapter 5.6 it was shown that trivalent metal ions are incorporated into the crystal lattice under specific conditions and therefore leave the process within the product. This point creates the problem of impure product, but if purity is not the critical parameter for the product quality as in case of fertilizers the incorporation is also a chance to reduce the amount of purge which has to be removed from the process. If the incorporation of trivalent metal ions is hindered due to the addition of oxalic acid (Fig. 5.29 in Chapter 5.6) an enrichment of impurities in the mother liquor could be expected which causes the need for an increasing purge (removal of mother liquor from the process). Purge always decreases the profitability of the process due to loss of product on the one hand and by creating costs for the waste disposal on the other hand.

As a consequence an optimization has to be done regarding both, the product purity and the costs for an increasing purge and for the additive oxalic acid.

6.4 Incorporation of Impurities

In Chapter 5.6 the results for the incorporation of trivalent metal ions into the crystal lattice of ammonium sulfate were shown. Due to the relevance for industrial applications the integration of impurities often was a subject in research. Especially, in academic research the compounds KDP (potassium dihydrogen phosphate) and AO (ammonium oxalate monohydrate) were investigated concerning segregation coefficients of different impurities. So Zaitseva et al. [Zai99] observed the incorporation of different impurities into KDP crystals. Thereby it was distinguished between the incorporation into the two characteristic faces (101) and (100) (Fig. 6.7) [Zai99]. For the three trivalent ions it was proven that they are predominantly incorporated into the (100) face and nearly no impurity built in could be detected in the (100) face. For instance, crystals grown from a solution containing 900 ppm Al^{3+} were observed and in the growth region of the face (100) 4400 ppm Al^{3+} could be found and in the growth region of face (101) only 200 ppm Al^{3+} could be detected [Zai99]. Fig. 6.16 A shows the incorporation of Cr^{3+} into the crystal lattice of KDP vividly. This is in agreement with the effects of these impurities on the growth of KDP crystals (see e.g. [Mae06] and [Ras97]) since these faces are blocked predominantly which later contain a higher amount of incorporated impurity. Similar results were reported by Veintemillas-Verdaguer [Vei86] and Hirota [Hir02] who also showed images of KDP crystals grown in the presence of a dye (see Figure 6.16 B).

A   **B**

Fig. 6.16: Face-specific incorporation of Cr^{3+} (A) [Zai99] and a dye (B) [Hir02] into the crystal lattice of potassium dihydrogen phosphate

Another example is given by Mielniczek-Brzoska [Mie00] who observed the incorporation of Cu^{2+} ions into AO crystals and determined the segregation coefficients of this system concerning the dependence on supersaturation. Thereby it

was shown that the segregation coefficient increases with an increasing supersaturation which implies a higher incorporation [Mie00]. Moreover, the segregation coefficient increases with decreasing impurity concentration. These results were confirmed by Sangwal et al. [San02] who observed the segregation coefficient of different other cationic impurities (Fe^{3+} and Cr^{3+}) in AO crystals.

By concluding these two given examples concerning the incorporation of impurities it can be stated that the incorporation correlates with the adsorption of impurity molecules on the crystal surface. According to this, the adsorption is the first step followed by the coverage of the impurity molecule by growth layers before desorption of the impurity molecule can take place. In the existing literature no pH depending incorporation of impurities was reported up to now. In Chapter 5.3.2 the effect of the pH value on the impurity effect was shown for the three trivalent metal ions Fe^{3+}, Cr^{3+} and Al^{3+}. Thereby the first hydrolysis product $[Me(H_2O)_5OH]^{2-}$ was identified to be responsible for widening the MZW of ammonium sulfate and in Chapter 6.1 this was related to the adsorption onto the crystal surface. For the incorporation similar dependencies were observed concerning the pH and these results were shown in Chapter 5.4. Concluding these facts it can be suggested that the impurity is incorporated due to the adsorption at the crystal surfaces. It was mentioned in Chapter 5.4 that the effect of completely coverage (Fig.5.28) of the incorporation can be contributed to the adsorption isotherms. This context was already explained in Chapter 6.1.4 in connection to the decreasing slope of impurity effect (e.g. on MZW) with increasing impurity concentration due to the adsorption isotherm exemplary shown in Fig. 6.9. According to this complete coverage, the amount of impurity incorporated in the crystal will not increase without an increase in the adsorbed amount of impurities.

An open question arises from the decrease in the incorporated amount of Fe^{3+} by adding different concentrations of oxalic acid. As already shown in Chapter 6.3 the effect of oxalic acid has its source in the reduction of Fe^{3+} to Fe^{2+}. Thus by adding oxalic acid not the incorporation of Fe^{3+} is diminished, but the Fe^{3+} is changed into Fe^{2+} which is not incorporated into the crystal lattice of ammonium sulfate.

6.5 Consequences for industrial crystallization processes

One of the main aims of this work defined in Chapter 3 was the identification of process windows of the relevant impurities observed in this work concerning product quantity and quality derived from an industrial crystallization process. Maintaining the order used within this work at first the changes in crystal morphology will be discussed which were shown in Chapter 5.2. It was shown that the crystal morphology is changed significantly by adding small quantities of different metal ions and exemplary for the observed trivalent metal ions the crystal shape turns into needle like crystals. As already mentioned before, a change in crystal morphology can have several negative effects. A first major disadvantage of needle-like crystals compared to compact product crystals is their higher susceptibility to mechanical stress. Already within the crystallization process needle-like crystals will lead to an increasing rate of secondary nucleation and therefore a shift of the CSD (Crystal Size Distribution) to smaller crystals [Mas66].

Further problems of needle-like crystals are caused during the solid-liquid phase separation which in the industry is often realized by filtration or centrifugation steps. Equation 6.12 defines the specific cake resistance α_v which is valid for the cake filtration of monodispers spheres [Sti94].

$$\alpha_v = C \cdot 36 \cdot \frac{(1-\varepsilon)^2}{\varepsilon^3} \cdot \frac{1}{D_{32}^2} \qquad (6.12)$$

Chances in particle shape are taken into account by introducing a shape factor Ψ. Therefore Eq. 6.12 will change into Eq. 6.13.

$$\alpha_v = \frac{C}{\Psi^2} \cdot 36 \cdot \frac{(1-\varepsilon)^2}{\varepsilon^3} \cdot \frac{1}{D_{32}^2} \qquad (6.13)$$

The shape factor Ψ is 1 for spheres and smaller than 1 for particles with a shape deviating from spheres. Consequently, the specific cake resistance increases and the filtration deteriorate due to a change in morphology from compact to needle-like.

After the solid-liquid separation step the product has to be further dried, transported and stored. For these process steps a needle-like product would tend to break and form fines which can increase the tendency of caking.

It can be concluded that concerning their effects on the morphology of ammonium sulfate crystals the concentration of trivalent metal ions should be kept as low as possible. Since a completely removal of these impurities is not possible under an economic point of view, the steady state concentration of a continuous process should not exceed a critical level. With reference to the results shown in Chapter 5.2 and 5.5 it can be suggested to keep the concentration for Fe^{3+} and Cr^{3+} below 20 ppm and for Al^{3+} a critical value of 50 ppm can be defined. For the other observed impurities no critical limit could be detected up to 1000 ppm concerning their effect on the crystal morphology of ammonium sulfate.

For the effects on the MZW a different picture emerges. It has to be kept in mind that most of the industrial crystallization processes are performed within the metastable zone width to avoid primary nucleation and therefore a critical undercooling or supersaturation could be defined depending on the width of the metastable zone. A widening caused by impurities as shown in Chapter 5.3.1 can be seen as a positive aspect due to the enhancement of the critical supersaturation. Only the concentration of Zn^{2+} which tends to decrease the MZW has to be controlled since primary nucleation could be induced and the CSD will be shifted to smaller crystals.

In Chapter 5.4 the effects of the observed impurities on the crystal growth rates are shown. Especially the trivalent metal ions tend to decrease the growth rate of ammonium sulfate crystals until growth stoppage as the worst case and therefore reduce the yield and profitability of the process. As in case of the MZW the concentration of trivalent metal ions should be hold as low as possible. Despite the steep decrease in crystal growth rate the change in crystal morphology is the bottle neck for the process concerning the effect of impurities. First of all the investigations were performed to a supersaturation of 2 K and with increasing supersaturations the growth will be enhanced. Secondly the growth retardation induced by the impurities can be compensated slightly by the increase in MZW due to the increase in the critical supersaturation (primary nucleation).

The application of oxalic acid also has to be discussed with regard to industrial crystallization processes. It was shown that the addition of oxalic acid reduces the effects of the trivalent metal ions. On the first view this is the solution to a number of the problems since the process will deliver uniform, compact and pure product crystals with desired shape and growth rates after oxalic acid treatment. But it could also be shown (Chapter 5.6) that the impurity incorporation into the crystal lattice is

diminished or removed by adding oxalic acid. This causes the problem of impurity enrichment within the continuous process and induces the need for an increasing purge of mother liquor. Hence, for every process the optimal balance between purity, crystal morphology and growth rates (yield) on the one hand and costs for the additive oxalic acid and the loss through mother liquor discharge has to be found.

7. Conclusions and Outlook

Based on the experimental observations, following conclusions can be draw with respect to the aims defined in Chapter 3:

- The pH value plays an important role for the impurity effect since it changes the species of impurities existing in aqueous solutions (hydrolysis of metal ions).
- The first hydrolysis products of Fe^{3+}, Cr^{3+} and Al^{3+} ($[Me(H_2O)_5OH]^{2+}$) was identified to be active in widening the MZW and to be incorporated into the crystal lattice.
- For the results concerning crystal growth rates, MZW, morphology and incorporation the order of the strength of effect is: $Fe^{3+}>Cr^{3+}>Al^{3+}$ which can be related to impurity adsorption at the surface of ammonium sulfate crystals.
- All observed effects were caused by impurity adsorption induced by the affinity between impurity molecule and crystal surface.
- Molecular modeling is a useful tool to discuss and explain the effects regarding the change in morphology of the crystals (impurity – surface interactions).

These results contribute some new pieces in the puzzle called general understanding in the mode of action of impurities on inorganic compounds like ammonium sulfate. They can be used to give some general recommendation for an industrial crystallization process:

- The monovalent ions K^+ and Na^+ and the divalent ions Zn^{2+} and Fe^{2+} do not significantly affect the crystallization process or the product crystals up to concentrations of 1000 ppm → no critical impurity concentration necessary.
- For the trivalent metal ions some critical concentrations can be defined concerning growth rate retardation and the change in crystal morphology:
  → Fe^{3+} and Cr^{3+} should be kept below 20 ppm and Al^{3+} below 50 ppm.
- Oxalic acid proved to be a promising additive to remove the negative effects caused by trivalent impurities.

For further research the following points could be of great interest:

- Establishing molecular modeling as a tool to predict the effects caused by trivalent metal ions and therefore performing simulations in terms of impurity – crystal surface interactions for different metal-aquo-complexes → quantitative analysis.
- Performing face-specific adsorption experiments for the trivalent metal ions to prove the predictions given by molecular modeling.
- Verify the obtained results by changing the model substance to another inorganic salt like sodium chloride or potassium sulfate.

8. Summary

Industrial crystallization processes of inorganic mass products like ammonium sulfate are often continuous, large scale and use waste streams of other chemical reaction pathways as raw materials in order to reduce costs. Therefore a critical problem arises due to the impurities present in these feed streams. Impurities can affect the crystallization at important points such as crystal growth rate, MZW, crystal morphology or crystal purity.

In the available literature there is a lack of coherent information concerning the effects of frequently occurring impurities like e.g. Fe^{3+}, Cr^{3+}, and Al^{3+} on the crystallization as mentioned above. Therefore systematic research on these effects was conducted by using established measurement techniques and instrumentation: fluidized bed crystallizer, batch crystallization, microscope cell and ultrasound velocity measurements. Both, the impurity concentration and the pH value of the solution were varied throughout the experiments.

It was proven that mono- and divalent ions do not significantly influence any of the observed parameters. In the contrary, the trivalent metal ions affected considerable the MZW, the growth rates and the crystal morphology of ammonium sulfate. The MZW of ammonium sulfate was increased by traces of trivalent metal ions due to a shift of the nucleation curve. Furthermore, the growth rates were decreased by adding even small amounts of trivalent metal ions until the growth was completely stopped at a critical concentration. The obtained data were successfully fitted to the Kubota-Mullin-model. The growth retarding effect was identified to be face specific which led to a change in crystal morphology from compact to needle-like crystals. In general, the order of effectiveness was identified to be $Fe^{3+}>Cr^{3+}>Al^{3+}$ at a pH value of 4.

Moreover, it was noted that the pH value has a substantial influence on the effect of the trivalent metal ions. Impurity specific curve shapes including maxima were reported. Similar results with regard to the curve shapes were obtained for the incorporation of trivalent metal ions into the product crystals. Based on the hydrolysis of metal ions in aqueous solution which depend on the pH, a distribution of metal-aquo-complexes was simulated and compared to the pH dependent effect on the MZW and the impurity incorporation. Thereon the first hydrolysis product

$[Me(H_2O)_5OH]^{2+}$ was identified to be active in terms of widening the MZW and changing the morphology of the crystals. The application of oxalic acid as an additive to prevent the effects of trivalent metal ions was proven successfully. The mode of action was discussed based on the chemistry in an aqueous solution including the reduction of Fe^{3+} to Fe^{2+} and the formation of chromium-oxalate-complexes.

All effects described above were discussed with regard to an adsorption of the impurities onto the crystal surface and a first approach was made concerning a molecular modeling as an useful tool to explain the observed results.

The concluded findings were finally discussed with respect to an industrial crystallization process of ammonium sulfate, critical impurity concentrations for the trivalent metal ions were defined and some open questions concerning impurity adsorption and molecular modeling were pointed out which have to be observed further in future.

Symbols

Latin Symbols

Symbol	Unit	Description
$c_i(x)$	ppm	concentration of the impurity
k_d	-	constant for diffusion term
k_r	-	constant for reaction term
m_i	mg	mass of the salt to achieve a desired c_i
m_{tot}	kg	total mass of the solution
m_{start}, m_{end}	g	mass before and after fluidized bed experiment
p	bar	pressure
pKa	-	hydrolysis constant
r	m	radius of the nuclei
r^*_{2D}	m	critical radius for two-dimensional nucleation
r^*_{3D}	m	critical radius for three-dimensional nucleation
t	s	time
t_{ind}	s	induction time for nucleation
t_r	s	relaxation time
t_n	s	time to form stable nuclei
t_g	s	time to grow to a detectable size
$v(R)$	ms^{-1}	crystal growth velocity
v_0	ms^{-1}	crystal growth velocity at pure conditions
v_{US}	ms^{-1}	ultrasound velocity
z	-	stoichiometric number
A	m^2	area
A_1	-	constant for nucleation rate
A_2 and A_3	-	constants for the B+S model
A_4 and A_5	-	constants for the BCF model
G_L and G_W	ms^{-1}	growth rate into length and into width
G_G and G_D	ms^{-1}	growth rate and dissolution rate
I	M	ionic strength
J	$\#*m^{-3}*s^{-1}$	nucleation rate
K	ppm^{-1}	adsorption constant (e.g. Langmuir)
L_1	µm	arithmetic average of the sieve fraction

M_i and $M_{i,tot}$	$gmol^{-1}$	molar mass of the impurity ion and total molar mass of the salt
T	°C	temperature

Greek Symbols

Symbol	Unit	Description
α	-	impurity effectiveness factor
β_{ad}		adiabatic compressibility
γ	$J*m^2$	solid-liquid interfacial energy
ρ	$kg*m^{-3}$	density
σ (S)	-	supersaturation level
ΔG	J	total free energy
ΔG_S	J	surface excess free energy
ΔG_V	J	volume excess free energy
ΔH	$kJ*mol^{-1}$	heat of solution
K	-	ratio of MZW with to MZW without impurities
Θ_{eq}	-	equilibrium surface coverage
Ω	m^3*mol^{-1}	molecular volume

Abbreviations

Abbreviation	Description
AO	ammonium oxalate
conc.	concentration
EU	eutectic
KDP	potassium dihydrogen phosphate
Me	metal
MZW	metastable zone width
ppm	parts per million
SOL	solution
T_{nuc}	nucleation temperature
T_{sol}	solubility temperature

References

[AlA08]   A. Al-Atia: Crystallization of Inorganic Compounds – Scaling in Seawater Desalination. PhD thesis (2008), Martin-Luther University Halle-Wittenberg, published online:
http://sundoc.bibliothek.uni-halle.de/diss-online/08/09H003/index.htm

[Ald99]   L. Alderighi, P. Gans, A. Ienco, D. Peters, A. Sabatini, A. Vacca: Hyperquad simulation and speciation(HySS): a utility program for the investigation of equilibria involving soluble and partially soluble species. Coord. Chem. Rev. 184 (1999), 311-318

[AlJ01]   S. Al-Jibbouri, J. Ulrich: The influence of impurities on crystallization kinetics of sodium chloride. Cryst. Res. Technol. 36 (2001) 12, 1365-1375

[AlJ02]   S. Al-Jibbouri: Effects of Additives in Solution Crystallization, PhD thesis (2002), Martin-Luther University Halle-Wittenberg, published online:
http://sundoc.bibliothek.uni-halle.de/diss-online/02/03H046/index.htm

[AlS96]   A. Al-Sabbagh: Zur KCl- und NaCl-Kristallisation in Anwesenheit von Fremdstoffen. PhD thesis (1996), RWTH Aachen

[Asa07]   Y. Asakuma, M. Nishimura, M. Kimura, H.M. Ang, M.O. Tade, K. Maeda, K. Fukui: Experimental and theoretical study of recovery mechanism of impurity effect by the addition of EDTA. Cryst. Res. Technol. 42 (2007) 5, 424-431

[Asa08]   Y. Asakuma, L. Jee, M. Nishimura, H. Ming Ang, M. Tade, K. Maeda, K. Fukui: Quantum estimation of impurity effect for KDP crystal growth. J. Mol. Struct. 851 (2008) 225-231

[Asa09]   Y. Asakuma, S. Takeda, K. Maeda, K. Fukui: Kinetic and theoretical studies of metal ion adsorption in KDP solution. Appl. Surf. Sci. 255 (2009) 4140-4144

[Bli56]   G. Blisnakov, E. Kirkova: Der Einfluss der Adsorption auf das Kristallwachstum. Z. Phys. Chem. 206 (1957), 271-280

[Bae76]   C. Baes, R.E. Mesmer: The hydrolysis of cations. Wiley, New York, 1976

[Ban66]   D. Banerjea, M.S. Mohan: Kinetics and Mechanism of formation of Cis-diaquo-bis-oxalato-chromate(III) from the Mono-oxalato Complex and Oxalate Ions. ZAAC 347 (1966) 107-112

[Bar02]   P. Barrett, B. Glennon: Characterizing the metastable zone width and solubility curve using lasentec FBRM and PVM. Trans IChemE 80 (2002) 799-805

[Boi88]   R. Boistelle, J. P. Astier: Crystallization mechanism in solution. J. Cryst. Growth 90 (1988) 14-30

[Bro85]   P.L. Brown, R.N. Sylva, G.E. Batley, J. Ellis. The hydrolysis of metal ions. Part 8 Aluminum(III). J. Chem. Soc. Dalton Trans. (1967-1970)

[Byr00]   R.H. Byrne, Y.-R. Luo, R.W. Young: Iron hydrolysis and solubility revisited: observations and comments on iron hydrolysis characterizations. Mar. Chem. 70 (2000) 23-35

[Cab58]   N. Cabrera, D. A. Vermilyea: The growth of crystals from solution, in R.H. Doremus et al. (Eds.), Perfection of Crystals, Wiley, New York, 1958, 393-407

[Cha97]   C.M. Chang, M.K. Wang: Global relationship between the acitidy constants and structural stability in hexaaqua metal complexes. J. Mol. Struct. 417 (1997) 237-240

[Dav74]   R.J. Davey, J.W. Mullin: Growth of the {100} faces of ammonium dihydrogen phosphate crystals in the presence of ionic species. J. Cryst. Growth 26 (1974) 203-208

[Fab96]   J. Fabian: Untersuchungen zur Auflösungskinetik in der Lösungskristallisation. PhD thesis (1996), University Bremen

[Fie07]   A. Fiebig: Prediction of Crystal Morphology for a Limited Range of Impurity Concentrations. PhD thesis (2007), Martin-Luther University Halle-Wittenberg, Shaker Verlag, Aachen, 2008

[Gan96]   P. Gans, A. Sabatini, A. Vacca: Investigation of equilibria in solution. Determination of equilibrium constants with the HYPERQUAD suite of programs. Talanta 43 (1996) 10, 1739-1753

[Gar71]   J. Garside: The concept of effectiveness factors in crystal growth. Chem. Eng. Sci. 26 (1971) 1425-1431

[GES10]   GESTIS Stoffdatenbank des IFA downloaded at 29.09.2010 (http://biade.itrust.de/biade/lpext.dll?f=templates&fn=main-h.htm)

[Gou09]   M. Gougazeh, W. Omar, J. Ulrich: Growth and dissolution kinetics of potassium sulfate in pure solutions and in presence of Cr^{3+} ions. Cryst. Res. Technol. 44 (2009) 11, 1205-1210

[Guz97]   L.A. Guzman, K. Maeda, S. Hirota, M. Yokota, N. Kubota: Unsteady-state impurity effect of chromium (III) on the growth rate of potassium sulfate crystal in aqueous solution. J. Cryst. Growth 181 (1997) 272-280

[Guz98]   L.A. Guzman, K. Maeda, S. Hirota, N. Kubota: Adsorption of growth suppressor chromium (III) on potassium sulfate crystals in aqueous solution. J. Cryst. Growth 186 (1998) 438-445

[Ham53]   R.E. Hamm, R.E. Davis: Complex Ions of Chromium. 3. Reactions between Hexaquochromium(III) and Oxalate Ions. J. Amer. Chem. Soc. 75 (1953) 3085-3089

[Har55]   P. Hartmann, W.G. Perdok: On the relations between structure and morphology of crystals. Acta. Cryst. 8 (1955) 525-529

[Hay73]   T. Hayakawa, M. Matsuoka: Effect of heat transfer on crystal growth rate for inorganic salt-water systems. Japanese Research 2 (1973) 104-115

[Hir02]   S. Hirota, H. Miki, K. Fukui, K. Maeda: Coloring and habit modification of dyed KDP crystals as functions of supersaturation and dye concentration. J. Cryst. Growth 235 (2002) 541-546

[Hof04]   G. Hofmann: Kristallisation in der industriellen Praxis. Wiley-VCH, Weinheim, 2004

[Hys10]   Program HySS downloaded for free of charge from internet at 11.03.2009 http://www.chim1.unifi.it/group/vacsab/hyss.htm

[Kas02]   D. Kashchiev, A. Firoozabadi: Nucleation of gas hydrates. J. Cryst. Growth 243 (2002) 3-4, 476-489

[Kit92]   M. Kitamura, K. Ikemoto, Y. Kawamura, T. Nakai: Effect of Impurity of Cr^{3+} on Crystal-Growth Process of Ammonium Sulfate. Intern. Chem. Eng 32 (1992) 157-163

[Kru93]   M. Kruse: Zur Modellierung der Wachstumskinetik in der Lösungskristallisation. PhD thesis (1993), University Bremen, VDI Verlag, Reihe 3, Nr. 309, Düsseldorf, 1993

[Kub88]   N.Kubota, I. Uchiyama, K. Nakai, K. Shimizu: Change of solubility of potassium sulfate in water caused by traces of chromium (III). Ind. Eng. Chem. Res. 27 (1988) 930-934

[Kub95a]   N. Kubota, J. W. Mullin: A Kinetic Model for Crystal Growth from Aqeous Solution in the Presence of Impurity. J. Cryst. Growth 152 (1995) 203-208

[Kub95b]   N. Kubota, J. Fukazawa, H. Yashiro, J.W. Mullin: Impurity effect of chromium (III) on the growth and dissolution rates of potassium sulfate crystals. J. Cryst. Gowth 149 (1995) 113-119

[Kub97]   N. Kubota, M. Yokota, J.W. Mullin: Supersaturation dependence of crystal growth in solutions in presence of impurity. J. Cryst. Growth 182 (1997) 86-94

[Kub99]   N. Kubota, K. Katagiri, M. Yokota, A. Sato, H. Yashiro, K. Itai: Impurity effect of iron(III) on the growth of potassium sulfate crystal in aqueous solution. J. Cryst. Growth 196 (1999) 156-163

[Kub00]   N. Kubota, H. Otosaka, N. Doki, M. Yokota, A. Sato: Effect of lead impurity on the growth of sodium chloride crystals. J. Cryst. Growth 220 (2000) 135-139

[Lar73]   M.A. Larson, J.W. Mullin: Crystallization kinetics of ammonium sulphate. J. Cryst. Growth 20 (1973) 183-191

[Leu89]   V.W.-H. Leung, B.W. Darwell, A.P.-C. Chan: A rapid algorithm for solution of the equations of multiple equilibrium systems – RAMEDES. Talanta 35 (1989) 9, 713-718

[Lin79]   W.L. Lindsay: Chemical Equilibria in Soils. Wiley Interscience, New York, 1979, 385-422

[Lu03]   J.J. Lu: Predicting Crystal Morhology in the Presence of Additives by Molecular Modeling. PhD thesis (2003), Martin-Luther University Halle-Wittenberg, Shaker Verlag, Aachen, 2004

[Lüh96]   J. Lühmann: Optische on-line Meßtechnik zur Bestimmung der Kristall-wachstumsgeschwindigkeit. PhD thesis (1996), University Bremen, Verlag Mainz, Aachen, 1996

[Mae06]   K. Maeda, R. Tabuchi, Y. Asakuma, K. Fukui: Distribution of metallic ions in a single KDP crystal grown from aqueous solution. Cryst. Res. Technol. 41 (2006) 10, 955-960

[Mas66]   R.E.A. Mason, R.F. Strickland-Constable: Breeding of crystal nuclei. Trans. Faraday Soc. 62 (1966) 455-461

[Mat91]   M. Matsuoka, J. Garside: Non-Isothermal effectiveness factors and the role of heat transfer in crystal growth from solutions and melts. Chem. Eng. Sci 46 (1991) 1, 183-192

[May79]   H.M. May, P.A. Helmke, M.L. Jackson. Gibbsite solubility and thermodynamic properties of hydroxyl-aluminum ions in aqueous solution at 25 °C. Geochim. Cosmochim. Acta 43 (1979), 861-868

[Mes70]   Th. Messing: Probleme und ihre Lösung bei der Massenkristallisation. Chem. Ing. Tech. 42 (1970) 1141-1148

[Mul70]   J.W. Mullin, M. Chakraborty, K. Mehta: Nucleation and growth of ammonium sulfate crystals from aqueous solution. J. appl. Chem. 20 (1970) 367-371

[Mul79]   J.W. Mullin, S.J. Jancic: Interpretation of metastable zone width. IChemE 59 (1979) 188-193

[Mul93]   J.W. Mullin: Crystallization. 3th edition, Butterworth-Heinemann, Oxford, 1993

[Mye02]   A.S. Myerson: Handbook of Industrial Crystallization. 2nd edition, Butterworth-Heinemann, Woburn, 2002

[Nie95]   S. Niehörster, J. Ulrich: Designing Crystal Morphology by a Simple Approach. Cryst. Res. Technol. 30 (1995) 3, 389-395

[Nöl02]   J. Nölte: ICP Emissionsspektrometrie für Praktiker. Wiley-VCH , Weinheim, 2002

[Nyv62]   J. Nývlt: Der Einfluss von Additiven auf die Kristallisation von Ammoniumsulfat. Chemický Prumysl 12 (1962) 170-174

[Nyv70]   J. Nývlt, R. Rychlý, J. Gottfried, J. Wurzelová: Metastable zone width of some aqueous solutions. J. Cryst. Growth 6 (1970) 151-162

[Nyv85]   J. Nývlt, O. Söhnel, M. Matuchova, M. Broul: The kinetics of ndustrial crystallization. Elsevier, Amsterdam, 1985

[Nyv95]   J. Nývlt, J. Ulrich: Admixtures in Crystallization. Wiley-VCH, Weinheim (1995)

[Oma97]   W. Omar, J. Ulrich: Influence of the Fe^{2+} Ions on the Dissolution Rate of Potassium Chloride. Cryst. Res. Technol. 32 (1997) 6, 789-797

[Oma03]   W. Omar, J. Ulrich: Influence of crystallization conditions on the mechanism and rate of crystal growth of potassium sulfate. Cryst. Res. Technol. 38 (2003) 1, 34-41

[Ras97]   L.N. Rashkovich, N.V. Kronsky: Influence of Fe^{3+} and Al^{3+} ions on the kinetics of steps on the {100} faces of KDP. J. Cryst. Growth 182 (1997) 434-441

[Rau00]   M. Rauls, K. Bartosch, M. Kind, St. Kuch, R. Lacmann, A. Mersmann, The influence of impurities on crystallization kinetics – a case study on ammonium sulfate, J. Cryst. Growth 213 (2000) 116-128

[San02a] K. Sangwal, E. Mielniczek-Brzóska: Effect of Cr (III) ions on the growth kinetics of ammonium oxalate monohydrate crystals from aqueous solutions. J. Cryst. Growth 242 (2002) 421-434

[San02b] K. Sangwal, E. Mielniczek-Brzóska, J. Borc: Study of segregation coefficient of cationic impurities in ammonium oxalate monohydrate crystals during growth from aqueous solutions. J. Cryst. Growth 244 (2002) 183-193

[San04]   K. Sangwal, E. Mielniczek-Brzóska: Effect of impurities on metastable zone width for the growth of ammonium oxalate monohydrate crystals from aqueous solutions. J. Cryst. Growth 267 (2004) 662-675

[San07a] K. Sangwal, E. Mielniczek-Brzóska: Effect of cationic impurities on solubility and crystal growth processes of ammonium oxalate monohydrate: Role of formation of metal-oxalato-complexes. Cryst. Res. Technol. 42 (2007) 6, 531-543

[San07b] K. Sangwal: Additives and Crystallization Processes. Wiley&Sons, New York, 2007

[Sat88]   A. Sato, Y. Umetsu, N. Kubota: Effect of Traces of Al(III) on the growth and dissolution Processes of Potassium Sulfate Crystal. Iwate Daigaku Kogakubu Kenkyu Hokoku 41 (1988), 119-123

[Say01]   P. Sayan, J. Ulrich: Determination of the metastable zone width of ammonium sulfate in the presence of impurities by an ultrasound technique, in 8th International Workshop on Industrial Crystallization, BIWIC, Eds. P. Jansens, H. Kramer, M. Roelands,. Doc Vision Delft, Delft, Netherland, 2001, 269-276.

[Sch04]   H. Scherzberg, J. Bach, R. Schmitz: Gleichgewichtsdiagramme für die Kristallisation aus Lösungen und Schmelzen. In G. Hofmann: Kristallisation in der industriellen Praxis. Wiley-VCH, Weinheim, 2004

[Sei55]   H. Seifert: The problem of crystal shape and its industrial importance. Chem. Ing. Tech. (1955) 27, 135-142

[Sen10]   SensoTech GmbH, LiquiSonic 30 Users Manual, D-39179 Magdeburg-Barleben

[Ste07]   A. Stefansson: Iron (III) hydrolysis and solubility at 25 °C. Environ. Sci. Technol 41 (2007) 6117-6123

[Ste90]   M. Stepanski: Zur Wachstumskinetik in der Lösungskristallisation. PhD thesis, University Bremen, Verlag Mainz, Aachen 1990

[Sti94]   M. Stieß: Mechanische Verfahrenstechnik 2. Springer Verlag, Berlin, 1994

[Tav92]   N.S. Tavare: Ammonium sulfate crystallization in a cooling batch crystallizer. Sep. Sci. Technol. 27 (1992) 11, 1469-1487

[Tit02]   S. Titiz-Sargut, J. Ulrich: Influence of additives on the width of the Metastable Zone. Cryst. Growth Des. 2 (2002) 5, 371-374

[Tit03]   S. Titiz-Sargut: Application of a protected ultrasound sensor for the determination of the width of the metastable zone. Chem. Eng. and Proc. 42 (2003) 841-846

[Ulr89]   J. Ulrich: Growth Rate Dispersion – A Review. Cryst. Res. Technol. 24 (1989) 3, 249-257

[Ulr90]   J. Ulrich: Kristallwachstumsgeschwindigkeiten bei der Kornkristallisation - Einflussgrößen und Messtechniken. Habilitation, University Bremen, Shaker, Aachen, 1993

[Ulr04]   J. Ulrich: Fremdstoffbeeinflussung in der Kristallisation. In G. Hofmann: Kristallisation in der industriellen Praxis. Wiley-VCH, Weinheim, 2004

[Ull05]   K.H. Zapp: Ammonium Compounds. in Ullmann´s Encyclopedia of Industrial Chemistry, 6th Edition, Wiley-VCH, Weinheim, 2005, 1-29

[Uri48]   R.J. Urick: The Adsorption of sound in suspension of irregular Particles. J. Acoust. Soc. Am. 20 (1948) 283–289.

[vBr92]   G. von Brachel: Zur Beeinflussung der Kristallwachstumskinetik durch Fremdsalze. PhD thesis (1992), RWTH Aachen, Shaker Verlag, Aachen, 1992

[VDL89]   M. van der Leeden, G. van Rosmalem, K. de Vreugd, G. Witkamp: Einfluss von Additiven und Verunreinigungen auf Kristallisationsprozesse. Chem.-Ing.-Tech. 61 (1989) 5, 385-395

[Vei86]   S. Veintemillas Verdaguer, R. Rodriguez Clemente: Crystal growth of KDP from boiling solutions in the presence of impurities. J. Cryst. Growth 79 (1986), 198-204

[Xu98]   J. Xu, D. Imre, R. McGraw, I. Tang: Ammonium sulfate – Equilibrium and Metastability Phase Diagrams from 40 to -50 °C. J. Phys. Chem. B (1998) 102, 7462-7469

[Zai99]   N. Zaitseva, L. Carman, I. Smolsky, R. Torres, M. Yan: The effect of impurities and supersaturation on the rapid growth of KDP crystals. J. Cryst. Growth 204 (1999) 521-524

[Zhu08]   Z. Zhu, Z. Zhu, P. Yin: Influence of Solubility of ammonium sulfate caused by decreasing pH or addin Fe^{3+} from 288.15 K to 359.15 K. J. Eng. Data 53 (2008) 564-565

Statement of Authorship

I declare that this document and the accompanying code have been composed by myself, and describe my own work, unless otherwise acknowledged in the text. It has not been entered in any previous application for a degree. All verbatim extracts have been distinguished by quotation marks, and all sources of information have been specifically acknowledged.

Halle/Saale, the 01.06.2011

Robert Buchfink

Curriculum Vitae

Personal Details

Born at 18. April in 1983 in Oschatz, Germany
unmarried

Internships

03/2007 – 09/2007	Sanofi-Aventis, Frankfurt/M.
02/2006 – 03/2006	Fraunhofer Institute, Halle (Saale)

Education

05/2008 – 12/2010	PhD thesis, Thermal Process Technology, Halle (Saale) Stipendiary of the AIP e.V.
09/2007 – 03/2008	Diploma thesis, Thermal Process Technology, Halle (Saale)
09/2002 – 03/2008	Study, Engineering, Martin-Luther-University Halle-Wittenberg
08/1993 – 06/2001	Gymnasium, Oschatz
08/1989 – 08/1993	Primary school, Borna

Community Service

08/2001 – 05/2002	Saxony Hospital Hubertusburg, Wermsdorf

Professional Life

Since 01/2011	Sales Manager, GEA Messo PT, Duisburg

Halle (Saale), the 01.06.2011

List of Publications

[1]   R. Buchfink, A. Tischer, G. Patil, R. Rudolph, C. Lange: Ionic liquids as refolding additives: Variation of the anion. J. Biotechnol. (2010), doi:10.1016/j.biotec.2010.07.003

[2]   R. Buchfink, C. Schmidt, J. Ulrich: Fe^{3+} as an example of the effect of trivalent additives on the crystallization of inorganic compounds, here ammonium sulfate. Cryst. Eng. Comm. (2010), doi:10.1039/C0CE00107D

[3]   R. Buchfink, J. Ulrich: The influence of trivalent metal ions on the metastable zone width of ammonium sulfate. Chem. Eng. Technol. (2010), under review

[4]   R. Buchfink, J. Ulrich: The influence of trivalent metal ions on the metastable zone width of ammonium sulfate. Poster presentation, proceedings, BIWIC 2010, Halle/Saale, September 2010

[5]   D. Pertig, R. Buchfink, S. Petersen, T. Stelzer, J. Ulrich: In-line analyzing of industrial crystallization processes by innovative ultrasonic probe technique. Poster presentation, proceedings, BIWIC 2010, Halle/Saale, Cuvillier Verlag, Göttingen, September 2010

[6]   D. Pertig, R. Buchfink, S. Petersen, T. Stelzer, J. Ulrich: In-line analyzing of industrial crystallization processes by innovative ultrasonic probe technique. Chem. Eng. Technol. (2010), submitted

[7]   R. Buchfink, J. Ulrich: Einfluss von Fremdstoffen auf wichtige Kristallisations-parameter von Düngemittelkomponenten. Poster presentation, Fachausschuss Kristallisation, Magdeburg, March 2010

[8]   R. Buchfink, J. Ulrich: The importance of additives and the pH on crystalline product qualities. Oral presentation, Achema 2009, Frankfurt, May 2009